

Electronic Thesis and Dissertation Repository

3-13-2018 3:00 PM

Design and Probabilistic Analysis of Mid- and High-rise Wood Buildings Subjected to Earthquake Excitations

Shucheng Yang
The University of Western Ontario

Supervisor
Dr. H.P. Hong
The University of Western Ontario

Graduate Program in Civil and Environmental Engineering
A thesis submitted in partial fulfillment of the requirements for the degree in Doctor of Philosophy
© Shucheng Yang 2018

Follow this and additional works at: <https://ir.lib.uwo.ca/etd>



Part of the [Structural Engineering Commons](#)

Recommended Citation

Yang, Shucheng, "Design and Probabilistic Analysis of Mid- and High-rise Wood Buildings Subjected to Earthquake Excitations" (2018). *Electronic Thesis and Dissertation Repository*. 5244.
<https://ir.lib.uwo.ca/etd/5244>

This Dissertation/Thesis is brought to you for free and open access by Scholarship@Western. It has been accepted for inclusion in Electronic Thesis and Dissertation Repository by an authorized administrator of Scholarship@Western. For more information, please contact wlsadmin@uwo.ca.

Abstract

Mass timber products, such as the glulam or cross laminated timber (CLT), are less frequently used construction materials at present for mid- and high-rise buildings. The study investigates the feasibility and possible advantages of these materials for constructing mid- and high-rise buildings. One of the issues that needs to be addressed for the use of heavy timber materials is the safety of such constructions under seismic excitations. To address this issue, the nonlinear inelastic seismic responses and capacity curves of a wood buildings must be assessed. For this, the 10-, 15- and 20-storey buildings are designed using heavy timber structural members considering the requirements stipulated in applicable Canadian design codes and standards.

When considering the buildings under unidirectional ground motion, the structural capacity curves along the structural axes in the horizontal plane are identified using well accepted approaches such as the incremental dynamic analysis (IDA) and nonlinear static pushover analysis (NSPA). The capacity curve is used as the basis to develop equivalent nonlinear inelastic single-degree-of-freedom (SDOF) system. The equivalent SDOF system is then employed for the structural reliability. The results indicate that the estimated reliabilities of the designed timber buildings are similar to those of steel frame structures designed according to Canadian practice.

To consider the effect of the bidirectional ground motions on the building responses and their seismic reliability, a procedure is proposed to develop the capacity surface based on the results from the IDA and NSPA. Also, a procedure is proposed to establish equivalent nonlinear inelastic two-degree-of-freedom (2DOF) system based on the capacity surface. The use of the equivalent 2DOF system largely simplifies the reliability analysis of the buildings under bidirectional ground motions. The analysis results indicate that the failure probabilities under bidirectional ground motions are about 3 to 8 times greater than those obtained under unidirectional ground motions. Therefore, the consideration of bidirectional

ground motions in assessing the reliability of building under seismic ground motions can be important for seismic risk modeling and emergency preparedness.

Keywords

Design, cross laminated timber, building, seismic, nonlinear inelastic behaviour, capacity surface, equivalent system, reliability.

Co-Authorship Statement

The material presented in Chapters 2, 3, 4 and 5 of this thesis are to be submitted for possible publication in peer-reviewed journals.

A version of Chapter 2 that contains the structural design co-authored by H.P. Hong and F.M. Bartlett, will be submitted for possible publication in a journal.

A version of Chapter 3 describing the reliability analysis under unidirectional ground motion co-authored by H.P. Hong will be submitted for possible publication in a journal.

A version of Chapter 4 describing the assessment of capacity surface co-authored by H.P. Hong will be submitted for possible publication in a journal.

A version of Chapter 5 presenting the reliability analysis under bidirectional ground motions co-authored by H.P. Hong will be submitted for possible publication in a journal.

Dedication

This thesis is dedicated to all my beloved family.

Also, it is dedicated in memory of my mother, my grandfather Yang, my grandfather Jiang, my grandmother, and my uncle, who have gone on to an even brighter side.

Acknowledgments

First of all, I would like to express my greatest gratitude to Dr. H.P. Hong, who has devoted his time and energy for providing invaluable guidance, comments and suggestions to this work. His intelligence, as well as amicableness, considerateness, diligence, and patience throughout the completion of this thesis are much appreciated. He has acted not only as my supervisor in the field of academia, but also a mentor for life. I am grateful to him for providing the opportunity to complete this degree.

Secondly, I would like to thank to my great friends and outstanding colleagues. It is always a pleasure to remind those fine people in Civil and Environmental Engineering Department for the delightful working environment. In particular, I would like to express my gratitude to Dr. Michael Bartlett for the discussion on research ideas and offering feedback on the subjects of my work.

The financial support from the China Scholarship Council (CSC) is gratefully acknowledged. The financial supports received from the multi-disciplinary NSERC strategic research Network for Engineered Wood-based Building Systems (NEWBuilds) and University of New Brunswick for supporting me to attend the conferences are acknowledged. I also acknowledge the financial support from the University of Western Ontario throughout the duration of my program.

Finally, I am extremely grateful to my family for their unwavering support through all of this and for encouraging me to pursue my aspirations in a foreign country.

Table of Contents

Abstract	i
Co-Authorship Statement.....	iii
Dedication	iv
Acknowledgments.....	v
Table of Contents	vi
List of Tables	ix
List of Figures	x
Nomenclature	xiv
Chapter 1	1
1 Introduction.....	1
1.1 Introduction	1
1.2 Objectives and thesis outline.....	3
1.3 References	5
Chapter 2.....	9
2 Seismic Responses and Capacity Curves of Mid- and High-rise Wood Buildings under Uni-directional Seismic Excitations	9
2.1 Introduction	9
2.2 Design considerations for mid- and high-rise wood buildings	11
2.2.1 Basic considerations	11
2.2.2 Design procedure and criteria.....	12
2.3 Finite element modelling of designed buildings	21
2.3.1 Designed buildings	21
2.3.2 Finite element modelling	28
2.4 Response characteristics and capacity curves	34

2.4.1	Response characteristics of the designed buildings.....	34
2.4.2	Estimation of capacity curves.....	36
2.5	Conclusions.....	44
2.6	References.....	44
Chapter 3.....		49
3	Reliability Assessment of Mid- and High-rise Wood Buildings under Uni-directional Seismic Excitations.....	49
3.1	Introduction.....	49
3.2	Seismic response characteristics of designed prototype wood buildings.....	51
3.3	Equivalent nonlinear inelastic SDOF system for the buildings.....	57
3.4	Seismic demand, reliability evaluation procedure and results.....	63
3.4.1	Seismic demand and reliability evaluation procedure.....	63
3.4.2	Analysis results.....	68
3.5	Conclusions.....	71
3.6	References.....	71
Chapter 4.....		76
4	Assessing the Capacity Surface of Mid- and High-rise Wood Buildings under Bidirectional Seismic Excitations.....	76
4.1	Introduction.....	76
4.2	Response characteristics of designed wood buildings under bidirectional horizontal seismic load.....	79
4.2.1	Designed tall wood buildings.....	79
4.2.2	Evaluation of the capacity surface under bidirectional horizontal ground motions.....	81
4.2.3	Effect of record-to-record variability on the response surface.....	92
4.2.4	Comparison of the mean IDA surface and nonlinear static pushover analysis results	97

4.3	Conclusions	103
4.4	References	103
Chapter 5.....		108
5	Reliability Assessment of the Mid- and High-rise Wood Buildings under Bidirectional Seismic Excitations.....	108
5.1	Introduction	108
5.2	Seismic response characteristics of designed prototype wood buildings.....	110
5.3	Approximating bisymmetric buildings using equivalent 2DOF system	114
5.3.1	Equation of motion	114
5.3.2	Incorporating design consideration	118
5.3.3	Fitting the equivalent model based on the capacity surface	120
5.4	Seismic demand, reliability evaluation procedure and results	123
5.4.1	Seismic demand and reliability evaluation procedure	123
5.4.2	Estimated failure probability	134
5.5	Conclusions	138
5.6	References	138
Chapter 6.....		141
6	Conclusions and Recommendations for Future Work.....	141
6.1	Conclusions	141
6.2	Recommendations for future work.....	143
Curriculum Vitae		144

List of Tables

Table 2.1. Design data of a residential building located at a site classified as “D” in North Vancouver.	14
Table 2.2a. Distribution of lateral load from earthquake effect.....	24
Table 2.2b. Distribution of lateral load from wind effect.	25
Table 2.3a. Connections used in the 10-storey wood building and the number of fasteners and their spacing.	26
Table 2.3b. Connections used in the 15-storey wood building and the number of fasteners and their spacing.	27
Table 2.3c. Connections used in the 20-storey wood building and the number of fasteners and their spacing.	27
Table 2.4. Material properties of CLT and glulam.	29
Table 2.5. Characterized connector parameters for the connection model.	32
Table 2.6. Vibration periods of designed buildings.....	34
Table 2.7. Selected records for North Vancouver.	37
Table 2.8a. Values of capacity curve at selected load levels for designed wood buildings considering the E-W direction.....	43
Table 2.8b. Values of capacity curve at selected load levels for designed CLT buildings considering the S-N direction.	43
Table 3.1. Parameters used to calculate the design based shear and the characteristics of the designed wood buildings.....	53
Table 3.2. Estimated model parameters for the equivalent SDOF systems along two horizontal orthogonal structural axes.....	61
Table 3.3. Estimated probabilities of the incipient damage P_D	68
Table 4.1. Selected ground motion records.	82
Table 4.2. Characterizing of capacities for designed CLT buildings considering different directions.....	99
Table 5.1. Parameters used to calculate the design based shear for and the characteristics of the designed wood buildings along X-axis and Y-axis.	120
Table 5.2. Estimated model parameters.	122

List of Figures

Figure 2.1. Illustration of screw-type connections for adjacent shear wall panels and the wall-to-floor brackets (FPInnovations, 2011): a) half-tapped joint; b) spline joint; c) Brackets installed at upper or lower side of the floor.	17
Figure 2.2. Illustrations of connections: a) simplified kinematics model of CLT wall panel subjected to horizontal load; b) illustration of connection system (dimension in mm).	19
Figure 2.3. Three-dimensional model of the designed wood buildings: a) 10-storey wood building; b) 15-storey wood building; c) 20-storey wood building.	23
Figure 2.4. Designed connection system for the wood buildings: a) 10-storey; b) 15-storey; c) 20-storey.	28
Figure 2.5. Illustration of the orientation for defining the material properties: a) CLT panel; b) glulam member.	29
Figure 2.6. Illustration of the modelling of floor panels.	30
Figure 2.7. Model and comparison of predicted and test results: a) sketch of hysteretic model and definition of model parameters, b) illustration of fitted model for the steel bracket; c) illustration of fitted model for the equivalent connectors used for parallel panels.	33
Figure 2.8. Inter-storey drifts of wood buildings under seismic loadings.	36
Figure 2.9. Inter-storey drifts of wood buildings under wind loadings.	36
Figure 2.10. Capacity curves obtained from IDA presented by roof drift ratio and spectral acceleration S_a	39
Figure 2.11. Capacity curves obtained from IDA presented by base shear versus top displacement.	40
Figure 2.12. Capacity curves obtained from mean of IDA curves and from NSPA by using inverted-triangle triangle or first sway mode load pattern.	41
Figure 3.1. Designed 10-storey wood building and its seismic response.	54
Figure 3.2. Designed 15-storey wood building and its seismic response.	55
Figure 3.3. Designed 20-storey wood building and its seismic response.	56
Figure 3.4. Illustration of force-deformation curve of the Bouc-Wen hysteretic models subjected to harmonic excitations with increasing amplitude: a) smooth hysteretic and	

quasi-bilinear models; b) smooth hysteretic models with different post-yield and unloading slopes.....	60
Figure 3.5. Hysteresis curves of equivalent SDOF systems and capacity curves of designed three wood buildings along two horizontal orthogonal structural axes.	62
Figure 3.6. Estimated ductility demand for the equivalent SDOF systems.	65
Figure 3.7. Samples of maximum ductility demand presented in the (shifted) Frechet distribution paper.	67
Figure 3.8. Estimated annual failure probability P_C : a) $v_{\mu_R} = 0.2$; b) $v_{\mu_R} = 0.3$; c) $v_{\mu_R} = 0.4$	70
Figure 4.1. Designed 10-Storey wood building	80
Figure 4.2. Designed 15-Storey wood building.	80
Figure 4.3. Designed 20-Storey wood building.	81
Figure 4.4. Definition of the earthquake incidence angle α	83
Figure 4.5. Capacity of the 10-storey wood building under bidirectional horizontal orthogonal ground motions by considering Record # 4 listed in Table 4.1: a) Trajectory of the maximum displacement projected in the horizontal plane; b) capacity curve; c) capacity surface considering the base shear; d) capacity surface using $S_{2A}(T_1, \xi)$ as the ground motion measure.....	84
Figure 4.6. Capacity of the 10-storey wood building under bidirectional horizontal orthogonal ground motions by considering Record # 8 listed in Table 4.1: a) Trajectory of the maximum displacement projected in the horizontal plane; b) capacity curve; c) capacity surface considering the base shear; d) capacity surface using $S_{2A}(T_1, \xi)$ as the ground motion measure.....	87
Figure 4.7. Capacity of the 15-storey wood building under bidirectional horizontal orthogonal ground motions by considering Record # 4 listed in Table 4.1: a) Trajectory of the maximum displacement projected in the horizontal plane, b) capacity curve, c) capacity surface considering the base shear, d) capacity surface using $S_{2A}(T_1, \xi)$ as the ground motion measure.....	88
Figure 4.8. Capacity of the 15-storey wood building under bidirectional horizontal orthogonal ground motions by considering Record # 8 listed in Table 4.1: a) Trajectory of the maximum displacement projected in the horizontal plane; b) capacity curve; c) capacity surface considering the base shear; d) capacity surface using $S_{2A}(T_1, \xi)$ as the ground motion measure.....	89

Figure 4.9. Capacity of the 20-storey wood building under bidirectional horizontal orthogonal ground motions by considering Record # 4 listed in Table 4.1: a) Trajectory of the maximum displacement projected in the horizontal plane; b) capacity curve; c) capacity surface considering the base shear; d) capacity surface using $S_{2A}(T_1, \xi)$ as the ground motion measure.....	90
Figure 4.10. Capacity of the 20-storey wood building under bidirectional horizontal orthogonal ground motions by considering Record # 8 listed in Table 4.1: a) Trajectory of the maximum displacement projected in the horizontal plane; b) capacity curve; c) capacity surface considering the base shear; d) capacity surface using $S_{2A}(T_1, \xi)$ as the ground motion measure.....	91
Figure 4.11. The obtained mean and standard deviation of capacity surfaces by using base shear for wood buildings: a) 10-storey; b) 15-storey; c) 20-storey.	94
Figure 4.12. The obtained mean and standard deviation of capacity surfaces by using $S_{2A}(T_1, \xi)$ for wood buildings: a) 10-storey; b) 15-storey; c) 20-storey.	96
Figure 4.13. Capacity surfaces obtained by using the NSPA and by using the mean of IDA surface and the relative difference respect to the mean of IDA surface (conditioned on the same roof displacement) for the 10-storey building.	100
Figure 4.14. Capacity surfaces obtained by using the NSPA and by using the mean of IDA surface and the relative difference respect to the mean of IDA surface (conditioned on the same roof displacement) for the 15-storey building.	101
Figure 4.15. Capacity surfaces obtained by using the NSPA and by using the mean of IDA surface and the relative difference respect to the mean of IDA surface (conditioned on the same roof displacement) for the 20-storey building.	102
Figure 5.1. Designed 10-storey wood building and its mean capacity surface by considering bidirectional ground motions.	111
Figure 5.2. Designed 15-storey wood building and its mean capacity surface by considering bidirectional ground motions.	112
Figure 5.3. Designed 20-storey wood building and its mean capacity surface by considering bidirectional ground motions.	113
Figure 5.4. Structural axes and definition of the θ -axis and illustration of the inelastic 2DOF system (from Lee and Hong 2010).	115
Figure 5.5. Contour for the incipient yield defined by the biaxial Bouc–Wen model... ..	118
Figure 5.6. Contours of incipient yield identified based on the mean of the IDA surface for the designed wood buildings: a) 10-storey wood building; b) 15-storey wood building; c) 20-storey wood building.	122

Figure 5.7. Calculated force-deformation curves along the X-axis and along the Y-axis, trajectory of displacement projected in the horizontal plane, $\mu_{b,\max}$ and $D_{b,PA}^*$ (for $\lambda = 0.1$) for a selected record (NGA#756, Loma Prieta, Dublin - Fire Station) for the 2DOF system representing 10-storey wood building.	127
Figure 5.8. Calculated force-deformation curves along the X-axis and along the Y-axis, trajectory of displacement projected in the horizontal plane, $\mu_{b,\max}$ and $D_{b,PA}^*$ (for $\lambda = 0.1$) for a selected record (NGA#756, Loma Prieta, Dublin - Fire Station) for the 2DOF system representing 15-storey wood building.	128
Figure 5.9. Calculated force-deformation curves along the X-axis and along the Y-axis, trajectory of displacement projected in the horizontal plane, $\mu_{b,\max}$ and $D_{b,PA}^*$ (for $\lambda = 0.1$) for a selected record (NGA#756, Loma Prieta, Dublin - Fire Station) for the 2DOF system representing 20-storey wood building.	129
Figure 5.10. Estimated mean and standard deviation (σ) of $\mu_{b,\max}$	130
Figure 5.11. Estimated mean and standard deviation (σ) of $D_{b,PA}^*$	131
Figure 5.12. Plots of the samples of $\mu_{b,\max}$ and $D_{b,PA}^*$ in Frechet or lognormal probability papers for selected sets of (ζ_x, ζ_y) values.	133
Figure 5.13. Estimated $P_{C,b}$: and $P_{C,PA}$ for the model representing 10-storey: a) Estimated $P_{C,b}$; b) Estimated $P_{C,PA}$	136
Figure 5.14. Estimated $P_{C,b}$: and $P_{C,PA}$ for the model representing 15-storey: a) Estimated $P_{C,b}$; b) Estimated $P_{C,PA}$	136
Figure 5.15. Estimated $P_{C,b}$ and $P_{C,PA}$ for the model representing 20-storey: a) Estimated $P_{C,b}$; b) Estimated $P_{C,PA}$	137
Figure 5.16. Estimated failure probability P_C by considering the unidirectional ground motion with the equivalent structural model shown in tables 5.1 and 5.2.	137

Nomenclature

The nomenclature used throughout the thesis is listed by chapter as follows (code specific values for Chapter 2 are indicated in parenthesis):

Chapter 2

A_{eff}	effective bending area
C_e	exposure factor
C_{eH}	exposure factor at the top of the building
C_g	gust effect factor
C_P	external pressure coefficient
D	lateral displacement at the top of the wall (m)
E_x, E_y, E_z	Young's moduli
F	gust energy ratio
F_a	acceleration-based site coefficients
F_b	factored bending strength
F_c	compressive strength parallel to the grain
F_i	static wind force of i -th storey
F_t	a portion of the shear force concentrated at the top of the building
F_{tp}	factored tensile strength parallel to the grain
F_x	horizontal load applied at the height h_x (N)
F_v	velocity-based site coefficient
$F(D)$	applied lateral force on the wall as function of D
G	total gravity load acting along the middle of the panel
G_{yz}, G_{zx}, G_{xy}	shear moduli
H	width of the wall panel

I_w, I_s, I_E	importance factors for wind, snow, and earthquake loads
I_{eff}	effective moment of inertia (mm^6)
J	reduction coefficient for the overturning moment
K	factor related to the surface roughness of the terrain
L	length of the wall panel
M_f	factored bending moment due to seismic lateral load
M_r	factored bending moment resistance
M_V	factor to account for higher mode effect on base shear
M_x	overturning moment at the height h_x
N	number of total storeys
P_f	factored compressive axial load
P_r	factored compressive load resistance parallel to grain
R_o	overstrength factor
R_d	ductility related reduction factor
$S(T_a)$	spectral acceleration at T_a , in fraction of gravitational acceleration
$S_a(T)$	design spectral acceleration at T given in the NBCC (2010)
T_a	fundamental natural vibration period (s)
T_f	factored tensile axial load
T_r	factored tensile load resistance parallel to grain
V_d	design base shear
V_H	mean wind speed at the top of structure
V_k	shear reaction of the k -th connector between wall panels
W	total building dead load plus 25% of the snow load (N)
W_x	weight at the height h_x (N)
W_i	weight at the i -th floor level (N)

X_i	horizontal drift of i -th storey (mm)
a_D	mean of the peak along-wind acceleration (m/s^2)
a_W	mean of the peak across-wind acceleration (m/s^2)
a_l	distance between the centroid of the first lamina and the centroid of the panel cross-section
b	CLT member width
d_a	along-wind effective depth (m)
d_1	deflection of the floor under a concentrate point load of 1 kN at the centre
f_i	reaction force of the i -th wall-to-floor connector
f_n	lowest natural frequency of the structure under wind load
f_{nD}	natural vibration frequencies in the along-wind direction
f_{nW}	natural vibration frequencies in the across-wind directions
f_1	fundamental vibration frequency of the floor system (Hz)
g_p	peak factor
h_{eff}	summation of thickness of panels parallel to the axial load (mm)
h_i	height of the i -th floor
h_n	total height of the building (m)
h_x	height above the ground (m)
h_l	thickness of the first (outermost) lamina
l_i	distance from the i -th wall-to-floor connector to the compression corner of the panel
m	total number of connectors between the wall panels
n	total number of connectors between the wall and the floor diaphragm
p	external pressure perpendicular to the wind (kPa)
q	reference wind velocity pressure (kPa)
s	size reduction factor

w	across-wind effective width
β_D	fraction of critical damping in along-wind direction
β_W	fraction of critical damping in across-wind direction
γ_1	connection efficiency factor
Δ	maximum wind-induced lateral deflection at the top of the building (m)
$\nu_{yx}, \nu_{zx}, \nu_{zy}$	Poisson's ratios
ρ_B	density of building

Chapter 3

I_E	importance factors for earthquake load
L	ratio of the seismic hazard in terms of the spectral acceleration
M	total mass of the structure
M_V	factor to account for higher mode effect on base shear
P_D	probability of incipient damage
P_C	probability of incipient collapse
R_o	overstrength factor
R_d	ductility related reduction factor
$S_A(T_n, \xi)$	annual maximum spectral acceleration for a SDOF system
$S_{A-\chi}(T_n, \xi)$	design spectral acceleration
$S(T_n)$	spectral acceleration at T_n (g)
\bar{S}_{A0}	average SA given the base shear equals f_0
T_n	natural vibration period (s)
V_d	design base shear
V_{sy}	capacity to sustain base shear of the constructed building

W	total building dead load plus 25% of the snow load (N)
c	viscous damping coefficient
f_y	force at yield
f_0	peak values of the earthquake-induced resisting force in the corresponding linear elastic system
\bar{f}_0	average base shear of the building given a selected spectral acceleration value S_{A0} of the corresponding linear elastic SDOF system
$h(z, \varepsilon)$	pinching function
k	stiffness
m	mass
\tilde{m}	generalized mass
m_L	mean of L
m_{R_n}, ν_{R_n}	mean and cov of R_n
m_{μ_R}, ν_{μ_R}	mean and cov of μ_R
$m_{\ln(\zeta)}, \sigma_{\ln(\zeta)}$	mean and standard deviation of $\ln(\zeta)$
u, \dot{u}, \ddot{u}	translational displacement, velocity, and acceleration, respectively
\ddot{u}_g	ground motion
u_y	displacement at yield
u_0	peak values of the earthquake-induced displacement and resisting force in the corresponding linear elastic system
z	hysteretic displacement
α	ratio of post-yield stiffness to initial stiffness
β, γ, n	Bouc-Wen model shape parameters
Γ	modal participation factor
δ_η, δ_ν	Bouc-Wen model degradation parameters

ε	dissipated energy at time t
ζ	equal to ϕ
Λ	effective modal mass (or the effective mass for the considered loading profile)
μ	ductility demand
μ_{\max}	peak ductility demand
μ_R	ductility capacity
ν_s	coefficient of variation (cov) of $S_A(T_n, \xi)$
ξ	damping ratio
ϕ	normalized yield strength
$\Phi^{-1}(\bullet)$	inverse standard normal distribution function
ω_n	natural vibration frequency (rad/s)

Chapter 4

D	maximum roof displacement
D_{px}	trajectory of displacement along the X -axis
D_{py}	trajectory of displacement along the Y -axis
D_x	displacement along the X -axis at time t_{\max}
D_y	displacement along the Y -axis at time t_{\max}
$D_x(t)$	roof displacement along the X -axis at time t
$D_y(t)$	roof displacement along the Y -axis at time t
M_x	modal mass for the sway mode along the X -axis
M_y	modal mass for the sway mode along the Y -axis
P	an intensity factor

$S_{2A}(T_1, \xi)$	maximum of the spectral acceleration by considering each of the horizontal ground motion components
T_1	fundamental vibration of the structure
V	maximum base shear
$V_x(t)$	base shear along the X -axis at time t
$V_y(t)$	base shear along the Y -axis at time t
m_i	mass associated with the i -th element of ψ_x (and ψ_y)
$p_{effx}(t)$	effective earthquake force along the X -axis at time t
$p_{effy}(t)$	effective earthquake force along the Y -axis at time t
t_{max}	time leading to D
$\ddot{u}_{gx}(t)$	horizontal component of ground motions applied along the X -axis
$\ddot{u}_{gy}(t)$	horizontal component of ground motions applied along the Y -axis
α	earthquake incidence angle equal
Γ_x	modal participation factor for the sway mode along the X -axis
Γ_y	modal participation factor for the sway mode along the Y -axis
ξ	damping ratio
ψ_x	first sway vibration mode along the X -axis
ψ_y	first sway vibration mode along the Y -axis
$\psi_{x,i}$	the i -th element of ψ_x
$\psi_{y,i}$	the i -th element of ψ_y

Chapter 5

$D_{b,PA}$	Park-Ang damage index under the biaxial excitations (Park and Ang 1985)
$E_{n,b}$	normalized dissipated hysteretic energy for biaxial response
F_{Ex}	force corresponding to d_x

F_{Ey}	force corresponding to d_y
$F_{y,x}$	yield force corresponding to yield displacement Δ_x
$F_{y,y}$	yield force corresponding to yield displacement Δ_y
I_E	importance factors for earthquake load
L_x	ratio of the seismic hazard in terms of the SA for the structural X-axis
L_y	ratio of the seismic hazard in terms of the SA for the structural Y-axis
M	total mass of the structure
M_V	factor to account for higher mode effect on base shear
$P_{C,b}$	probability of incipient collapse of the system subjected to bidirectional seismic excitations
$P_{C,PA}$	probability of incipient collapse of the system subjected to bidirectional seismic excitations assessed by using $D_{b,PA}$
$P_{D,b}$	probability of incipient yield (or damage) of the system subjected to bidirectional seismic excitations
Q_x	yield forces along the X-axis
Q_y	yield forces along the Y-axis
R_d	ductility related reduction factor
R_{nx}	ratio between $V_{yield, x}$ to V_{dx}
R_{ny}	ratio between $V_{yield, y}$ to V_{dy}
R_o	overstrength factor
$S_A(T_n, \xi)$	annual maximum spectral acceleration
$S_{Ax}(T_{nx}, \xi_x)$	spectral acceleration for the considered record component along the X-axis
$S_{Ay}(T_{ny}, \xi_y)$	spectral acceleration for the considered record component along the Y-axis
$S_{A-\chi}(T_n, \xi)$	design spectral acceleration (for a system with the natural vibration period T_n and a damping ratio ξ) representing $(1 - \chi)$ -fractile of SAa

T_n	natural vibration period (s)
T_{nx}	first sway vibration period along X -axis
T_{ny}	first sway vibration period along Y -axis
V_d	design base shear
V_{dx}	design base shear along the X -axis
V_{dy}	design base shear along the Y -axis
$V_{yield, x}$	base shear along the X -axis at incipient yield of a designed structure
$V_{yield, y}$	base shear along the Y -axis at incipient yield of a designed structure
W	total building dead load plus 25% of the snow load (N)
c_x	viscous damping coefficient along the X -axis
c_y	viscous damping coefficient along the Y -axis
d_x	earthquake-induced displacement in the corresponding linear elastic system along the X -axis
d_y	earthquake-induced displacement in the corresponding linear elastic system along the Y -axis
k_x	stiffness along the X -axis
k_y	stiffness along the Y -axis
m	mass
m_{L_x}	mean of L_x
m_{L_y}	mean of L_y
$m_{R_{nx}}, v_{R_{nx}}$	mean and cov of R_{nx}
$m_{R_{ny}}, v_{R_{ny}}$	mean and cov of R_{ny}
$m_{\mu_{x, cap}}, v_{\mu_{x, cap}}$	mean and cov of $\mu_{x, cap}$
$m_{\mu_{y, cap}}, v_{\mu_{y, cap}}$	mean and cov of $\mu_{y, cap}$
$m_{\ln(\zeta_x)}, \sigma_{\ln(\zeta_x)}$	mean and standard deviation of $\ln(\zeta_x)$

$m_{\ln(\zeta_y)}, \sigma_{\ln(\zeta_y)}$	mean and standard deviation of $\ln(\zeta_y)$
$u_x, \dot{u}_x, \ddot{u}_x$	translational displacement, velocity, and acceleration along the X -axis, respectively
$u_y, \dot{u}_y, \ddot{u}_y$	translational displacement, velocity, and acceleration along the Y -axis, respectively
\ddot{u}_{gx}	horizontal component of ground motions applied along the X -axis
\ddot{u}_{gy}	horizontal component of ground motions applied along the Y -axis
z_x	hysteretic displacement along the X -axis
z_y	hysteretic displacement along the Y -axis
α	ratio of post-yield stiffness to initial stiffness
β, γ, n	Bouc-Wen model shape parameters
δ_η	parameter controls the stiffness degradation
δ_v	parameter controls the strength degradation
Δ	yield displacement for a rectilinear displacement passing through θ
Δ_x	yield displacements along the X -axis
Δ_y	yield displacements along the Y -axis
ζ_x	equal to ϕ_x
ζ_y	equal to ϕ_y
η, v	parameters related to the degradation in the Bouc-Wen model
θ	counterclockwise rotation in the $X-Y$ plane
Λ_x	effective modal mass along the X -axis
Λ_y	effective modal mass along the Y -axis
λ	coefficient for cyclic loading

$\mu_{b,max}$	inelastic seismic demand for the 2DOF system
μ_x	inelastic seismic demand along the X -axis
μ_y	inelastic seismic demand along the Y -axis
$\mu_{x,cap}$	ductility capacity of the structure along the X -axis
$\mu_{y,cap}$	ductility capacity of the structure along the Y -axis
ν_{sx}	coefficient of variation (cov) of $S_{Ax}(T_{nx}, \xi_x)$
ν_{sy}	coefficient of variation (cov) of $S_{Ax}(T_{ny}, \xi_y)$
ξ_x	damping ratio associated with the structural dynamic response along the X -axis
ξ_y	damping ratio associated with the structural dynamic response along the Y -axis
ω_{nx}	vibration frequency corresponding to the fundamental sway vibration mode along the X -axis (rad/s)
ω_{ny}	vibration frequency corresponding to the fundamental sway vibration mode along the Y -axis (rad/s)
ϕ_x	normalized yield strength along the X -axis
ϕ_y	normalized yield strength along the Y -axis
$\Phi^{-1}(\bullet)$	inverse standard normal distribution function

Chapter 1

1 Introduction

1.1 Introduction

Wood is a traditional construction material and commonly used for houses and low-rise buildings at present. The application of wood laminating technique has led to wood composites with improved engineering properties as compared to sawn timbers. Engineered wood composites such as structural composite lumber (SCL), laminated veneer lumber (LVL) and cross-laminated timber (CLT) could be used to construct tall wood buildings. The improved stiffness and stability of the manufactured CLT panels facilitates their use as floor and wall elements reducing construction time. However, the most commonly used mid-rise and tall building construction materials in Canada at present are the reinforced concrete and steel. The use of heavy timber products is uncommon because the height of the timber structures is typically limited to 4 storeys partly due to the fire safety consideration. Recently, changes are made to allow up to six storeys timber structures in British Columbia, Ontario and Quebec in Canada. Furthermore, several prototype designs of the mid- or high-rise buildings up to 20 storeys were considered (Pang et al. 2010; Gagnon et al. 2010; MGB 2012; NEWBuildS 2015) by mainly using mass timber structural members. Some of the designs followed the provisions in the National Building Code of Canada (NBCC) (NRCC 2010) and CAN/CSA O86-09 (CSA 2009). However, none of the prototype designs are constructed, although an 18 storeys (53 metres, about 174 feet) wood hybrid building was recently completed four months ahead of schedule in Vancouver, Canada (<https://news.ubc.ca/2016/09/15/structure-of-ubcs-tall-wood-building-now-complete/>). The structure was completed less than 70 days using the prefabricated components that are delivered to the construction site. The building is the first mass wood, steel and concrete hybrid building that is taller than 14 storeys in the world. The design consists of a concrete podium and two concrete cores, with 17 storeys of CLT floors supported on glue-laminated wood columns.

As the detailed design information of a prototype mid-rise or tall wood building is rare, it is not clear whether such a design is governed by serviceability or ultimate limit state

conditions under wind load or earthquake load even if the building is located at a seismic zone. In addition, the wood buildings subjected to seismic excitations can undergo nonlinear inelastic deformation mainly due to the behaviour of the fasteners among the wood panels or assemblies. Therefore, an adequate modeling of the connections (Christovasilis et al. 2009; Pei et al. 2013; Shen et al. 2013) is essential to predict the overall seismic response of mid- and high-rise wood buildings. The predicted linear and nonlinear seismic responses of the designed prototype mid- or high-rise buildings can provide the evidence of the feasibility of constructing taller wood buildings.

The studies on the nonlinear inelastic behaviour of timber or composite timber buildings are limited. This is partly due to that the wood could be idealized as linear-brittle material (Keenan 1986), and there are difficulties to accurately represent connections in timber buildings because of unavailability of experimental data for all possible combinations of connection configurations. It is noted that several experimental studies focused on the seismic behaviour of CLT were available in the literature. These include the pseudo-dynamic tests of a one-storey 3D specimen in three different layouts (Lauriola and Sandhaas 2006), shake table tests of a 10 m high, three-storey building (Ceccotti 2008), and a full-scale shaking table test of a seven-storey CLT building at the E-Defense facility in Miki, Japan (Ceccotti et al. 2013). Also, the nonlinear dynamic time-history analyses to assess the ductile behaviour of a wood building are reported and the implications of the results for design are discussed in Pang et al. (2010) and Pei et al. (2013). An investigation of the failure mechanisms of a two-storey CLT structure (Popovski and Gavric 2015) indicates that the sliding of connections between wood panels is the predominant mode of deformation, and the CLT panels respond mainly linear under the dynamic lateral loads.

It should be noted that, one of the issues that needs to be addressed for the use of heavy timber material in constructing mid-rise and tall buildings is related to their reliability under seismic loads. To our knowledge, such a reliability assessment of mid- or high-rise wood buildings is currently unavailable in the literature, although reliability estimates of wood shear walls, wood frame houses, and low-rise wood frame buildings are reported (Foliente et al. 2000; van de Lindt and Walz 2003; Lee and Rosowsky 2006; Pang et al. 2009). For assessing the probability of incipient yield and probability of incipient collapse of a

building, appropriate simplified model is often developed and; the probabilistic structural capacity analysis and the seismic hazard assessment are separated into two distinct tasks (Cornell et al. 2002; Hong et al. 2010), facilitating the reliability analysis. Note that both the incremental dynamic analysis and the nonlinear static pushover analysis are often employed to assess structural capacity under seismic load. The seismic hazard assessment for Canadian sites are reported in Adams and Halchuk (2003), Adams and Atkinson (2003), Hong et al. (2006) and Adams et al. (2015). It must be noted that the assessment of reliability of buildings is most frequently carried out for structures under unidirectional ground motions. Simple procedure to assess the structural reliability under bidirectional horizontal ground motions, even for bisymmetric building, is rarely discussed. Also, there is no consensus on how to define the capacity of a building under bidirectional ground motions.

As the experience with and the reliability of the mid-rise and tall wood buildings under seismic excitations are unavailable, an assessment of the linear and nonlinear inelastic responses of the mid-rise and high-rise building as well as the reliability of the buildings under uni- and bi-directional horizontal seismic excitations are valuable to the structural design code makers, the practicing engineers, and potentially to the emergency management under rare earthquakes.

1.2 Objectives and thesis outline

The overall objective of this study is to design mid- and high-rise wood buildings according to applicable Canadian design codes and standards and, to assess their reliability under unidirectional and bidirectional ground motions. To achieve this overall objective, several tasks are carried out and are described in Chapters 2 to 5. Each chapter with its own objectives are summarized below.

The main objectives of Chapter 2 are to design and model 10-, 15- and 20-storey wood buildings with CLT and glulam structural members, and to assess the nonlinear inelastic responses as well as the capacity curve of the designed wood buildings under unidirectional seismic excitations using the incremental dynamic analysis (IDA) and nonlinear static pushover analysis (NSPA). For the design, the CLT panels are used for walls and

floors, and the glulam structural members are used for the building frames. Nonlinear hysteretic models for different connections are assembled based on experimental results available in the literature, and finite element models of the designed buildings are developed. Capacity curves for the designed wood buildings by applying the IDA and NSPA are obtained and compared.

In Chapter 3, a reliability assessment is carried out for three mid- and high-rise wood buildings designed according to the requirements stipulated in the NBCC (NRCC 2010) and described in Chapter 2. For the assessment, the seismic response characteristics of the designed structures are used to develop equivalent single-degree-of-freedom (SDOF) systems with Bouc-Wen hysteretic model (Foliente 1995; Foliente et al. 2000; Ma et al. 2004). Nonlinear inelastic responses of the equivalent systems are evaluated using more than 500 ground motion records from the NGA database (<http://peer.berkeley.edu/nga/index.html>). Probabilistic ductility demand model for the equivalent SDOD systems are developed and used together with the probabilistic seismic characteristics at the site of interest to estimate probability of incipient yield and probability of incipient collapse.

The main objectives of Chapter 4 are to evaluate the responses of the designed mid- and high-rise wood buildings according to the NBCC (NRCC 2010) under bidirectional seismic excitations, to characterize the capacity surface under bidirectional seismic excitations, and to discuss the major differences between the capacity curve and capacity surface under seismic loading. The evaluation of the responses needed to define the capacity surface is carried out by using the IDA considering bidirectional orthogonal horizontal seismic ground motions. Also, the use of the nonlinear static pushover analysis (NSPA) is considered as a simple practical alternative. To account for the effect of the incidence angle of bidirectional excitations on the structural capacities, the analysis is carried out by rotating the axes of the bidirectional horizontal excitations relative to the structural axis. The obtained responses from IDA and NSPA for each incidence angle are used to form the capacity surface; the implication of the obtained capacity surface for the performance-based design procedures of the mid- and high-rise wood buildings is discussed.

The main objectives of Chapter 5 are to establish a simple procedure to estimate reliability of 3D bisymmetrical structures under bidirectional ground motion, to apply the procedure to estimate the reliability of wood buildings under bidirectional orthogonal ground motions, and to compare the estimated reliabilities by considering uni- and bi-directional ground motions. The procedure considers that the bisymmetric buildings can be approximated by a nonlinear inelastic two-degree-of-freedom system (2DOF). The equivalent systems are used to represent three designed tall wood buildings. Statistics of the ductility demand for the equivalent nonlinear inelastic 2DOF systems are assessed based on 381 selected ground motion records, and probability of incipient yield and probability of incipient collapse are estimated.

Finally, conclusions and observations from the results obtained in each of the previous chapters are presented. Also, potential future research topics of interests are given.

1.3 References

- Adams, J., and Atkinson, G. (2003). Development of seismic hazard maps for the proposed 2005 edition of the National Building Code of Canada. *Canadian Journal of Civil Engineering*, 30(2), 255-271.
- Adams, J., and Halchuk, S. (2003). Fourth generation seismic hazard maps of Canada: Values for over 650 Canadian localities intended for the 2005 National Building Code of Canada (p. 155). *Geological Survey of Canada*.
- Adams, J., Halchuk, S., Allen, T., and Rogers, G. C. (2015). Canada's 5th generation seismic hazard model, as prepared for the 2015 National Building Code of Canada. *In The 11th Canadian Conference on Earthquake Engineering*, Victoria, BC. Paper (No. 93775).
- CSA. (2009). Engineering Design in Wood Standard, CSA O86-09. *Canadian Standards Association*, Mississauga, Ontario, Canada.
- Ceccotti, A. (2008). New technologies for construction of medium-rise buildings in seismic regions: the XLAM case. *Structural Engineering International*, 18(2), 156-165.

- Ceccotti, A., Sandhaas, C., Okabe, M., Yasumura, M., Minowa, C., and Kawai, N. (2013). SOFIE project—3D shaking table test on a seven - storey full - scale cross - laminated timber building. *Earthquake Engineering and Structural Dynamics*, 42(13), 2003-2021.
- Christovasilis, I. P., Filiatrault, A., Constantinou, M. C., and Wanitkorkul, A. (2009). Incremental dynamic analysis of wood frame buildings. *Earthquake Engineering and Structural Dynamics*, 38(4), 477-496.
- Cornell, C. A., Jalayer, F., Hamburger, R. O., and Foutch, D. A. (2002). Probabilistic basis for 2000 SAC federal emergency management agency steel moment frame guidelines. *Journal of Structural Engineering*, 128(4), 526-533.
- Foliente, G. C. (1995). Hysteresis modeling of wood joints and structural systems. *Journal of Structural Engineering*, ASCE, 121(6), 1013-1022.
- Foliente, G. C., Paevere, P., Saito, T., and Kawai, N. (2000). Reliability assessment of timber shear walls under earthquake loads. In *Proc., 12th World Conf. Earthquake Engineering*.
- Gagnon, S., Munoz, W., Mohammad, M., and Below, K. D. (2010, July). Design guidelines for an 8-storey hybrid wood-concrete multi-family building. In *Structures and Architecture* (Proceedings of the First International Conference on Structures and Architecture, Guimaraes, Portugal, 21-23 July 2010), CRC Press, Leiden, The Netherlands (pp. 109-110).
- Hong, H. P., Goda, K., and Davenport, A. G. (2006). Seismic hazard analysis: a comparative study. *Canadian Journal of Civil Engineering*, 33(9), 1156-1171.
- Hong, H.P., Hong, P. and Wang, W. (2010) Reliability of steel frames designed in accordance with the NBCC seismic provisions and implication in codified design, *Engineering Structures*, Volume 32, Issue 5, May 2010, Pages 1284-1291
- Keenan F. J. (1986). Limit states design of wood structures. *Morrison Hershfield Ltd.*

- Lauriola, M.P. and Sandhaas, C., (2006). November. Quasi-static and pseudo-dynamic tests on XLAM walls and buildings. In *COST E29 International Workshop on Earthquake Engineering on Timber Structures*, Coimbra, Portugal.
- Lee, K. H., and Rosowsky, D. V. (2006). Fragility analysis of woodframe buildings considering combined snow and earthquake loading. *Structural Safety*, 28(3), 289-303.
- Ma, F., Zhang, H., Bockstedte, A., Foliente, G. C., and Paevere, P. (2004). Parameter analysis of the differential model of hysteresis. *Journal of Applied Mechanics*, 71(3): 342-349.
- MGB Architecture and Design. (2012). Tall Wood Report. *MGB Architecture and Design*.
- NEWBuilds. (2015). Application of Analysis Tools from NEWBuildS Research Network in Design of a High-Rise Wood Building, Network on Innovative Wood Products and Building Systems (NEWBuildS), *University of New Brunswick*, Fredericton, New Brunswick, Canada.
- NGA database. Next Generation Attenuation <http://peer.berkeley.edu/nga/index.html>. 325 *Davis Hall, University of California, Berkeley, CA 94720-1792*
- NRC Canada (2010). National Building Code of Canada, *NRC Canada*, Ottawa, Ontario, Canada.
- Pang, W., Rosowsky, D. V., Ellingwood, B. R., and Wang, Y. (2009). Seismic fragility analysis and retrofit of conventional residential wood-frame structures in the central United States. *Journal of structural engineering*, 135(3), 262-271.
- Pang, W., Rosowsky, D. V., Pei, S., and Van De Lindt, J. W. (2010). Simplified direct displacement design of six-storey woodframe building and pretest seismic performance assessment. *Journal of structural engineering*, 136(7), 813-825.
- Pei, S., Popovski, M., and van de Lindt, J. W. (2013). Analytical study on seismic force modification factors for cross-laminated timber buildings. *Canadian Journal of Civil Engineering*, 40(9), 887-896.

- Popovski, M., and Gavric, I. (2015). Performance of a 2-storey CLT House Subjected to Lateral Loads. *Journal of Structural Engineering*, E4015006.
- Shen, Y. L., Schneider, J., Tesfamariam, S., Stiemer, S. F., and Mu, Z. G. (2013). Hysteresis behaviour of bracket connection in cross-laminated-timber shear walls. *Construction and Building Materials*, 48, 980-991.
- van de Lindt, J. W., and Walz, M. A. (2003). Development and application of wood shear wall reliability model. *Journal of Structural Engineering*, 129(3), 405-413.

Chapter 2

2 Seismic Responses and Capacity Curves of Mid- and High-rise Wood Buildings under Uni-directional Seismic Excitations

2.1 Introduction

Wood is a construction material traditionally used for houses and low-rise buildings. The application of wood laminating techniques has led to wood composites with improved mechanical properties as compared to sawn timbers. Engineered wood composites such as structural composite lumber (SCL), laminated veneer lumber (LVL) and cross-laminated timber (CLT) could be used to construct tall wood buildings. The improved stiffness and stability of the manufactured CLT panels facilitates their use as floor and wall elements reducing construction time. However, the most commonly used materials for mid-rise and tall buildings in Canada at present are reinforced concrete and steel. The use of heavy timber products is uncommon because the height of the timber structures is typically limited to 4 storeys partly due to the fire safety consideration. Recently, changes have been made in to allow timber structures up to six storeys in British Columbia, Ontario and Quebec in Canada, showing that the wood material is gaining acceptance for taller buildings. Furthermore, several prototype designs of the mid- or high-rise buildings up to 20 storeys were considered (Pang et al. 2010; Gagnon et al. 2010; MGB 2012; NEWBuildS 2015) by mainly using mass timber structural members. Some of the designs followed the provisions in the National Building Code of Canada (NBCC) (NRCC 2010a) and CAN/CSA O86-09 (CSA 2009). However, none of the prototype designs have been constructed, although an 18-storey wood hybrid building (53 metres, about 174 feet) was recently completed four months ahead of schedule in Vancouver, Canada.

Wood buildings subjected to seismic excitations can undergo nonlinear inelastic deformation mainly due to the behaviour of the fasteners among the wood panels or assemblies. Therefore, adequate modeling of the connections (Christovasilis et al. 2009; Pei et al. 2013; Shen et al. 2013) is essential to predict the overall seismic response of the mid-rise and high-rise wood buildings. The predicted linear and nonlinear seismic

responses of the designed prototype mid- or high-rise buildings could provide the needed evidence of their feasibility, and so could encourage practicing engineers to use composite wood materials in mid- and high-rise buildings.

The studies on the nonlinear inelastic behaviour of wood or composite timber buildings are limited. This is partly due to that the wood could be idealized as linear-brittle material (Keenan 1986), and there are difficulties to accurately represent the response of connections in timber buildings because representative experimental data for possible connection configurations are unavailable. Several experimental studies focused on the seismic behaviour of CLT are available in the literature. These include the pseudo-dynamic tests of a one-storey 3D specimen with three different layouts (Lauriola and Sandhaas 2006), shake table tests of a 10 m high, three-storey building (Ceccotti 2008), and a full-scale shaking table test of a seven-storey CLT building at the E-Defense facility in Miki, Japan (Ceccotti et al. 2013). Also, nonlinear dynamic time-history analyses to assess the ductile behaviour of a wood building are reported and the associated implications for design are discussed in Pang et al. (2010) and Pei et al. (2013). In addition, Christovasilis et al. (2009) carried out incremental dynamic analyses for low-rise wood frame buildings under seismic excitations, where the connections are represented by nonlinear springs. Shen et al. (2013) investigated the hysteretic behaviour of bracket connection in cross-laminated-timber shear walls. Dickof et al. (2014) investigated the inelastic response of a CLT-steel hybrid system based on static pushover analysis. An investigation of the failure mechanisms of a two-storey CLT structure (Popovski and Gavric 2015) indicates that the sliding of connections between wood panels is the predominant mode of deformation, and the response of the CLT panels is essentially linear under the dynamic lateral loads. In general, all the mentioned studies suggest that the connections between timber structural members and assemblies under dynamic loads can undergo inelastic deformation and dissipate energy. However, the overall nonlinear responses and capacity curves of mid- or high-rise wood buildings have not been investigated.

The main objectives of this chapter are to design and model 10-, 15- and 20-storey wood buildings with CLT and glulam structural members, and to assess the nonlinear inelastic responses and the capacity curve of the designed wood buildings under uni-directional

seismic excitations using the incremental dynamic analysis (IDA) and nonlinear static pushover analysis (NSPA). For the design, the CLT panels are used for walls and floors, and the glulam structural members are used for the building frames. Nonlinear hysteretic models for different connections are created based on experimental results available in the literature, and finite element models of the designed buildings are developed. Capacity curves for the designed wood buildings determined by applying the IDA and NSPA are obtained and compared. The shape of the capacity curves and the implied post-yield stiffness are discussed. The impact of the record-to-record variability on the capacity curve is also investigated.

2.2 Design considerations for mid- and high-rise wood buildings

2.2.1 Basic considerations

Structural design takes into account the experience, commonly accepted practice, and engineering and architectural considerations. As the actual mid- and high-rise timber buildings are rare and only prototype designs are evaluated (MGB 2012), the design experience and recorded performance of such structures subjected to strong earthquakes are lacking. The design of the timber buildings in the presented chapter is carried out using the information in MGB (2012) and NEWBuildS (2015) as a guide. The lateral resistance of the designed system is mainly provided by the elevator shaft and shear walls, which are constructed using 2200 mm wide manufactured CLT panels.

The designed system must resist lateral loads caused by wind or earthquake, and vertical gravity loads. The thick CLT panels are used for slabs to provide rigid floor diaphragm action; they rest on single-span simply-supported glulam beams. The glulam frame members are selected according to CWC (2010) to form the gravity load resisting system (GLRS) to withstand the vertical loads. As the size of the available CLT panels is constrained by the fabrication and transportation processes, the elevator shaft and shear walls must be comprised of “standard” panels that are to be connected using appropriately designed mechanical fasteners. The same footprint (i.e., 24 m × 23.2 m) is considered for the design of the 10-, 15-, and 20-storey wood buildings but with different member

dimensions or shear wall layouts. The height of the first storey is 4.4 m and the other storeys is 3.2 m.

The wood buildings are assumed to be located at North Vancouver, BC, and could experience extreme earthquake, wind and rain loads specified in NBCC (2010a). According to the NBCC (2010a), the minimum specified loads are shown in Table 2.1 for a structure classified as having “normal” importance and at a site with class “D” classification. Also, the importance factors for wind, snow, and earthquake loads, denoted as I_W , I_S , and I_E , respectively, are equal to 1.0 if the ultimate limit state (ULS) is considered; I_W , I_S , and I_E equal 0.75, 0.9 and 1.0, respectively, if the serviceability limit state (SLS) is considered.

2.2.2 Design procedure and criteria

The design of the buildings is an iterative process. Basically, a preliminary design is carried out for the gravity loads (i.e., dead load and live load due to use and occupancy). Seismic design load is then calculated based on the estimated fundamental vibration period and the adequacy of the preliminary design is checked. If it is necessary, the lateral load resisting system consisting of the elevator shaft, shear walls and frame to resist the seismic design load is redesigned by considering ultimate limit state and serviceability requirements. A design checking is then carried out by considering the wind loads for both ultimate and serviceability requirements given in the NBCC (2010a); a redesign is carried out whenever it is necessary. Also, a design checking is carried out for ultimate and serviceability requirements under earthquake load by considering the fundamental vibration period (in sway mode for the considered orientation) that is obtained from a 3D finite element model of the designed structure. If all the design requirements are satisfied and without significant overdesign for earthquake and wind loads, the design is accepted.

It is observed that the designs of the considered 10-, and 15-storey buildings are governed by the drift requirement for earthquake load specified in the NBCC, while the design of 20-storey building is governed by the drift requirement for wind load specified in the NBCC. This is because that as the number of storeys increases the timber building becomes more flexible and prone to vibration. More specifically, for the preliminary

design of the lateral load resisting system (LLRS) of the buildings, the fundamental natural vibration period (for the sway mode in the direction of consideration) T_a (s) is estimated by using an empirical equation given in the NBCC (2010a) for shear wall structures,

$$T_a = 0.05(h_n)^{3/4} \quad (2.1)$$

where h_n (m) represents the total height of the building. The 10-, 15- and 20-storey have total heights of 33.2 m, 49.2 m, and 65.2 m, respectively, resulting in T_a of 0.69 s, 0.93 s, and 1.15 s. Although the estimated fundamental natural vibration periods are likely to differ from the actual designed and constructed buildings, they are used to determine the spectral acceleration at T_a , $S(T_a)$, to calculate the seismic force in the preliminary design. The seismic force is reduced by the overstrength factor R_o and the ductility related reduction factor R_d according to the NBCC seismic design procedure. As the values of R_o and R_d are not specified for wood buildings in the NBCC, $R_d = 2.0$ and $R_o = 1.5$ are assumed based on the results given in FPInnovation (2011) and Pei et al. (2012). The implication of using these values will be discussed shortly.

Using the estimated $S(T_a)$, the design base shear V_d is calculated using,

$$V_d = S(T_a)M_v I_E W / (R_d R_o) \quad (2.2)$$

where $S(T_a)$ is in fraction of gravitational acceleration; M_v is a factor to account for the effect of higher modes on base shear that is taken equal to 1.0 for the considered buildings with “coupled walls” in this study; I_E is the earthquake importance factor, taken as 1.0; and W (N) represents the total building dead load plus 25% of the snow load. The elastic seismic design spectral acceleration $S(T)$ for a structure located in North Vancouver, BC with the fundamental vibration period T (s) can be linearly interpolated based on the values shown in Table 2.1,

$$S(T) = \begin{cases} F_a S_a(0.2) & T \leq 0.2 \text{ s} \\ \min\{F_a S_a(0.2), F_v S_a(0.5)\} & T = 0.5 \text{ s} \\ F_v S_a(1.0) & T = 1.0 \text{ s} \\ F_v S_a(2.0) & T = 2.0 \text{ s} \\ F_v S_a(2.0) / 2 & T \geq 4.0 \text{ s} \end{cases} \quad (2.3)$$

where the values of $S_a(T)$ are given in the NBCC (2010) for a damping ratio of 5% (see Table 2.1); and F_a and F_v are acceleration-based and velocity-based site coefficients,

respectively. For the site class “D”, F_a and F_v are taken equal to 1.1 and 1.16, respectively.

Table 2.1. Design data of a residential building located at a site classified as “D” in North Vancouver.

Parameter		Minimum specified load
D (Dead load) (kPa) ⁽¹⁾	Floor	2.80
	Partitions	0.50
	Roof	3.00
L (Live load)	Floor	1.90
	Roof	1.00
W (Wind load) (kPa)	Based on 50-year return period value for the ULS	0.45
	Based on 10-year return period value for assessing wind induced acceleration	0.35
S (Snow load) (kPa) ⁽²⁾	S_S (Snow)	3.00
	S_r (Rain)	0.30
E (Earthquake load, PSA) (g) ⁽³⁾	$S_a(0.2)$	0.88
	$S_a(0.5)$	0.61
	$S_a(1.0)$	0.33
	$S_a(2.0)$	0.17
	PGA	0.44

Notes: 1) The floor dead load shown in the table is not specified in the code but calculated using the area mass of CLT floors equal to 150 kg/m^2 (FPInnovations 2011) and a 65 mm thick concrete topping with normal density 2400 kg/m^3 . The thickness of 65 mm is suggested by O’Neill (2013) to provide acoustic and fire separation;

2) The snow load S is based on 50-year return period values and calculated by $S = I_S[S_S(C_b C_w C_S C_a) + S_r]$, where S_S is the 50-year return period value of the ground snow load in kPa and S_r is the 50-year return period value of the rain load in kPa; parameters C_b , C_w , C_S , C_a are all equals to 1.0 in this case;

3) The earthquake load E is defined based on PSA for a damping ratio of 5%, $S_a(T)$, and for $T = 0.2 \text{ s}$, 0.5 s , 1.0 s , and 2.0 s . The values represent the 2475-year return period value (i.e., 2% probability of exceedance in 50 years) of the PSA.

For timber structures, a damping ratio of 1% for light frame wood structures is considered by Ellingwood et al. (2008), Folz and Filiatrault (2004a, 2004b) and Chen et al. (2013); a damping ratio of 2% for wood structures is considered by Filiatrault and Folz (2002) and Filiatrault et al. (2003); and an average damping ratio of 12% and 10% for the CLT wall panels are considered by FPInnovations (2011) and Gavric et al. (2015a, 2015b),

respectively. Based on these studies, and considering that there are no full-scale test results for the type of timber structures considered in this study, a damping ratio of 5% is assumed for design and analysis. The implication of this assumption is to be discussed in the following sections.

The NBCC (2010a) also stipulates that V_d shall not be less than $S(4.0)M_v I_E W / (R_d R_o)$ for wall-frame systems and not be greater than $(2/3) \times S(0.2) I_E W / (R_d R_o)$ for building located on sites other than Class “F” and having an LLRS with a R_d equal to or greater than 1.5. V_d is distributed along the height of the building according to,

$$F_x = (V_d - F_t) W_x h_x / \left(\sum_{i=1}^n W_i h_i \right) \quad (2.4)$$

where F_x (N) is the horizontal load applied at the height h_x (m) above ground; W_x (N) is the weight at the height h_x , W_i (N) is the weight at the i -th floor level; h_i is the height of the i -th floor; and F_t (N) is a portion of the shear force assumed to be concentrated at the top of the building. The value of F_t is taken equal to $0.07T_d V_d$, but need not exceed $0.25V_d$ and is taken as zero for the vibration period less than 0.7 (s). The overturning moment M_x at elevation x is determined using.

$$M_x = J_x \sum_{i=x}^n F_i (h_i - h_x) \quad (2.5)$$

where $J_x = 1.0$ for $h_x \geq 0.6h_n$, or $J_x = J + (1 - J)(h_x / 0.6h_n)$ for $h_x < 0.6h_n$ in which J is a reduction coefficient for the overturning moment specified in NBCC (2010). The value of J is calculated by linear interpolation based on $J = 1.0, 0.9$, and 0.8 for $T \leq 0.5$ s, $T = 2.0$ s and $T \geq 4.0$ s, respectively.

In addition, according to NBCC, the lateral deflection of each storey derived by response spectrum analysis shall be multiplied by $R_d R_o / I_E$ to give realistic values of anticipated deflections, and the inter-storey drift shall be less than $2.5\% h_i$ to satisfy the serviceability requirement of the structure.

The selected thickness of the CLT wall panels for the shear walls or elevator shaft depends on available thicknesses manufactured (Structurlam 2011). The CLT Handbook (FPInnovations 2011) recommends the use of the method given in CSA O86-09 (2009) to

calculate the resistance of wood members subjected to bending and axial load. According to this method, only the CLT layers oriented parallel to the axial force carry the load. The specified design criteria are;

$$\frac{P_f}{P_r} + \frac{M_f}{M_r} \leq 1.0 \quad (2.6)$$

and

$$\frac{T_f}{T_r} + \frac{M_f}{M_r} \leq 1.0 \quad (2.7)$$

where P_f (N) is the factored compressive axial load; M_f (N) is the factored bending moment due to lateral load; T_f (N) is the factored tensile axial load; and P_r , M_r , and T_r are the factored compressive load resistance parallel to grain, factored bending moment resistance, and factored tensile load resistance parallel to grain, respectively.

For the capacities of the CLT wall panel, P_r , M_r , and T_r are determined using the following equations (FPInnovations 2011):

$$P_r = \phi_1 F_c A_{eff} \quad (2.8)$$

$$M_r = \phi_2 F_b \frac{I_{eff}}{(\gamma_1 a_1 + 0.5 h_1)} \quad (2.9)$$

and,

$$T_r = \phi_3 F_{tp} A_{eff} \quad (2.10)$$

where $\phi_1 = 0.8$ and $\phi_2 = \phi_3 = 0.9$; F_c , F_b and F_{tp} are the compressive strength parallel to the grain, factored bending strength and factored tensile strength parallel to the grain determined according to CSA O86-09 (2009). The effective bending area (i.e., of the layers oriented parallel to the axial load) A_{eff} is calculated by,

$$A_{eff} = b \cdot h_{eff} \quad (2.11)$$

where b (mm) is taken as 1000 mm (FPInnovations 2011), and h_{eff} (mm) is the summation of thickness of panels parallel to the axial load; I_{eff} (mm⁶) is the effective moment of inertia, which is a function of the thickness of panels oriented parallel to the axial load; γ_1 is the connection efficiency factor, taken as 0.9; a_1 is the distance between the centroid of the first lamina and the centroid of the panel cross-section, and h_1 is the thickness of the first

(outermost) lamina. Note that the values of F_c , F_b and F_{tp} are material related factors. All longitudinal laminae are assumed to be spruce-pine-fir (S-P-F) No.1/No.2.

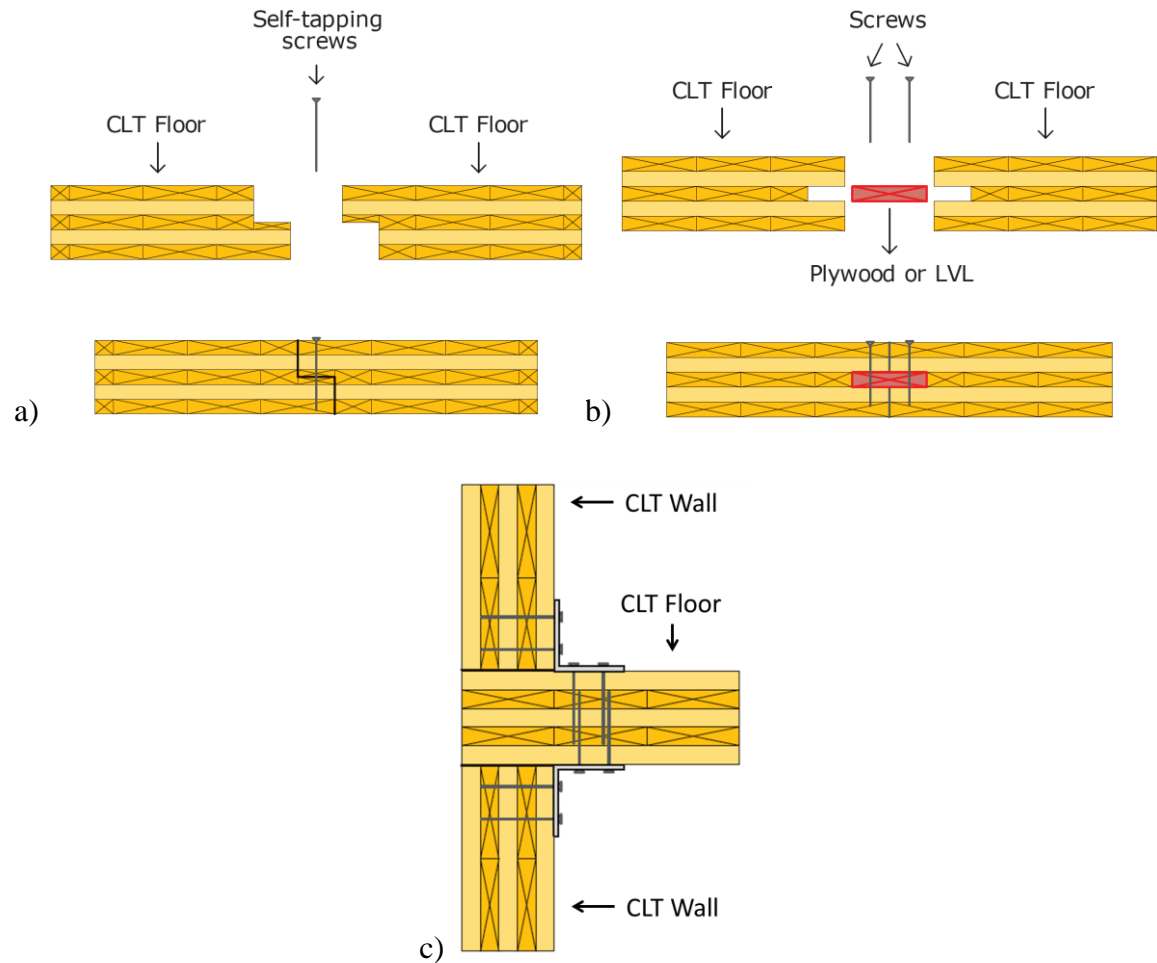


Figure 2.1. Illustration of screw-type connections for adjacent shear wall panels and the wall-to-floor brackets (FPInnovations, 2011): a) half-tapped joint; b) spline joint; c) Brackets installed at upper or lower side of the floor.

Two screw-type connections are often used to connect parallel CLT panels as shown in Figures 2.1a and 2.1b (FPInnovations 2011). Figure 2.1a shows a half-lapped joint with 50 mm overlapping length of adjacent panels, and the long self-tapping screws that are installed perpendicular to the plane. Figure 2.1b shows a spline joint with 28 mm thick and 180 mm wide LVL strip embedded in the notched edge and fastened to the panels with a double row of self-tapping screws. Metal brackets and hold-downs fastened by screws, nails or bolts are used to connect the wall panels to horizontal members as shown

in Figure 2.1c. Test results of the performance of the mentioned connectors can be found in the literature, including those in Gavric et al. (2015a, 2015b).

Since the response of wood is essentially linear elastic brittle, with negligible plastic deformation, lateral wall deformations are primarily due to extension of connections when the wall panel rotates about its corner as shown in Figure 2.2.a. Based on the kinematics model proposed in Pei et al. (2013), the reaction at each connector is a function of its location and the panel geometry, and the force equilibrium condition in the horizontal direction leads to:

$$F(D) = \sum_{i=1}^n \frac{l_i f_i}{H} \times \frac{l_i D}{H} + 2mV_k \times \frac{D}{H} + \frac{LG}{2H} \quad (2.12)$$

where $F(D)$ (N) is the applied lateral force on the wall as function of D ; L (m) is length of the wall panel; H (m) is the width of the wall panel; G (N) is total gravity load acting along the middle of the panel; D (m) is the lateral displacement at the top of the wall determined based on a drift ratio of 2.5%; n is total number of connectors between the wall and the floor diaphragm; f_i (N) is the reaction force of the i -th wall-to-floor connector; l_i (m) is the distance from the i -th wall-to-floor connector to the compression corner of the panel; m is the total number of connectors between the wall panels; and V_k (N) is shear reaction of the k -th connector between wall panels assumed to act on both sides of the panel along the edge. By using this equation, the demand on each individual connector can be estimated once the panel configuration (connection layout, number of connectors and panel geometry), the design lateral load and the maximum drift of the considered CLT wall panel are known. An illustration of the panel to panel and panel to floor connection systems is illustrated in Figure 2.2b.

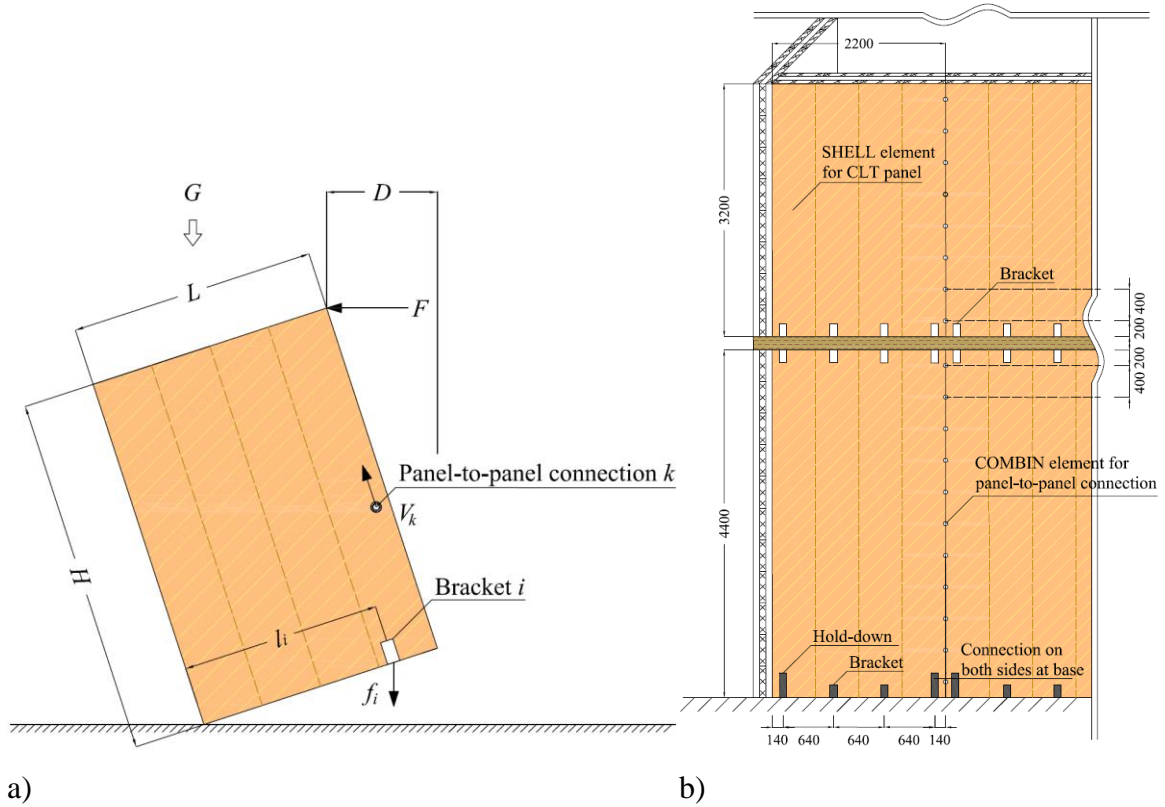


Figure 2.2. Illustrations of connections: a) simplified kinematics model of CLT wall panel subjected to horizontal load; b) illustration of connection system (dimension in mm).

Finally, the floor and roof panels are selected based on the design guideline suggested in Structurlam (2011). The factored load effects on beams and girders are calculated based on their respective tributary areas; the structural member sizes are selected based on the analysis recommended in CWC (2010) and the deflection requirements (i.e., less than span/360). In addition, the loss of serviceability due to walking-induced vibration needs to be considered. According to Hu et al. (2001), a designed floor system is adequate if the following condition is satisfied:

$$f_1 / d_1^{0.44} > 18.7 \quad (2.13)$$

where f_1 (Hz) is the fundamental vibration frequency of the floor system; and d_1 (mm) is the deflection of the floor under a concentrate point load of 1 kN at the centre.

Since the serviceability requirements for the wind load control the design of the 20-storey

building, these requirements are presented for completeness. According to the NBCC (2010a), the specified external pressure acting on a surface of the structure that is perpendicular to the wind, p (kPa), can be calculated using,

$$p = I_w q C_e C_g C_p \quad (2.14)$$

where q (kPa) is the reference wind velocity pressure; C_e is the exposure factor; C_g is the gust effect factor; C_p is the external pressure coefficient, which is 0.8 or -0.5 for windward and leeward side, respectively. For North Vancouver, q equals 0.45 kPa (i.e., the hourly-mean wind speed of 97.58 km/hr). There are two analysis procedures for wind loads: the static procedure and dynamic procedure; C_e and C_g for static procedure differ from those for the dynamic procedure. If the lowest natural frequency of the structure, f_n , calculated by using the static procedure (NRCC 2010b) and

$$f_n = \frac{1}{2\pi} \sqrt{\frac{\sum_{i=1}^N F_i X_i}{\sum_{i=1}^N W_i X_i^2}} \quad (2.15)$$

is within the range of 0.25 Hz to 1.0 Hz, the dynamic procedure must be used to calculate the structural response. In Eq. (2.15), i is the storey number and N is the total number of storeys; F_i (N) is the static wind force applied to the i -th storey calculated by multiplying the exposure area of each storey to the static wind pressure computed using Eq. (2.14); X_i (mm) is the horizontal drift of the i -th storey caused by F_i computed using numerical model described shortly in Section 2.3.2; W_i (N) is the associated weight of the i -th storey. Also, the dynamic procedure must be used if the building height is greater than 4 times of its minimum effective width, or greater than 60 m, the NBCC (2010a).

The inter-storey drift ratio of the designed wood building under wind load is limited to 1/500. The mean of the peak along-wind acceleration, a_D (m/s²) and the mean of the peak across-wind acceleration a_W (m/s²) caused by the dynamic wind loading must be less than 1.5% of the gravitational acceleration to satisfy the building vibration requirement (NRCC 2010b). According to (NRCC 2010b), a_D and a_W can be calculated using,

$$a_D = 4\pi^2 f_{nD}^2 g_p \sqrt{\frac{KsF}{C_{eH}\beta_D}} \cdot \frac{\Delta}{C_g} \quad (2.16)$$

and,

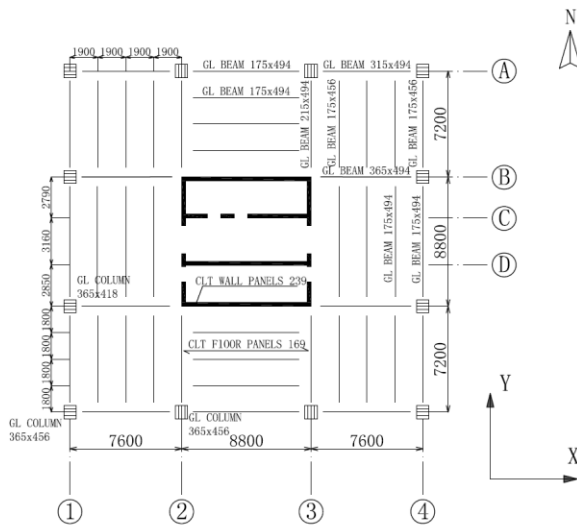
$$a_w = f_{nw}^2 g_p \sqrt{wd_a} \cdot \frac{a_r}{\rho_B g \sqrt{\beta_w}} \quad (2.17)$$

where f_{nD} and f_{nW} are the natural vibration frequencies (Hz) in the along- and across-wind directions, respectively; g_p is the peak factor; K is a factor related to the surface roughness of the terrain, and equals 0.10 for Exposure B; s is the size reduction factor; F is gust energy ratio evaluated at the natural frequency of the structure; C_{eH} is exposure factor at the top of the building; β_D and β_W are fractions of critical damping in the along- and across-wind directions, respectively, and are taken as 0.015 (NEWBuildS 2015); Δ is the maximum wind-induced lateral deflection at the top of the building (m); w and d_a are the across-wind effective width and along-wind effective depth (m), respectively; and a_r is equal to $0.0785(V_H / f_{nW} \sqrt{wd_a})^{3.3}$ in N/m^3 , in which V_H (m/s) is mean wind speed at the top of structure (based on the 10-year return period value); and ρ_B (kg/m^3) is the density of the building.

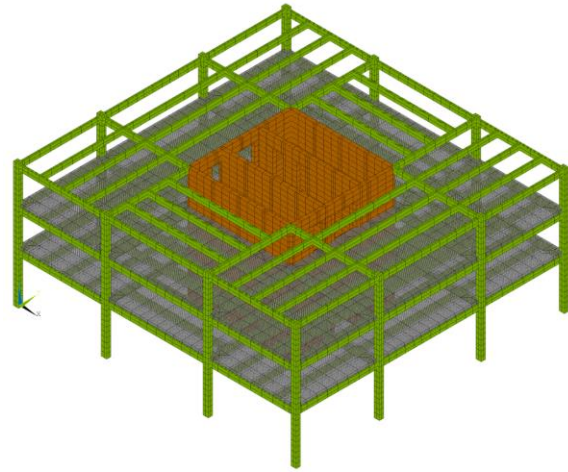
2.3 Finite element modelling of designed buildings

2.3.1 Designed buildings

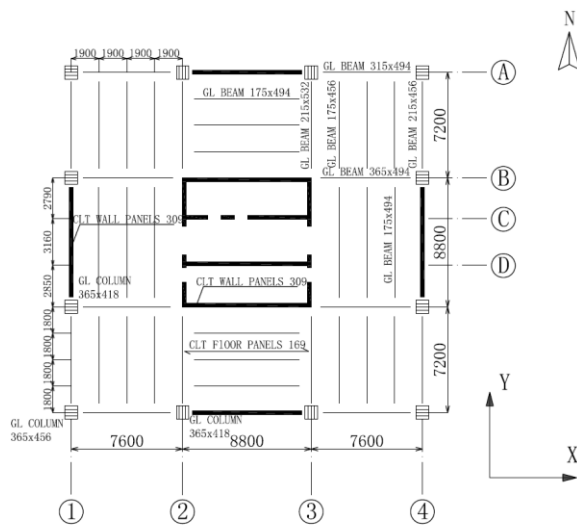
Following the procedures and requirements given in the previous section, the designed 10-, 15- and 20-storey wood buildings are shown in Figure 2.3, illustrating the dimensions of the structural members (i.e., beams, columns and walls). The (unfactored) associated specified lateral loads for earthquake and wind are shown in Tables 2.2a and Table 2.2b, respectively. The earthquake loads in the two directions differ because the natural (sway) vibration periods for the two orthogonal structural directions are different. The lowest frequencies f_n calculated using Eq. (2.15) for the 10-, 15- and 20-storey buildings are 0.67 Hz, 0.59 Hz, and 0.48 Hz, respectively. The pressure shown in Eq. (2.14) is calculated according to the code requirements for the case when the dynamic procedure is used to calculate the responses. The calculated wind loads in the E-W and N-S directions also differ because the exposure areas are different. As the earthquake load factor is 1.0 and the wind load factor is 1.4, the calculated design base shear due to earthquake load is greater than that due to wind load. This implies that for the ultimate limit states, the design is governed by the earthquake load.



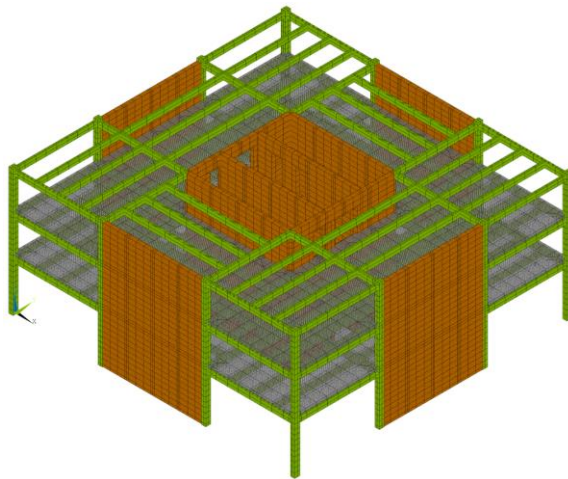
10 STOREY DESIGN FLOOR PLAN



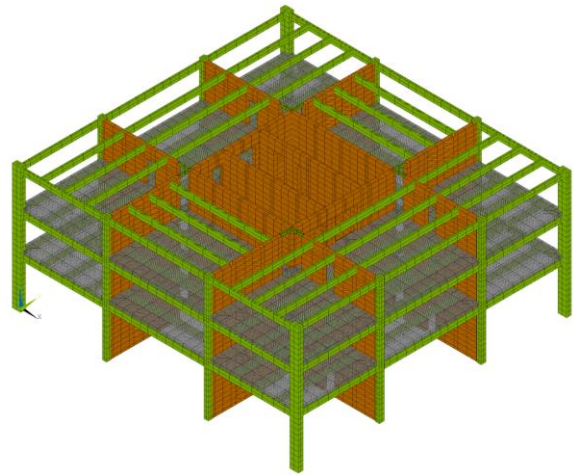
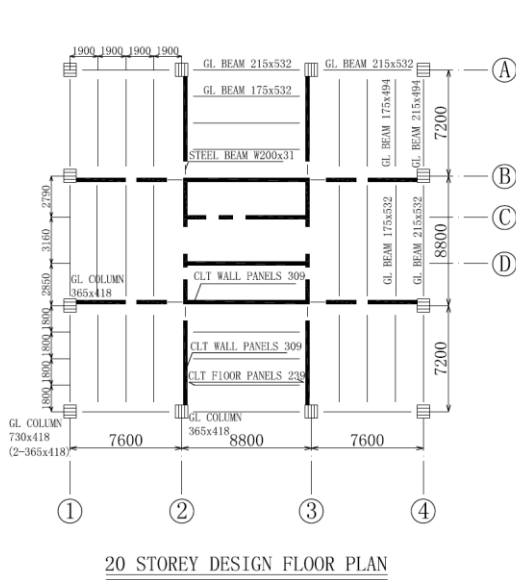
a)



15 STOREY DESIGN FLOOR PLAN



b)



c)

Figure 2.3. Three-dimensional model of the designed wood buildings: a) 10-storey wood building; b) 15-storey wood building; c) 20-storey wood building.

Table 2.2a. Distribution of lateral load from earthquake effect.

Storey	Height (m)	10-Storey		15-Storey		20-Storey	
		Design load (kN)		Design load (kN)		Design load (kN)	
		Earthquake		Earthquake		Earthquake	
		E-W	N-S	E-W	N-S	E-W	N-S
1	4.4	36	28	19	24	17	15
2	3.2	62	49	33	42	29	27
3	3.2	88	69	47	60	41	38
4	3.2	114	90	61	77	53	49
5	3.2	140	111	75	95	66	60
6	3.2	166	131	89	113	78	71
7	3.2	192	152	103	130	90	82
8	3.2	217	172	117	148	102	94
9	3.2	243	193	131	166	114	105
10	3.2	459	399	145	183	127	116
11	3.2			159	201	139	127
12	3.2			173	219	151	138
13	3.2			187	236	163	150
14	3.2			201	254	175	161
15	3.2			464	532	188	172
16	3.2					200	183
17	3.2					212	194
18	3.2					224	205
19	3.2					237	217
20	3.2					604	584
sum	65.2	1715	1394	2005	2481	3010	2788

Table 2.3b. Distribution of lateral load from wind effect.

Storey	Height (m)	10-Storey		15-Storey		20-Storey	
		Design load (kN)		Design load (kN)		Design load (kN)	
		Wind		Wind		Wind	
		E-W	N-S	E-W	N-S	E-W	N-S
1	4.4	74	77	73	76	70	72
2	3.2	54	56	53	55	51	53
3	3.2	54	56	54	56	51	53
4	3.2	56	58	56	58	53	55
5	3.2	60	62	59	61	57	59
6	3.2	63	65	63	65	60	62
7	3.2	66	68	66	68	63	65
8	3.2	69	71	70	72	66	68
9	3.2	71	73	71	73	69	71
10	3.2	73	76	74	77	73	76
11	3.2			75	78	77	80
12	3.2			77	80	81	84
13	3.2			78	81	83	86
14	3.2			80	83	87	90
15	3.2			82	85	90	93
16	3.2					93	96
17	3.2					95	98
18	3.2					96	99
19	3.2					98	101
20	3.2					100	103
sum	65.2	640	662	1032	1068	1512	1564

The connection systems shown in Figure 2.4 are designed to facilitate fast erection of the buildings. The floor panels rest directly on the wall panels and the frame to form a platform for subsequent floors. CLT panels, with widths up to 2200 mm and lengths up to 4400 mm, are used for the shear walls. Screw-type connections illustrated in Figure 2.1a and Figure 2.1b are used to connect parallel wall panels. Steel brackets are installed at the upper and lower sides of the floor as illustrated in Figure 2.1c to connect the wall and floor panels. Steel hold-downs connect the concrete base to the inner and outer sides of the shear walls. Connection details, including the number of connectors and their spacing, are listed in Tables 2.3a, 2.3b, and 2.3c, for 10-, 15-, and 20-storey buildings, respectively. The connection layouts for the three buildings differ because their shear walls are laid out differently, as shown in Figure 2.3.

Based on the availability of manufactured CLT products, and considering the design guideline suggested in Structurlam (2011) for the floor and roof systems, the use of the SLT 5 (169 mm) and SLT 9 (309 mm) CLT panels is adequate for the floor and roof, respectively. The serviceability vibration criterion, shown in Eq. (2.13), is satisfied. The fundamental frequencies of the floor systems, consisting of CLT floor panels and supporting frames, are 7.8 Hz, 8.8 Hz, and 8.9 Hz for 10-, 15-, and 20-storey designs, respectively.

Table 2.4a. Connections used in the 10-storey wood building and the number of fasteners and their spacing.

Connection type	Connection description
Wall anchoring (first storey)	E-W: 60 WHT 540 hold-downs with twelve 4 × 60 mm annular ring nails N-S: 30 WHT 540 hold-downs with fourteen 4 × 60 mm annular ring nails
Wall anchoring (upper storeys)	E-W: 64 BMF 100 × 100 × 90 × 3 mm brackets with twelve 3.9 × 89 mm spiral nails and two HBS 4 × 60 mm screws N-S: 62 BMF 90 × 116 × 48 × 3 mm brackets with eleven 4 × 60 mm annular ring nails with one Φ 12 bolts
Parallel panel to panel	E-W: Half-lapped joint with 2 × HBS Φ 8×80 mm screws spaced at 160 mm N-S: Half-lapped joint with 4 × HBS Φ 8×80 mm screws spaced at 120 mm

Table 2.5b. Connections used in the 15-storey wood building and the number of fasteners and their spacing.

Connection type	Connection description
Wall anchoring (first storey)	E-W: 92 WHT 540 hold-downs with six 4 × 60 mm annular ring nails N-S: 63 WHT 540 hold-downs with eight 4 × 60 mm annular ring nails
Wall anchoring (upper storeys)	E-W: 128 BMF 100 × 100 × 90 × 3 mm brackets with ten 3.9 × 89 mm spiral nails and two HBS 4 × 60 mm screws N-S: 126 BMF 100 × 100 × 90 × 3 mm brackets with ten 3.9 × 89 mm spiral nails and two HBS 4 × 60 mm screws
Parallel panel to panel	E-W: Spline joint with 2 × HBS Φ 8×80 mm screws spaced at 120 mm N-S: Spline joint with 4 × HBS Φ 8×80 mm screws spaced at 180 mm

Table 2.6c. Connections used in the 20-storey wood building and the number of fasteners and their spacing.

Connection type	Connection description
Wall anchoring (first storey)	E-W: 88 WHT 540 hold-downs with nine 4 × 60 mm annular ring nails N-S: 62 WHT 540 hold-downs with twelve 4 × 60 mm annular ring nails
Wall anchoring (upper storeys)	E-W: 120 BMF 90 × 116 × 48 × 3 mm brackets with eleven 4 × 60 mm annular ring nails with one Φ 12 bolts N-S: 124 BMF 90 × 116 × 48 × 3 mm brackets with fifteen 4 × 60 mm annular ring nails with two Φ 12 bolts
Parallel panel to panel	E-W: Half-lapped joint with 4 × HBS Φ 8×80 mm screws spaced at 160 mm N-S: Half-lapped joint with 4 × HBS Φ 8×80 mm screws spaced at 120 mm

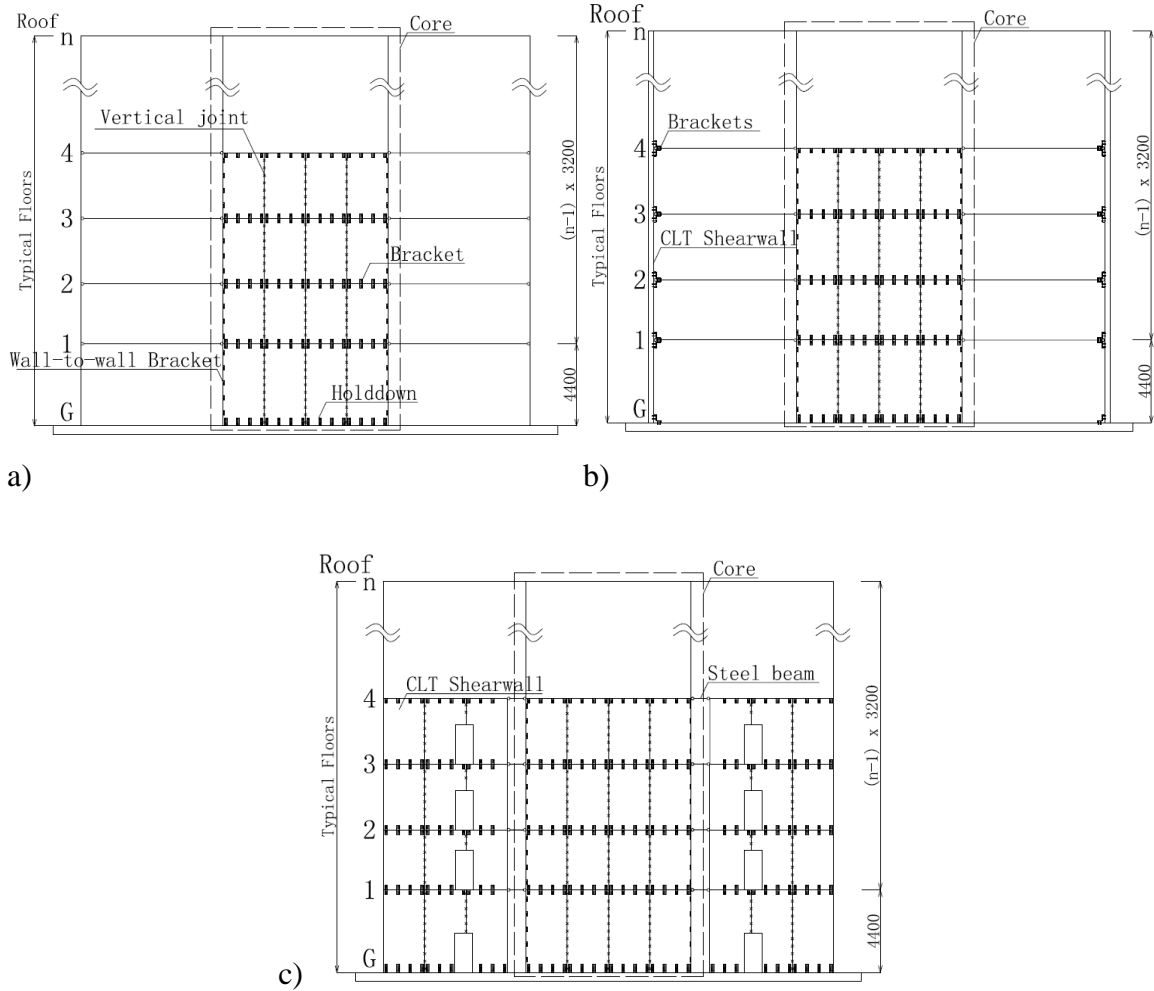


Figure 2.4. Designed connection system for the wood buildings: a) 10-storey; b) 15-storey; c) 20-storey.

2.3.2 Finite element modelling

Finite element models are developed using ANSYS Multiphysics 14.5 (2012). The CLT panels are modeled using a homogenized orthotropic shell element in ANSYS with the material properties shown in Table 2.4 (Gsell et al. 2007) for the orientation of the CLT panel illustrated in Figure 2.5a. In Table 2.4, E_x , E_y and E_z represent the Young's moduli, ν_{yx} , ν_{zx} and ν_{zy} are the Poisson's ratios, and G_{yz} , G_{zx} and G_{xy} are the shear moduli. The density of the CLT panel is as recommended in the CLT Handbook (FPInnovation 2011). Material properties for the glulam used for beams and columns are also shown in Table 2.4 (Zagari et al. 2009) for the orientation of the glulam illustrated in Figure 2.5b. Here, E_x

represents the elastic modulus along x -axis, and G_{xy} and G_{xz} denote the shear moduli in the xy and xz planes, respectively. The density shown is from CWC (2010).

Since research results (Fragiocomo et al. 2011; Gavric et al. 2015a, 2015b; Popovski and Gavric 2015) indicate that failure of massive timber panel building system usually occurs at connections, the composite timber materials are modelled as orthotropic linear elastic material.

Table 2.7. Material properties of CLT and glulam.

Parameter	CLT	Glulam
E_x (MPa)	8210	12000
E_y (MPa)	4630	-
E_z (MPa)	490	-
ν_{yx}	0.05	-
ν_{zx}	0.02	-
ν_{zy}	0.04	-
G_{yz} (MPa)	540	-
G_{zx} (MPa)	100	700
G_{xy} (MPa)	750	700
Density ($\times 10^3$ kg/m ³)	0.5	0.49

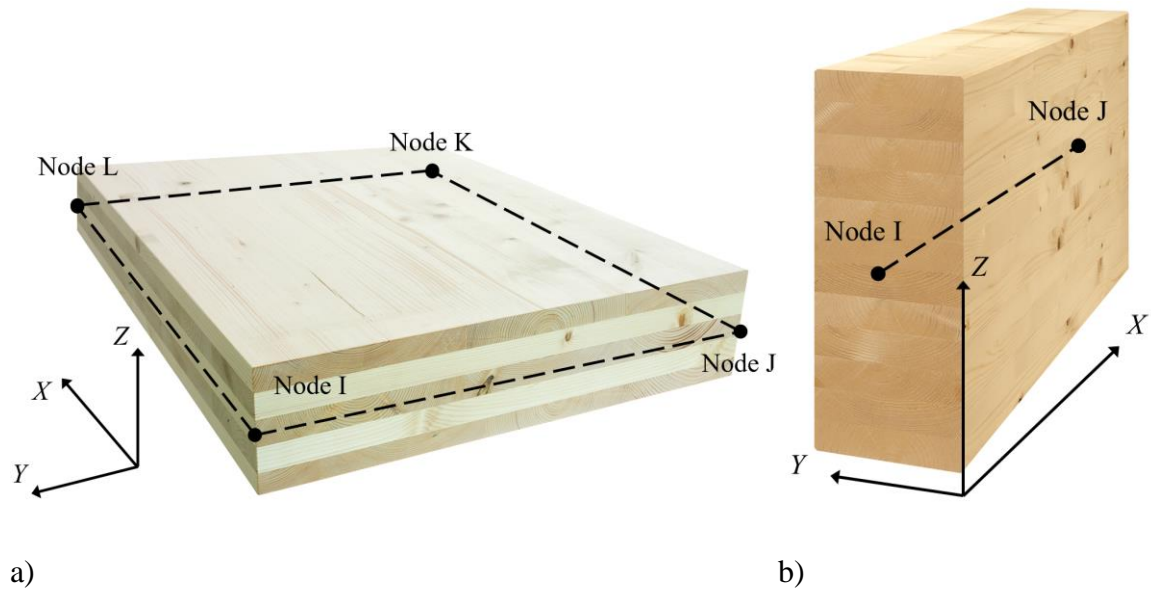


Figure 2.5. Illustration of the orientation for defining the material properties: a) CLT panel; b) glulam member.

The 4-node SHELL181 element is employed at the boundaries of the floor panel while the 8-node SHELL281 element is used for locations away from the boundaries of the floor panel so to reduce the total number of elements required, as shown in Figure 2.6. The floor panels are modelled as a rigid floor diaphragms, assuming their connections to the supporting horizontal frames are rigid (i.e., floor panels and supporting beam members are acting as a composite system). An equivalent density that accounts for the 65 mm normal weight concrete topping is considered, yielding densities of $1.0 \times 10^3 \text{ kg/m}^3$ or $0.83 \times 10^3 \text{ kg/m}^3$ for the floors with SLT 5 (169 mm) or SLT 9 (309 mm) CLT panels, respectively.

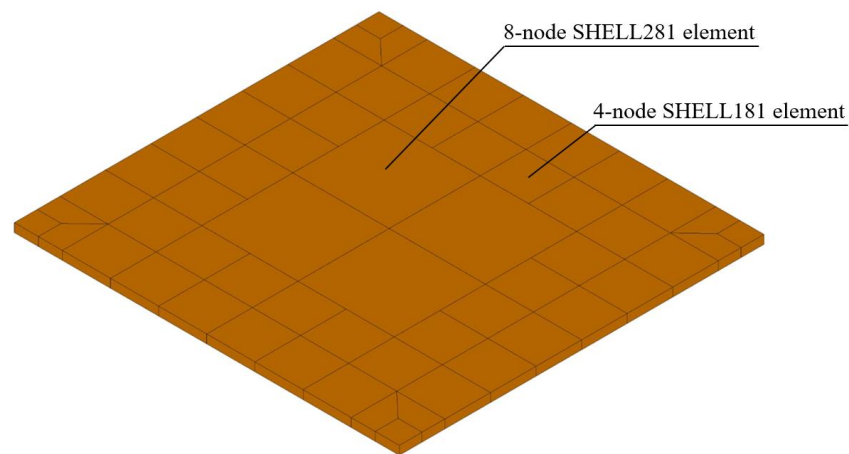


Figure 2.6. Illustration of the modelling of floor panels.

Each wall panel, represented by meshed shell elements, is connected to adjacent panel by connection elements. To simplify finite element model, equivalent connection elements are uniformly spaced at 400 mm whereas the actual spacing of fasteners for the designed buildings is already shown in Tables 2.3. The mechanical properties of an equivalent connection element between two wall panels are considered to be equal to the mechanical properties of a fastener times the ratio of the total number of actual fastener to the total number of connection elements spaced at 400 mm that is required. The steel brackets and hold-downs used to connect the vertical CLT panels to the floor are also modelled by the connection elements. More details on the modelling of the connection elements will be presented shortly.

The gravity load resisting system (GLRS) is designed using glulam beams and columns,

which are modeled using 2-node beam elements. To model the connections shown in Table 2.3, it is recognized that these connections can undergo inelastic deformation (Blasetti et al. 2008; Fragiocomo et al. 2011; Gavric et al. 2015a, 2015b; Popovski and Gavric 2015). The following assumptions were therefore made to model the response of the connection:

- 1) The inelastic behaviour is considered only in shear directions;
- 2) The withdrawal behaviour is assumed to be linear-brittle;
- 3) The axial behaviour to transfer compressive loads is to be rigid.

Following Blasetti et al. (2008), the inelastic dynamic behaviour in each direction of a fastener is modelled using two COMBIN40 elements: one to model the backbone envelope and the other for the loading and unloading paths. The slippage between the joint and wood members due to cyclic loading is idealized using the friction slider already included in the COMBIN40 element. The two elements are acting in parallel and the yield capacity of fastener is represented by the sum of the sliding capacity of both elements. Figure 2.7a illustrates the hysteretic loop of this model. However, values of the model parameters that pertain to connections for the CLT panels under lateral load are not provided in Blasetti et al. (2008).

To determine the model parameters of these connections identified in Figure 2.7a, test results of representative connectors given in Gavric et al. (2015a, 2015b) were considered. Finite element models of the test specimen, including the CLT panels and steel bracket or hold-down, are developed in the present study. First, a set of reasonable values of the parameters of the connection model (see Figure 2.7a) was assigned. A numerical analysis was then carried out following the actual test protocol. The time-history responses of the CLT panel from the numerical model were compared to the test results, and values of the model parameters were modified by trials and error until the maximum relative difference between the predicted and observed displacements is less than 2%. The estimated values of the model parameters are shown in Table 2.5, and the developed model is illustrated in Figure 2.7b, showing its adequacy.

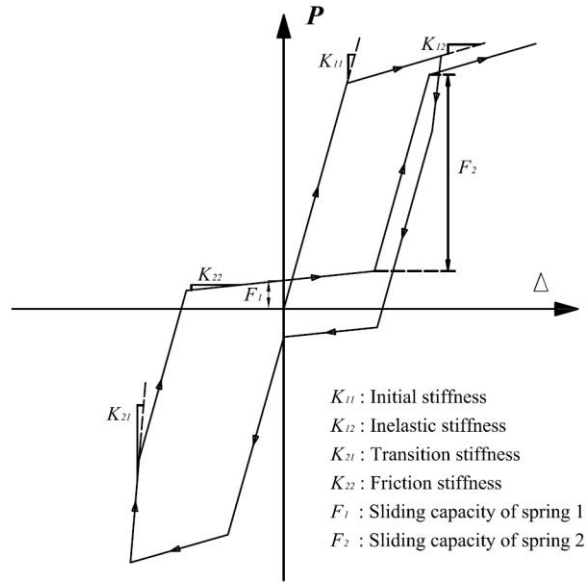
Similarly, analyses are carried out for the parallel panel to panel fasteners (i.e., screws) using the test results given in Gavric et al. (2015a) for spline and half-tapped joints, where

the panels are subjected to in-plane forces along the connection boundary. In other words, the screws are subjected to shear. Modeling each screw individually is an inconvenient and cumbersome task, especially given the number of screws in a typical building. To reduce the modeling effort and computing time, the connection system is represented by an equivalent system, with equivalent connection elements spaced at 400 mm along the connection boundary. The model parameters finally adopted are listed in Table 2.5 and the model is depicted in Figure 2.7c, illustrating its adequacy.

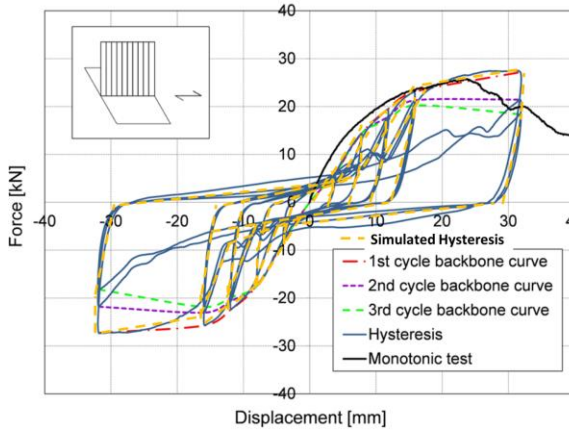
Table 2.8. Characterized connector parameters for the connection model.

Connector type	$K_{11}^{(1)}$	K_{12}	$F_1^{(2)}$	K_{21}	K_{22}	F_2
HTT4 WHT 540 hold-downs with twelve 4 × 60 mm annular ring nails	4.51	0.75	40.5	2.28	0.38	12.9
BMF 100 × 100 × 90 × 3 mm brackets with fourteen 3.9 × 89 mm spiral nails and two HBS 4 × 60 mm screws (Shear)	1.10	0.33	16.6	0.61	0.18	5.0
BMF 100 × 100 × 90 × 3 mm brackets with fourteen 3.9 × 89 mm spiral nails and two HBS 4 × 60 mm screws (Withdrawal)	2.98	0.51	11.1	1.64	0.14	0.8
BMF 90 × 116 × 48 × 3 mm brackets with eleven 4 × 60 mm annular ring nails with one Φ 12 bolts (Shear)	2.09	0.35	23.0	1.10	0.13	5.2
BMF 90 × 116 × 48 × 3 mm brackets with eleven 4 × 60 mm annular ring nails with one Φ 12 bolts (Withdrawal)	2.53	0.42	19.2	1.36	0.13	0.7
Half-lapped joint with 2 × 2 HBS Φ 8×80 mm screws spaced at 120 mm ⁽³⁾	1.24	0.325	3.2	0.400	0.035	0.8
Spline joint with 2 × 4 HBS Φ 8×80 mm screws spaced at 100 mm ⁽³⁾	0.84	0.100	4.9	0.430	0.034	1.3

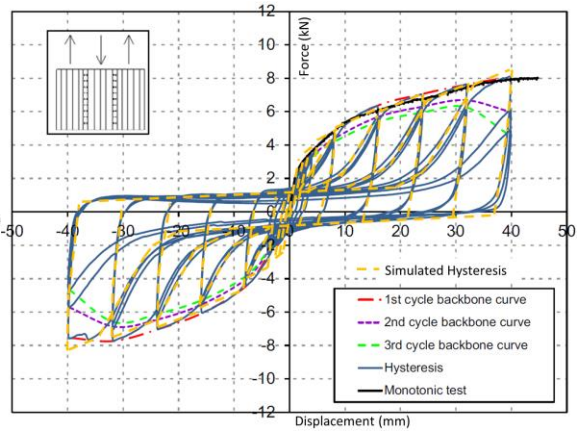
Notes: 1) The stiffness is in the unit of kN/mm; 2) The yield capacity is in kN; 3) The parameters calibrated are presented for a single connector.



a)



b)



c)

Figure 2.7. Model and comparison of predicted and test results: a) sketch of hysteretic model and definition of model parameters, b) illustration of fitted model for the steel bracket; c) illustration of fitted model for the equivalent connectors used for parallel panels.

2.4 Response characteristics and capacity curves

2.4.1 Response characteristics of the designed buildings

Free vibration analysis is carried out by using the developed finite element models of the designed buildings. The obtained first three lowest natural vibration periods for each of the designed buildings are shown in Table 2.6. The first vibration mode of the 10-, 15- and 20-storey buildings is not always side sway mode. In fact, the first vibration mode of the 20-storey building corresponds to the torsional vibration mode. Table 2.6 also indicates that the second vibration mode of the 10-storey building and the third vibration mode of the 15-storey building are the torsional vibration mode. These differences are due to different shear walls locations shown in Figure 2.3 that are necessary to satisfy the design requirements.

Table 2.9. Vibration periods of designed buildings.

Story	Period (s) from Eq. (3)	1 st -mode		2 nd -mode		3 rd -mode	
		Period (s)	Associated Vibration Mode	Period (s)	Mode	Period (s)	Mode
10-	0.692	1.629	N-S sway	1.383	Torsion	1.301	E-W Sway
15-	0.929	1.924	E-W sway	1.656	N-S sway	1.217	Torsion
20-	1.147	2.672	Torsion	2.111	N-S sway	1.973	E-W Sway

Using the calculated vibration periods for the lateral sway modes, the seismic design base shear along the E-W direction equals 1932 kN, 2298 kN and 3460 kN for the 10-, 15- and 20-storey wood buildings, respectively. These values become 1572 kN, 2839 kN and 3374 kN if the N-S direction is considered. A further analysis shows that the calculated natural vibration period for the first vibration mode of each of the design building is about twice of the value predicted by using Eq. (2.1). This can be explained by noting that Eq. (2.1) was developed for reinforced concrete buildings that are stiffer than the wood buildings, and so should not be applied in its present form to wood buildings.

Applying the response spectrum method, the displacement responses in the E-W or N-S directions are estimated using the design spectrum defined by Eq. (2.3) and the values

shown in Table 2.1. For the estimation, the first 20 vibration modes in each of the considered directions are considered. The estimated displacement are multiplied by $(R_d R_o / I_E)$ according to the NBCC requirement. The obtained values in terms of the inter-storey drift ratio are shown in Figure 2.8. The maximum inter-storey drift ratios are 2.2%, 1.6%, and 1.2% for the designed 10-, 15- and 20-storey wood buildings, respectively. In all cases, the maximum value of the drift ratio is less than the tolerable value of 2.5% stipulated in the NBCC (NRCC 2010a). The ratio of the specified limit to the maximum inter-storey drift equals 1.14, 1.56 and 2.08 for the 10-, 15- and 20-storey buildings, respectively, implying that the 10-storey building is only slightly overdesigned, whereas the 20-storey building is significantly overdesigned. The latter is due to the actual design of the 20-storey building being governed by the tolerable inter-storey drift ratio of wind load. The magnitude of overdesign for the 15-storey building is between those for the 10- and 20-storey buildings.

The lateral displacements for the wind load with $I_w = 0.75$ given in the NBCC commentary (NRCC 2010b) for serviceability requirement are estimated using the dynamic procedure. The estimated inter-storey drifts are shown in Figure 2.9, indicating that the maximum inter-storey drift ratio is 0.08%, 0.10% and 0.15% for the 10-, 15- and 20-storey wood buildings, respectively. All these values are less than the specified limit of 1/500 subjected to wind load (NRCC 2010b). The ratio of the specified limit to computed maximum inter-storey drift is 2.5, 2.0 and 1.33 for the 10-, 15- and 20-storey buildings. Inspection of the results shown in Figures 2.8 and 2.9 indicates that the inter-storey drift ratio varies rapidly for the first 20% of the building height, and the maximum inter-storey drift of the designed wood buildings occurs approximately within 20% to 40% of the total height.

The evaluation of displacements in the E-W and in the N-S directions subjected to wind load are repeated but with the 10-year return period value of the wind velocity pressure given in the NBCC (NRCC 2010a) to check building vibration. By using the evaluated displacements and Eqs. (2.16) and (2.17), the calculated maximum values of a_D (m/s^2) and a_W (m/s^2) are 0.005g, 0.006g and 0.011g for the 10-, 15- and 20-storey buildings, respectively. The ratio for the tolerable limit of 0.015g for residential occupancy (NRCC 2010b) to a_D equals 3.0, 2.5, and 1.36, for the 10-, 15-, and 20-storey buildings. These

ratios are consistently greater than those obtained for the inter-storey drift requirement, indicating that the overdesign for drift ratio limit is slightly greater than that for vibration. These values again indicate that the buildings are overdesigned: the 10- and 15-storey buildings are overdesigned for wind because their designs are governed by earthquake; whereas the overdesign is markedly less for the 20-storey building under wind.

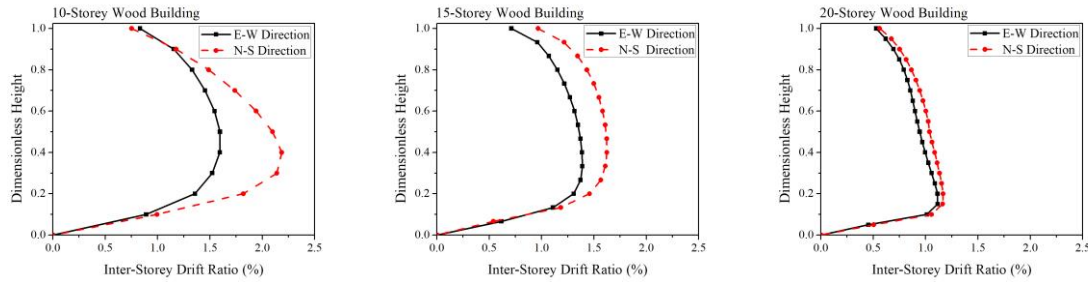


Figure 2.8. Inter-storey drifts of wood buildings under seismic loadings.

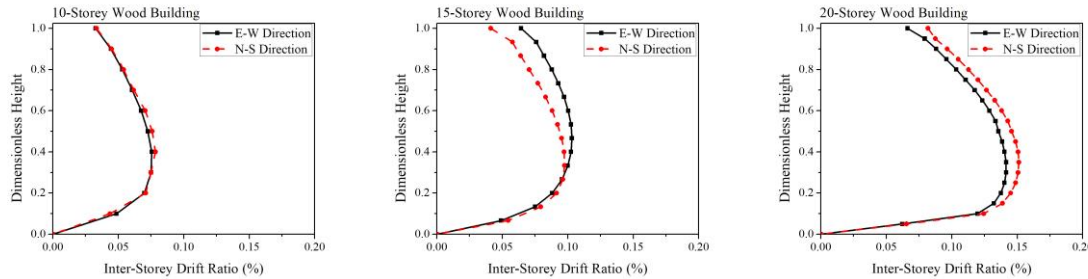


Figure 2.9. Inter-storey drifts of wood buildings under wind loadings.

2.4.2 Estimation of capacity curves

Two approaches, the nonlinear static pushover analysis (NSPA) and the incremental dynamic analysis (IDA), are often used to assess the capacity curves. The IDA (Vamvatsikos and Cornell 2002) consists of carrying out a series of nonlinear dynamic analyses by applying the scaled ground motion records with increased intensities. The scaling is often based on the Pseudo-spectral acceleration (PSA) at the fundamental natural vibration period. The obtained IDA curves, each for a selected record component, include the record-to-record variability, and require extensive computing time. Conversely, the NSPA does not take the record-to-record variability into account, but it is very efficient to assess the capacity curve. Both of the analysis methods are employed in this section to

evaluate the capacity curves of the three buildings and their relation to the seismic design demand.

For the IDA, a set of records is selected from the NGA database (<http://peer.berkeley.edu/nga/index.html>). The selection is based on the following criteria: 1) the moment magnitude of earthquake should be at least 6.0; 2) the records should be obtained at site with the site class “D” (e.g., 180-360 m/s average shear wave velocity in the uppermost 30 m); c) the closest horizontal distance to projected faults should be larger than 15 km; and, d) only a single record from each seismic event should be considered. The application of the criteria resulted in 11 records (i.e., 22 horizontal record components) from 11 seismic events which are shown in Table 2.7.

Table 2.10. Selected records for North Vancouver.

No.	NGA #	Event	Station	Moment Magnitude	PGA (g)
1	31	Parkfield	Cholame - Shandon Array #8	6.19	0.265
2	36	Borrego Mtn	El Centro Array #9	6.63	0.088
3	62	San Fernando	Colton - So Cal Edison	6.61	0.038
4	165	Imperial Valley-06	Chihuahua	6.53	0.270
5	463	Morgan Hill	Hollister Diff Array #1	6.19	0.094
6	718	Superstition Hills-01	Wildlife Liquef. Array	6.22	0.137
7	721	Superstition Hills-02	El Centro Imp. Co. Cent	6.54	0.293
8	744	Loma Prieta	Bear Valley #12, Williams Ranch	6.93	0.156
9	841	Landers	Boron Fire Station	7.28	0.103
10	960	Northridge-01	Canyon Country - W Lost Cany	6.69	0.436
11	1762	Hector mine	Amboy	7.13	0.194

The two horizontal orthogonal components are considered to be statistically independent as a standard practice. The use of 22 record components is aimed at gaining an understanding on the effect of the record-to-record variability on the estimated IDA curves for the designed wood buildings. By carrying out the IDA for each of the three buildings for the E-W and N-S directions, the obtained IDA curves are presented in Figure 2.10 in terms of the drift ratio and PSA. The computing time for a single point on a capacity curve is approximately 6 hours using a desktop computer with Intel Core i7, and 8G RAM.

To better visualize the nonlinear inelastic behaviour of these buildings, the IDA curves shown in Figure 2.10 are presented in terms of base shear versus roof displacement in Figure 2.11. For the plot of the IDA curves, the maximum roof displacement and the maximum base shear from the time history analysis are employed. The last point on an IDA curve represents the results obtained from the time history analysis for the scaled record component before the roof drift ratio becomes more than 2% or before convergence is not achieved. This drift ratio limit is consistent with those suggested by Filiatrault and Folz (2002), Ellingwood et al. (2008) and Pei et al. (2012). Figure 2.10 shows that there is significant record-to-record variability in the IDA curves which is consistent with that observed for reinforced concrete or steel buildings (Haselton et al. 2007; Hong et al. 2010). The figure also indicates that the wood buildings exhibit highly nonlinear inelastic behaviour with significant post-yield stiffness. The post-yield stiffness ratio to initial stiffness for the wood buildings is much greater than that for steel buildings shown in Hong et al. (2010). The post-yield stiffness can significantly influence the seismic ductility demand.

To reduce the computational time to assess the capacity curve, the NSPA can be used. For the analysis, an inverted triangle load pattern and a load pattern defined by the first (sway) vibration mode (Fajfar 2000) are adopted, and the lateral load is monotonically increased. The obtained results are shown in Figure 2.12. Comparison of the curves shown in the figure indicates that for a given displacement the capacity predicted by using the inverted triangle load pattern is greater than that by using the load pattern defined by the first sway vibration mode.

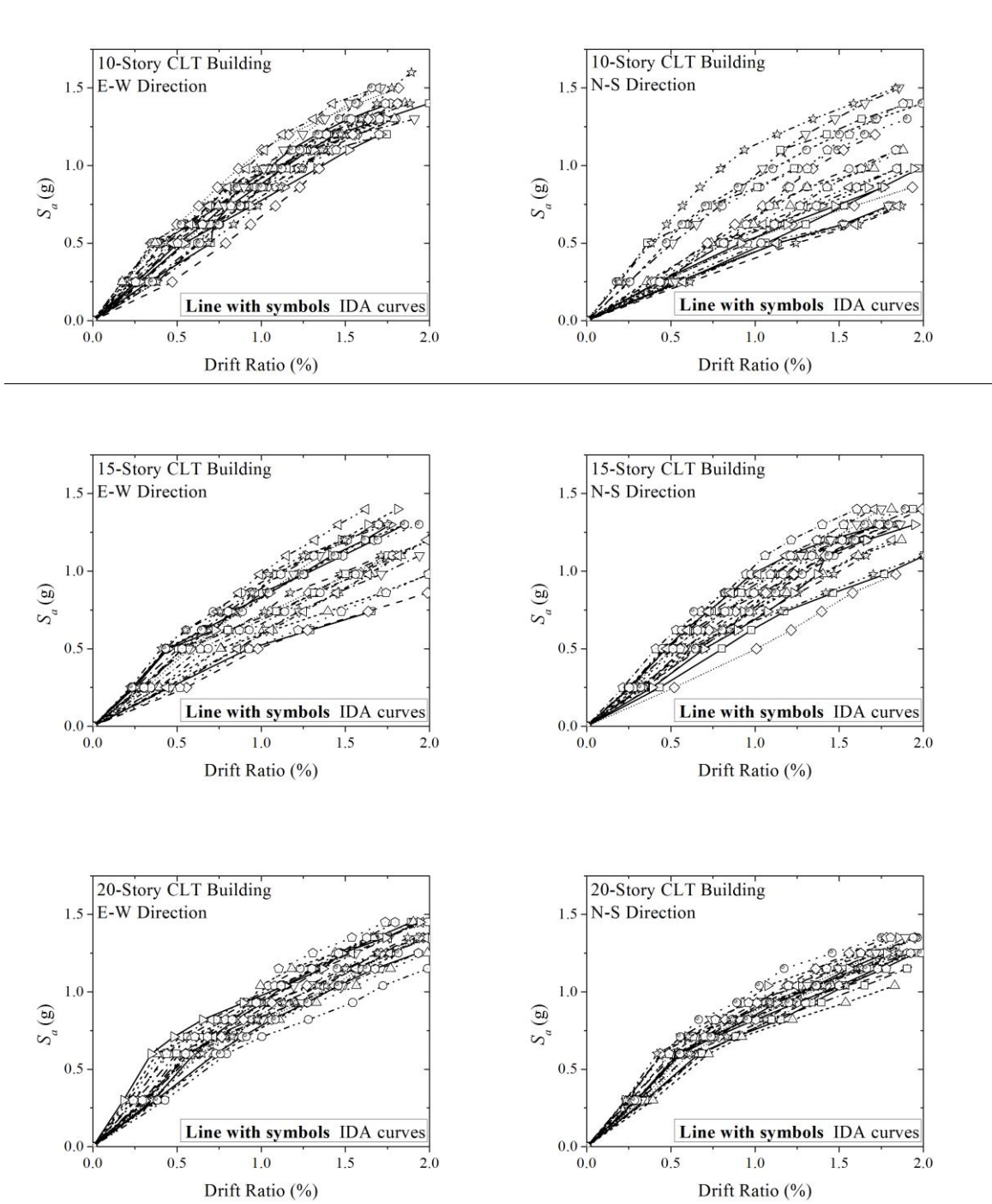


Figure 2.10. Capacity curves obtained from IDA presented by roof drift ratio and spectral acceleration S_a .

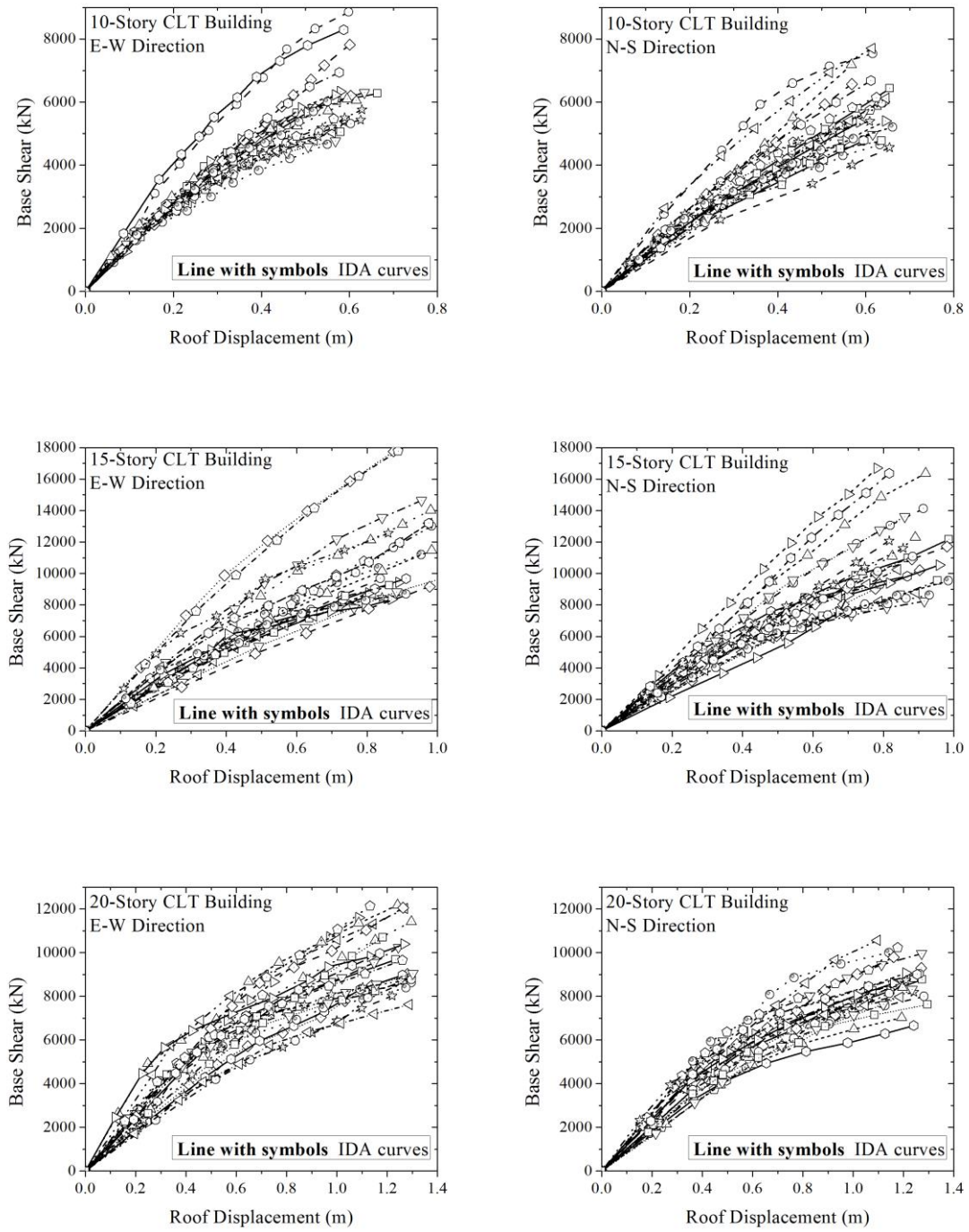


Figure 2.11. Capacity curves obtained from IDA presented by base shear versus top displacement.

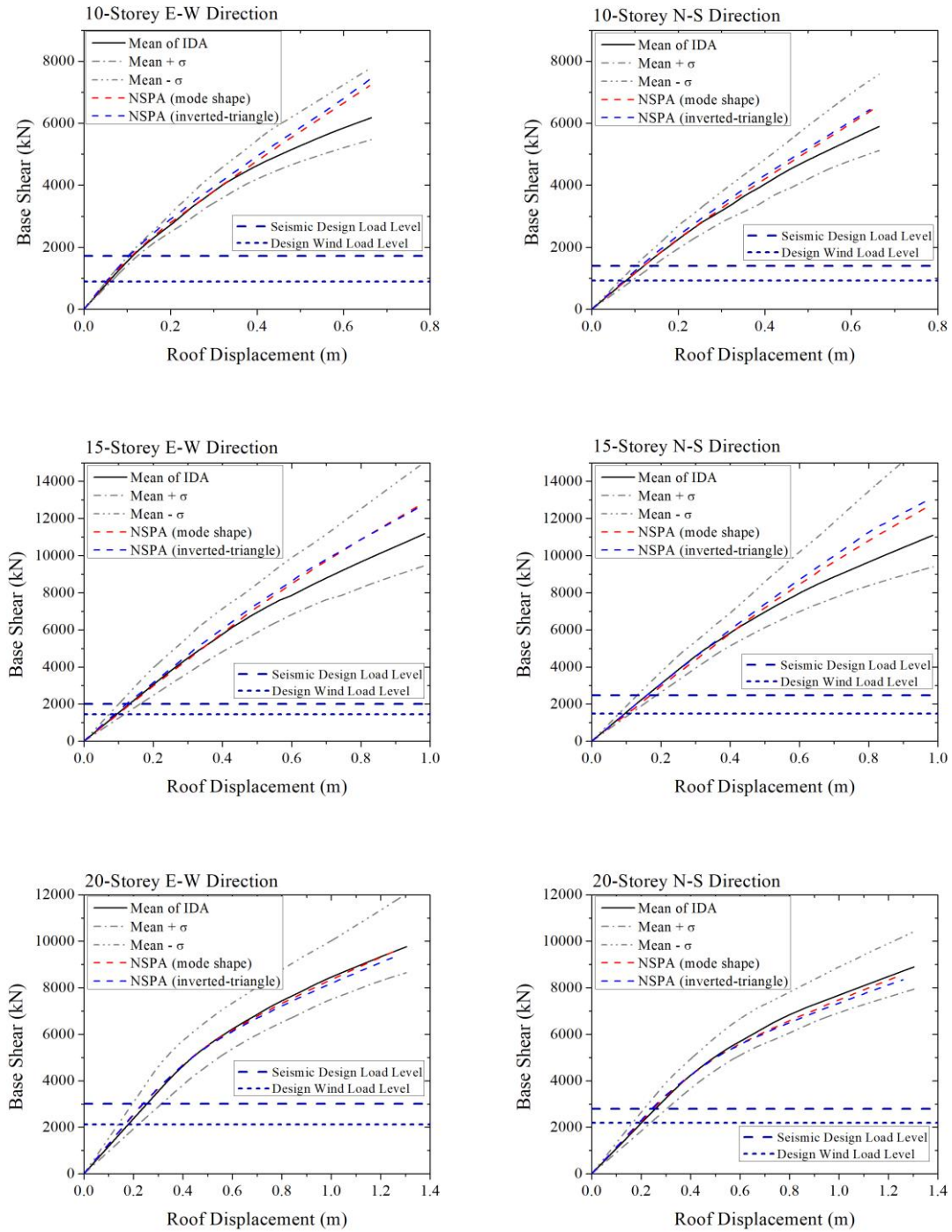


Figure 2.12. Capacity curves obtained from mean of IDA curves and from NSPA by using inverted-triangle triangle or first sway mode load pattern.

To see the differences between the capacity curves determined by the NSPA and IDA, the mean, and mean \pm one standard deviation of the IDA curves shown in Figure 2.11 are evaluated and are also included in Figure 2.12. The figure shows that the curves from the NSPA are in good agreement with the mean of the IDA curves, although the mean of the IDA curves leads to a predicted capacity that is slightly lower than that predicted by the NSPA. The differences between the mean of the IDA curves and the curve from the NSPA increases as the total applied load (i.e., base shear) increases. In all cases, the NSPA curves are within the mean \pm one standard deviation of the IDA curves. For a range of seismic load levels, the absolute differences between the displacement predicted by the mean IDA curve and the NSPA curve are shown in Table 2.8, where the design seismic load level, V_d , is calculated using Eq. (2.2).

To further appreciate these differences, values of the capacity curves at $2V_d$ and $3V_d$ are also shown in Table 2.8. The results indicate that the relative differences vary for the 10-, 15- and 20-storey buildings, and depend on the orientation of seismic excitations. The maximum relative differences are less than 2.5% at load level V_d , 2.7% at $2V_d$, and 7.8% at $3V_d$, which are considered to be small.

Table 2.11a. Values of capacity curve at selected load levels for designed wood buildings considering the E-W direction.

Load Level		Roof Displacement (m)							
		V_d			$2V_d$			$3V_d$	
Build ing	Mean IDA	NSPA	Relative difference	Mean IDA	NSPA	Relative difference	Mean IDA	NSPA	Relative difference
10-	0.112	0.112	0.7%	0.263	0.263	0.6%	0.479	0.444	7.8%
15-	0.133	0.132	0.6%	0.273	0.274	1.0%	0.417	0.411	1.4%
20-	0.242	0.240	0.8%	0.570	0.570	0.4%	1.180	1.184	0.3%

Table 2.12b. Values of capacity curve at selected load levels for designed CLT buildings considering the N-S direction.

Load Level		Roof Displacement (m)							
		V_d			$2V_d$			$3V_d$	
Build ing	Mean IDA	NSPA	Relative difference	Mean IDA	NSPA	Relative difference	Mean IDA	NSPA	Relative difference
10-	0.120	0.118	1.7%	0.253	0.245	2.7%	0.417	0.399	4.6%
15-	0.160	0.164	2.5%	0.327	0.332	1.5%	0.547	0.537	1.8%
20-	0.256	0.252	1.6%	0.578	0.579	0.3%	1.221	1.252	2.5%

2.5 Conclusions

Designs of 10-, 15- and 20-storey wood buildings are carried out according to the requirements stipulated in National Building Code of Canadian (NRCC 2010a, b) and CAN/CSA O86 (CSA 2009).

The hysteretic models used to model the fasteners for wood members are created and the model parameters are recommended for the structural analysis. It was found that the design of these structures are governed by inter-storey drift caused by earthquake or wind loads rather than the strength requirements.

3D finite element linear and nonlinear finite element models are developed for the designed buildings. An assessment of the capacity curves of the 10-, 15- and 20-storey buildings is carried out using the incremental dynamic analysis (IDA) and nonlinear static pushover analysis (NSPA). Comparison of the obtained capacity curves indicates that the NSPA curve approximates well the mean capacity curve estimated by using the IDA. The use of the NSPA cannot characterize, however, the uncertainty in the capacity curve caused by record-to-record variability, which is significant for the assessed wood buildings and comparable to that observed for steel frame structures designed according to Canadian design practice.

In addition, it is observed that the post-yield stiffness ratio to initial stiffness for the wood buildings is much greater than that for steel buildings. The post-yield stiffness can significantly influence the seismic ductility demand.

2.6 References

Ansys, (2012). ANSYS multiphasics version 14.5. *Ansys Inc., Canonsburg, PA.*

Blasetti, A. S., Hoffman, R. M., and Dinehart, D. W. (2008). Simplified hysteretic finite-element model for wood and viscoelastic polymer connections for the dynamic analysis of shear walls. *Journal of structural engineering*, 134(1), 77-86.

Ceccotti, A. (2008). New technologies for construction of medium-rise buildings in seismic regions: the XLAM case. *Structural Engineering International*, 18(2), 156-165.

- Ceccotti, A., Sandhaas, C., Okabe, M., Yasumura, M., Minowa, C., and Kawai, N. (2013). SOFIE project—3D shaking table test on a seven - storey full - scale cross - laminated timber building. *Earthquake Engineering and Structural Dynamics*, 42(13), 2003-2021.
- Chen, Z., Chui, Y. H., Ni, C., and Xu, J. (2013). Seismic response of midrise light wood-frame buildings with portal frames. *Journal of Structural Engineering*, 140(8), A4013003.
- Christovasilis, I. P., Filiatrault, A., Constantinou, M. C., and Wanitkorkul, A. (2009). Incremental dynamic analysis of woodframe buildings. *Earthquake Engineering and Structural Dynamics*, 38(4), 477-496.
- CWC. (2010). Wood Design Manual, *Canadian Wood Council*, Ottawa, Ontario, Canada.
- CSA. (2009). Engineering Design in Wood Standard, CSA O86-09. *Canadian Standards Association*, Mississauga, Ontario, Canada.
- Dickof, C., Stiemer, S. F., Bezabeh, M. A., and Tesfamariam, S. (2014). CLT–Steel Hybrid System: Ductility and Overstrength Values Based on Static Pushover Analysis. *Journal of Performance of Constructed Facilities*, 28(6), A4014012.
- Ellingwood, B. R., Rosowsky, D. V., and Pang, W. (2008). Performance of light-frame wood residential construction subjected to earthquakes in regions of moderate seismicity. *Journal of structural engineering*, 134(8), 1353-1363.
- Fajfar, P. (2000). A nonlinear analysis method for performance-based seismic design. *Earthquake spectra*, 16(3), 573-592.
- Filiatrault, A., and Folz, B. (2002). Performance-based seismic design of wood framed buildings. *Journal of Structural Engineering*, 128(1), 39-47.
- Filiatrault, A., Isoda, H., and Folz, B. (2003). Hysteretic damping of wood framed buildings. *Engineering Structures*, 25(4), 461-471.

- Folz, B., and Filiatrault, A. (2004a). Seismic analysis of woodframe structures. I: Model formulation. *Journal of Structural Engineering*, 130(9), 1353-1360.
- Folz, B., and Filiatrault, A. (2004b). Seismic analysis of woodframe structures. II: Model implementation and verification. *Journal of Structural Engineering*, 130(9), 1361-1370.
- FPIInnovations. (2011). CLT Handbook – Cross-Laminated Timber, *FPIInnovations*, Quebec, Quebec, Canada.
- Fragiacomo, M., Dujic, B., and Sustersic, I. (2011). Elastic and ductile design of multi-storey crosslam massive wooden buildings under seismic actions. *Engineering structures*, 33(11), 3043-3053.
- Gagnon, S., Munoz, W., Mohammad, M., and Below, K. D. (2010, July). Design guidelines for an 8-storey hybrid wood-concrete multi-family building. In *Structures and Architecture (Proceedings of the First International Conference on Structures and Architecture, Guimaraes, Portugal, 21-23 July 2010)*, CRC Press, Leiden, The Netherlands (pp. 109-110).
- Gavric, I., Fragiaco, M., and Ceccotti, A. (2015a). Cyclic behaviour of typical screwed connections for cross-laminated (CLT) structures. *European Journal of Wood and Wood Products*, 73(2), 179-191.
- Gavric, I., Fragiaco, M., and Ceccotti, A. (2015b). Cyclic behaviour of typical metal connectors for cross-laminated (CLT) structures. *Materials and structures*, 48(6), 1841-1857.
- Gsell, D., Feltrin, G., Schubert, S., Steiger, R., and Motavalli, M. (2007). Cross-laminated timber plates: evaluation and verification of homogenized elastic properties. *Journal of Structural Engineering*, 133(1), 132-138.
- Haselton, C. B., Liel, A. B., Dean, B. S., Chou, J. H., and Deierlein, G. G. (2007). Seismic collapse safety and behaviour of modern reinforced concrete moment frame buildings. In *Structural Engineering Research Frontiers* (pp. 1-14).

- Hu, L. J., Chui, Y. H., and Onysko, D. M. (2001). Vibration serviceability of timber floors in residential construction. *Progress in Structural Engineering and Materials*, 3(3), 228-237.
- Hong, H.P., Hong, P. and Wang, W. (2010) Reliability of steel frames designed in accordance with the NBCC seismic provisions and implication in codified design, *Engineering Structures*, Volume 32, Issue 5, May 2010, Pages 1284-1291
- Keenan F. J. (1986). Limit states design of wood structures. *Morrison Hershfield Ltd.*;
- Lauriola, M.P. and Sandhaas, C., (2006, November). Quasi-static and pseudo-dynamic tests on XLAM walls and buildings. In *COST E29 International Workshop on Earthquake Engineering on Timber Structures, Coimbra, Portugal*.
- MGB Architecture and Design. (2012). Tall Wood Report. *MGB Architecture and Design*.
- NEWBuilds. (2015). Application of Analysis Tools from NEWBuildS Research Network in Design of a High-Rise Wood Building, *Network on Innovative Wood Products and Building Systems (NEWBuildS)*, University of New Brunswick, Fredericton, New Brunswick, Canada.
- NGA database. Next Generation Attenuation <http://peer.berkeley.edu/nga/index.html>. 325 *Davis Hall, University of California, Berkeley, CA 94720-1792*
- NRC Canada (2010a). National Building Code of Canada, *NRC Canada*, Ottawa, Ontario, Canada.
- NRC Canada (2010b). *User's Guide – NBC 2010, Structural Commentaries (Part 4 of Division B)*, NRC Canada, Ottawa, Ontario, Canada.
- O'Neill, J. W. (2013). The Fire Performance of Timber Floors in Multi-Storey Buildings. Thesis.

- Pang, W., Rosowsky, D. V., Pei, S., and Van De Lindt, J. W. (2010). Simplified direct displacement design of six-storey woodframe building and pretest seismic performance assessment. *Journal of structural engineering*, 136(7), 813-825.
- Pei, S., Popovski, M., and van de Lindt, J. W. (2013). Analytical study on seismic force modification factors for cross-laminated timber buildings. *Canadian Journal of Civil Engineering*, 40(9), 887-896.
- Pei, S., van de Lindt, J. W., and Popovski, M. (2012). Approximate R-factor for cross-laminated timber walls in multistory buildings. *Journal of Architectural Engineering*, 19(4), 245-255.
- Popovski, M., and Gavric, I. (2015). Performance of a 2-storey CLT House Subjected to Lateral Loads. *Journal of Structural Engineering*, E4015006.
- Shen, Y. L., Schneider, J., Tesfamariam, S., Stiemer, S. F., and Mu, Z. G. (2013). Hysteresis behaviour of bracket connection in cross-laminated-timber shear walls. *Construction and Building Materials*, 48, 980-991.
- Structurlam (2011). Cross-Laminated Timber Design Guide. *Structurlam*, Canada.
- Vamvatsikos, D., and Cornell, C. A. (2002). Incremental dynamic analysis. *Earthquake Engineering and Structural Dynamics*, 31(3), 491-514.
- Zagari, G., Fortino, S., and Dill-Langer, G. (2009, September). FEM simulation of crack growth in Glulam by using a 3D orthotropic-viscoelastic model and cohesive elements. In *7th EUROMECH Solid Mechanics Conference* (pp. 7-11).

Chapter 3

3 Reliability Assessment of Mid- and High-rise Wood Buildings under Uni-directional Seismic Excitations

3.1 Introduction

The wood laminating techniques allow a wider application of wood material in civil engineering. Engineered wood composites such as structural composite lumber, laminated veneer lumber and cross-laminated timber (CLT) are used in constructing taller wood buildings. Because of the improved stiffness, quality control and stability of the wood composites, the manufactured CLT panels can be used for floor and wall assemblies. Structures constructed using the mass timber members and assemblies are likely to be different from the light-frame wood structures in terms of fire and acoustic performance, structural performance, and construction efficiency.

Designed mid- or high-rise wood buildings up to 20 storeys by using the CLT panels are presented in Pei et al. (2012), MGB (2012), NEWBuilds (2015), as well as in Chapter 2. These designs are often governed by the drift limits or serviceability requirements due to wind or earthquake loads. Some of the designs satisfy the provisions in the National Building Code of Canada (NBCC) (NRCC 2010a) and Canadian timber structural design practice (CWC 2010; CSA O86-09 2009). In all cases, they are only in the design stage, although an 18-storey (53 m, about 174 ft) wood hybrid building was recently constructed in Vancouver, Canada.

To provide the proof of the concept, and to encourage practicing engineers to use composite wood materials in mid- and high-rise buildings, one of the issues that needs to be addressed to use heavy timber material is related to the reliability of the wood buildings subjected to seismic or environmental loads. To our knowledge, a reliability assessment of mid- or high-rise wood buildings is currently unavailable in the literature, while reliability estimates of wood shear walls, wood frame houses, and low-rise wood frame buildings are presented in several studies, including Foliente et al. (2000), Rosowsky and Ellingwood (2002), van de Lindt and Walz (2003), Lee and Rosowsky (2006), and Pang et al. (2009).

To evaluate the probability of incipient yield and probability of incipient collapse of wood buildings, a probabilistic characterization of the inelastic response of the buildings or appropriate simplified modeling of inelastic behaviour of the structures under earthquake load is essential. This is because the direct use of simulation techniques to evaluate seismic reliability is inefficient by using a detailed inelastic 3D finite element model of a building, especially since each nonlinear inelastic time history analysis can take hours, and at least a few hundred thousands of time history analyses are needed to estimate the failure probability. Also, the use of the efficient first-order reliability method (Madsen et al. 2006) could breakdown for nonlinear inelastic structural system under dynamic loads (Koduru and Haukass 2010). An alternative is to characterize the probabilistic seismic response of the structure conditioned on a ground motion measure such as the pseudo-spectral acceleration (SA) and to evaluate exceedance probability of a specified drift ratio subjected to seismic load. The probabilistic characterization of the seismic responses conditioned on SA or another ground motion measure, which includes the effect of record-to-record variability, is computing time consuming since it calls for the incremental dynamic analysis (IDA) of the structure for multiple records (Vamvatsikos and Cornell 2002). The evaluation of the failure probability is carried out by using the probability distribution of the response conditioned on SA and the probability distribution of the SA obtained from seismic hazard assessment (Cornell et al. 2002). This approach effectively separates the probabilistic structural analysis and the seismic hazard assessment into two distinct tasks, facilitating the reliability analysis. Rather than establishing the limit state function based on the drift ratio, Hong et al. (2010) used the ductility capacity and ductility demand to establish the limit state function, and carried out the reliability analysis based on an equivalent nonlinear inelastic single-degree-of-freedom (SDOF) system. The equivalent system is developed based on the capacity curve obtained from the nonlinear static pushover analysis (NSPA). This largely simplifies the reliability analysis since it avoids the repeated nonlinear dynamic analysis of the (3D) building for multiple records, although a probabilistic assessment of the ductility demand for the equivalent nonlinear inelastic SDOF subjected to a set of ground motion records needs to be carried out with very moderate computing time. Additional efficiency is gained if the probabilistic model of the ductility demand for

the equivalent nonlinear inelastic SDOF system (Hong and Hong 2007; Goda et al. 2009) is readily developed and available.

In this chapter, a reliability assessment is carried out for three mid- and high-rise wood buildings designed to satisfy the requirements in the NBCC (NRCC 2010a) (see Chapter 2). The buildings are to be located in North Vancouver, BC. For the assessment, the seismic response characteristics of the designed structures are used to develop equivalent SDOF systems with Bouc-Wen hysteretic model (Foliente 1995; Foliente et al. 2000; Ma et al. 2004). Nonlinear inelastic responses of the equivalent systems are evaluated using more than 500 ground motion records extracted from the NGA database (<http://peer.berkeley.edu/nga/index.html>). The estimated inelastic responses are employed to develop probabilistic model of the ductility demand with include the record-to-record variability. Reliability analysis is carried out by using the developed model and the probabilistic seismic hazard characteristics at the site of interest.

In the following, the seismic response characteristics of the designed wood buildings are summarized. Equivalent SDOF systems with Bouc-Wen hysteretic model for three wood buildings are developed and explained. Results of nonlinear time-history analysis for the equivalent systems are used to probabilistically characterize the seismic ductility demand. Reliability analysis results are then presented and their implication for the design and construction of the wood buildings are discussed.

3.2 Seismic response characteristics of designed prototype wood buildings

The design of the wood building includes the consideration of appropriate design methodology, reasonable assumptions, and common practice in structural engineering and architecture. Details on the design procedure and the 10-, 15- and 20-storey buildings with footprint of 24 m × 23.2 m are given in Chapter 2. The essential considerations of the design and modeling are:

- 1) The height of the first storey is 4.4 m and the other storeys are 3.2 m.; the CLT panels are used for floors, roof, shear walls, elevator shaft; the glulam is used for beams and columns;

- 2) The design was carried out for seismic load and checked for wind load. It was concluded that the design is governed by inter-storey drift limits due to earthquake or wind, or vibration limit under wind load (NRCC 2010b); and
- 3). Finite element models are developed for three buildings by considering the nonlinear behaviour of fasteners among the wood panels or structural members.

The designed structural system, and the estimated mean and mean \pm one standard deviation of the IDA curves, and the NSPA curve using the first natural vibration mode in the direction of interest are presented in Figures 3.1 to 3.3. Both the IDA and NSPA are carried out using the finite element models of the buildings developed in ANSYS (2012) (see Chapter 2). The IDA curves are obtained by considering 22 record components. The results depicted in Figures 3.1 to 3.3 showed that the NSPA curve compare favorably to the mean of the IDA curves.

The designed seismic loads according to the NBCC (NRCC 2010a, b) by considering the overstrength related factor R_o of 1.5 and ductility related reduction factor R_d of 2.0 (FPInnovation 2011; Pei et al. 2012) are also shown in Figures 3.1 to 3.3. In addition, for comparison purpose, the base shears calculated using the factored design wind load as well as the (factored) design earthquake load (including the reduction due to overstrengthening and ductility factors) V_d for ultimate limit state design are also shown in the figures, where

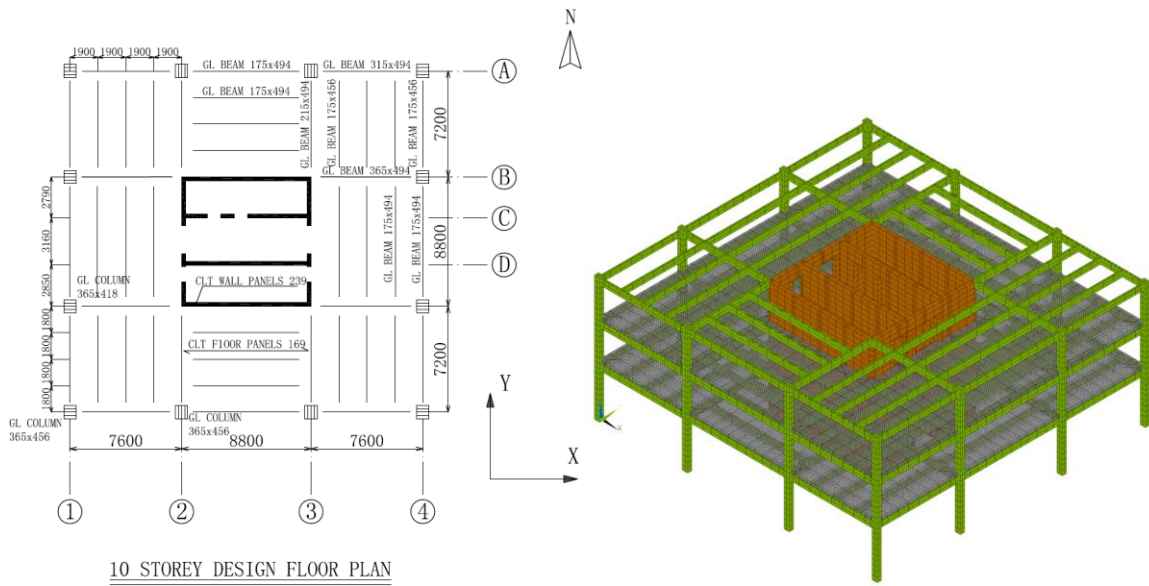
$$V_d = S_{A-\chi}(T_n, \xi) M_V I_E W / R_A, \quad (3.1)$$

in which $S_{A-\chi}(T_n, \xi)$ denotes the design spectral acceleration (for a system with the natural vibration period T_n and a damping ratio ξ) representing $(1-\chi)$ -fractile of SA with $\chi = 1/2475$; M_V is the higher mode factor that equals 1.0 for the considered structural systems; I_E is the importance factor that equals 1.0 if the ultimate limit state (ULS) is considered; W represents the building weight plus 25% of snow load and $R_A = R_o R_d$. Values of T_n , $S_{A-1/2475}(T_n, \xi)$ for $\xi = 5\%$, W and V_d considered for the design of the wood buildings are summarized in Table 3.1. Also shown in the table are the characteristics of the designed wood buildings.

Table 3.1. Parameters used to calculate the design based shear and the characteristics of the designed wood buildings.

Design	10-Storey		15-Storey		20-Storey	
$W (\times 10^3 \text{ kN})$	14.63		25.04		39.28	
Direction	E-W	N-S	E-W	N-S	E-W	N-S
T_n (s)	1.30	1.63	1.92	1.66	1.97	2.11
$S_{A-1/2475} (T_n, 5\%)$ (g)	0.33	0.27	0.22	0.27	0.21	0.19
V_d (kN)	1715	1394	2005	2481	3010	2788
v_s	2.29	2.35	2.45	2.36	2.47	2.71
L_m	1.81	2.05	1.74	1.98	1.77	1.91
m_{R_n}	1.87	1.85	2.90	2.21	1.76	1.75
v_{R_n}	0.23	0.28	0.20	0.29	0.17	0.12

The results presented in Figures 3.1 to 3.3 show that the base shear for the factored earthquake load is greater than that for the factored design wind load. It is emphasized that in all cases, the loads for the ultimate limit state design do not govern the design of the three buildings as mentioned earlier. The roof displacements corresponding to the factored design wind or earthquake loads are lower than the identified yield displacements.



10 STOREY DESIGN FLOOR PLAN

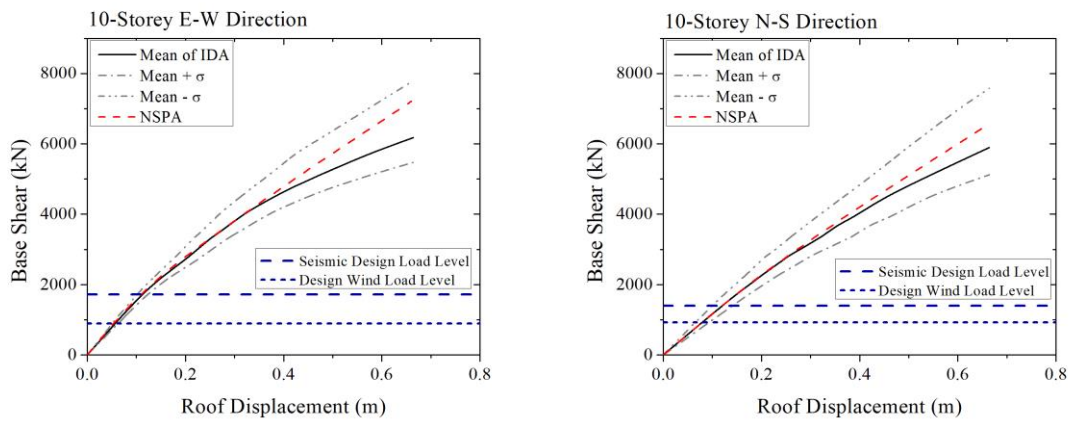


Figure 3.1. Designed 10-storey wood building and its seismic response.

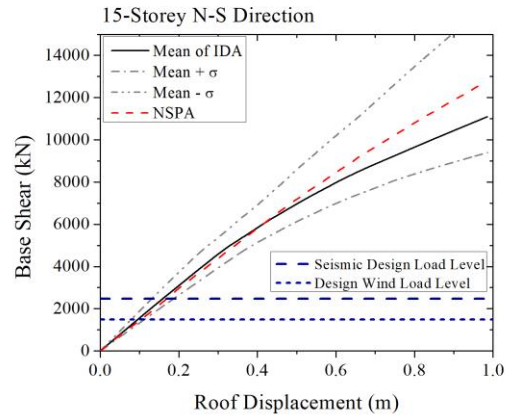
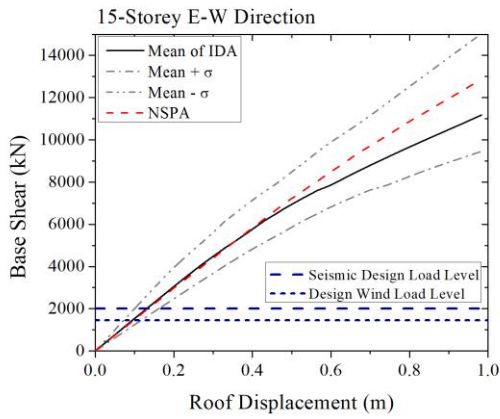
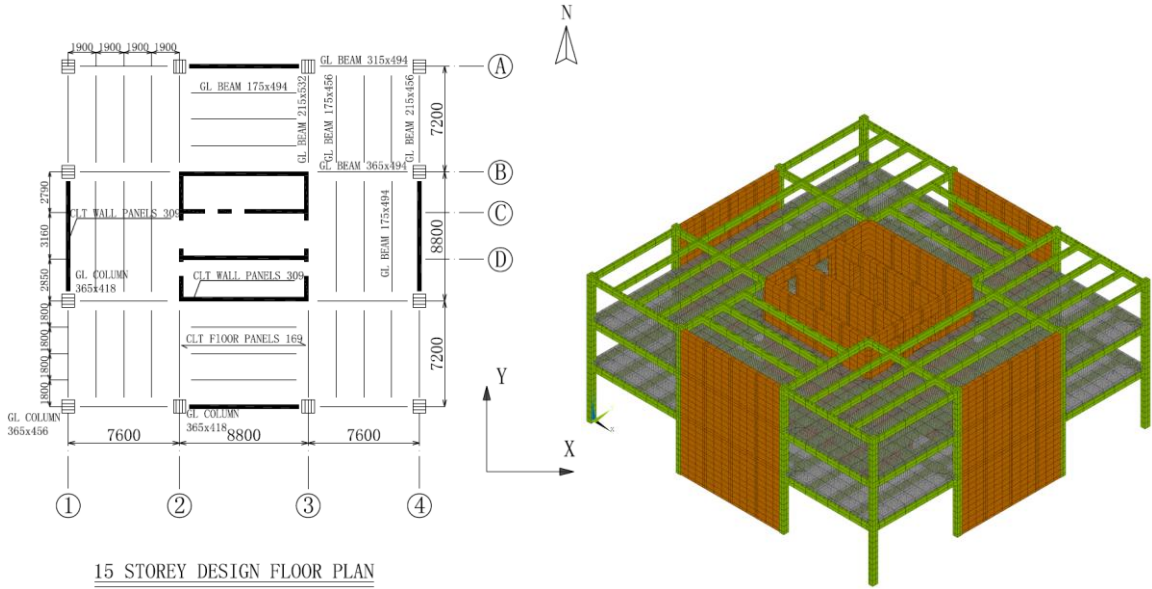


Figure 3.2. Designed 15-storey wood building and its seismic response.

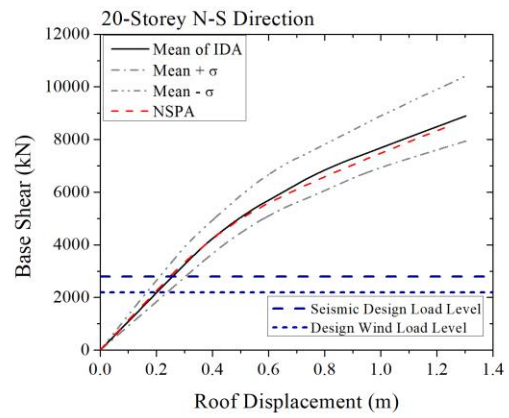
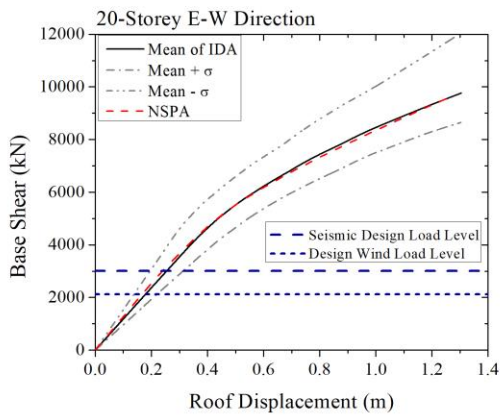
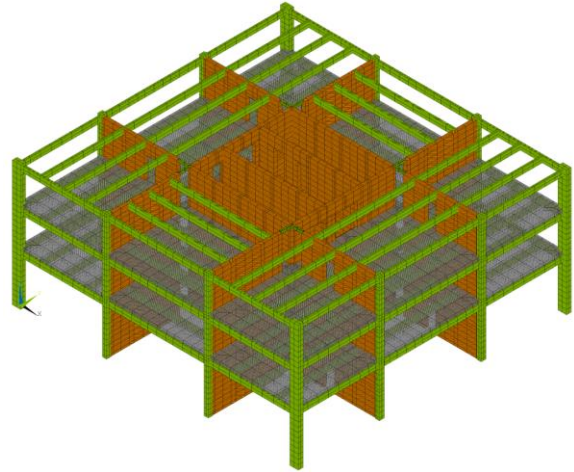
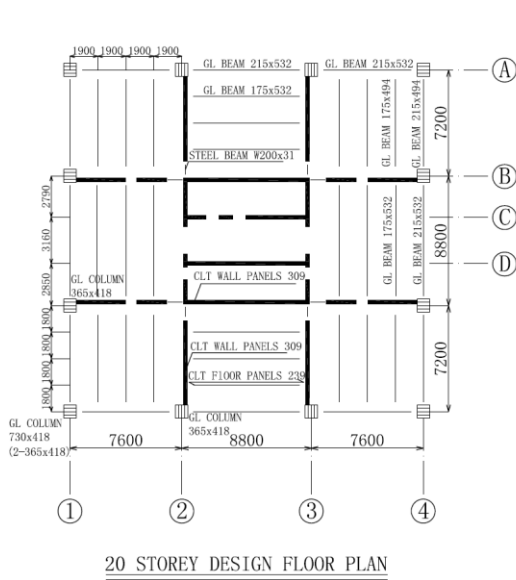


Figure 3.3. Designed 20-storey wood building and its seismic response.

3.3 Equivalent nonlinear inelastic SDOF system for the buildings

As mentioned in the introduction, one of the possible simplified approaches to carry out the reliability analysis of a building is to develop an equivalent nonlinear inelastic SDOF system based on the capacity curve of the building, so the probabilistic characterization of the inelastic seismic displacement or ductility demand can be efficiently evaluated. Rather than using a bilinear equivalent system (Hong and Hong 2007; Hong et al. 2010), the use of the SDOF system with Bouc-Wen hysteretic behaviour (Foliente 1995; Foliente et al. 2000; Ma et al. 2004; Goda et al. 2009) for such a purpose is considered in the following.

The equation of motion of the SDOF system with Bouc-Wen hysteretic behaviour subjected to the ground motion, \ddot{u}_g , can be expressed as,

$$m\ddot{u} + c\dot{u} + \alpha ku + (1 - \alpha)kz = -m\ddot{u}_g, \quad (3.2)$$

where u , \dot{u} , and \ddot{u} are the translational displacement, velocity, and acceleration, respectively; m is the mass, c is the viscous damping coefficient, k is the stiffness; α is the ratio of post-yield stiffness to initial stiffness; and z is the hysteretic displacement which is governed by (Foliente 1995; Ma et al. 2004),

$$\dot{z} = \frac{h(z, \varepsilon)}{1 + \delta_\eta \varepsilon} \left[\dot{u} - (1 + \delta_v \varepsilon) (\beta |\dot{u}| |z|^{n-1} z + \gamma \dot{u} |z|^n) \right], \quad (3.3)$$

in which $h(z, \varepsilon)$ is the pinching function, β , γ , and n are the shape parameters, δ_η and δ_v are the degradation parameters, and ε is the dissipated energy at time t through hysteresis given by,

$$\varepsilon = (1 - \alpha)k \int_0^t \dot{u}z d\tau, \quad (3.4)$$

The non-damping restoring force for the SDOF system with Bouc-Wen hysteretic behaviour is represented by $\alpha ku + (1 - \alpha)kz$. In particular, for a system without pinching and degradation (i.e., $h(z, \varepsilon) = 1$, $\delta_\eta = 0$, and $\delta_v = 0$), Eq. (3.3) becomes,

$$\dot{z} = \left[\dot{u} - (\beta |\dot{u}| |z|^{n-1} z + \gamma \dot{u} |z|^n) \right], \quad (3.5)$$

In such a case, the model that is represented by Eqs. (3.2) and (3.5) is simplified to have only four parameters $\{\alpha, \beta, \gamma, n\}$.

To facilitate the probabilistic characterization of the seismic ductility demand of a system described by Eqs. (3.2) and (3.5), let,

$$\mu = u / u_y, \quad (3.6a)$$

and,

$$\mu_z = z / u_y, \quad (3.6b)$$

where u_y is the displacement at yield with corresponding force at yield denoted by f_y . The substitution of Eqs. (3.6a) and (3.6b) into Eqs. (3.2) and (3.5) results in,

$$\ddot{\mu} + 2\xi\omega_n\dot{\mu} + \alpha\omega_n^2\mu + (1-\alpha)\omega_n^2\mu_z = -\ddot{u}_g / (\phi u_0), \quad (3.7)$$

and,

$$\dot{\mu}_z = \left[\dot{\mu} - \left(\beta_0 |\dot{\mu}| |\mu_z|^{n-1} \mu_z + \gamma_0 \dot{\mu} |\mu_z|^n \right) \right], \quad (3.8)$$

where $\beta_0 = \beta u_y^n$, $\gamma_0 = \gamma u_y^n$, $\xi = c / (2m\omega_n)$ is the damping ratio, ω_n is the natural vibration frequency, $\omega_n = \sqrt{k/m}$, in rad/s; ϕ is the normalized yield strength defined as (Chopra 2001),

$$\phi = u_y / u_0 = f_y / f_0, \quad (3.9)$$

where u_0 and f_0 are the peak values of the earthquake-induced displacement and resisting force in the corresponding linear elastic system, respectively, which can be obtained by solving Eq. (3.2) with α equal to unity for the given \ddot{u}_g .

If the capacity curve is obtained based on the NSPA for a specified loading profile (such as the first sway mode along a structural axis), and is used as the basis to develop the equivalent nonlinear inelastic SDOF system, m on the left-hand-side of Eq. (3.2) is replaced by the generalized mass, \tilde{m} , and m on the right-hand-side is replaced by $\Gamma\tilde{m}$, where Γ is the modal participation factor (Chopra 2001). The vibration frequency of the equivalent SDOF system $\omega_n = \sqrt{f_y / (u_y \tilde{m})}$.

If the mean of the IDA curves is employed to represent the capacity of the building, the

loading profile is unknown. In such a case, the vibration frequency of the equivalent SDOF system, could be considered to be equal to the natural vibration frequency for the first mode of the building, which is available from the free vibration analysis. The generalized mass \tilde{m} can then be estimated from $\tilde{m} = f_y / (u_y \omega_n^2)$, and the modal participation factor could be estimated using $\Gamma = (\bar{f}_0 / (\tilde{m} S_{A0}))^{1/2}$ or $\Gamma = (f_0 / (\tilde{m} \bar{S}_{A0}))^{1/2}$ where \bar{f}_0 represents the average base shear of the building obtained for the considered ground motions used for the IDA curves that are scaled to a selected spectral acceleration value S_{A0} of the corresponding linear elastic SDOF system, and \bar{S}_{A0} represents the average SA used to scale the i -th record to carry out the nonlinear dynamic analysis such that the base shear equals f_0 for the scaled i -th record. Note that the values \bar{f}_0 or \bar{S}_{A0} are already available or can be estimated from IDA curves. The use of $\Gamma = (f_0 / (\tilde{m} \bar{S}_{A0}))^{1/2}$ is considered in the following.

In addition, let R_n denote the ratio of the capacity to sustain base shear of the constructed building, V_{sy} , to the design base shear requirement shown in Eq. (3.1) (i.e., V_d). The ratio between the corresponding displacements is the same and equals R_n . By considering the above and using the similar argument employed in Hong and Hong (2007) for bilinear system, it can be shown that Eq. (3.7) can be re-written as,

$$\ddot{\mu} + 2\xi\omega_n\dot{\mu} + \alpha\omega_n^2\mu + (1-\alpha)\omega_n^2\mu_z = -\ddot{u}_g / (\zeta u_0), \quad (3.10)$$

where

$$\zeta = \frac{R_n}{R_o R_d} \frac{L_m}{L}, \quad (3.11)$$

in which $L_m = M / \Lambda$, M is the total mass of the structure and $\Lambda = \Gamma \tilde{m}$ represents the effective modal mass (or the effective mass for the considered loading profile), $L = S_A(T_n, \xi) / S_{A-\chi}(T_n, \xi)$ represents ratio of the seismic hazard in terms of the SA, $S_A(T_n, \xi)$ (for a SDOF system with $T_n = \omega_n / 2\pi$, and a damping ratio of ξ) to $S_{A-\chi}(T_n, \xi)$. Given the ground motion record \ddot{u}_g , u_0 in Eq. (3.10) represents the peak displacement of the linear elastic SDOF system with vibration period T_n and damping ratio ξ subjected to \ddot{u}_g , and the relation between the maximum ductility demand μ , μ_{\max} , and ζ can be

established by solving Eq. (3.10).

Before using the equivalent SDOF system with Bouc-Wen model hysteretic behaviour to approximate the designed wood buildings, and to assess the ductility demand, it is worth mentioning that the parameter n (see Eq. (3.8)) controls the transition from pre-yield to post-yield regions; as n increases, the transition from pre-yield to post-yield regions becomes sharper resulting a bilinear system. The parameter α represents the ratio of the post-yield to initial stiffness; the sum of the parameters β_0 and γ_0 equals one (Foliente 1995; Ma et al. 2004; Goda et al. 2009). β_0 and γ_0 could be taken equal to 0.5 for most cases (Goda et al. 2009). The sensitivity of hysteretic behaviour to n and α is illustrated in Figure 3.4.

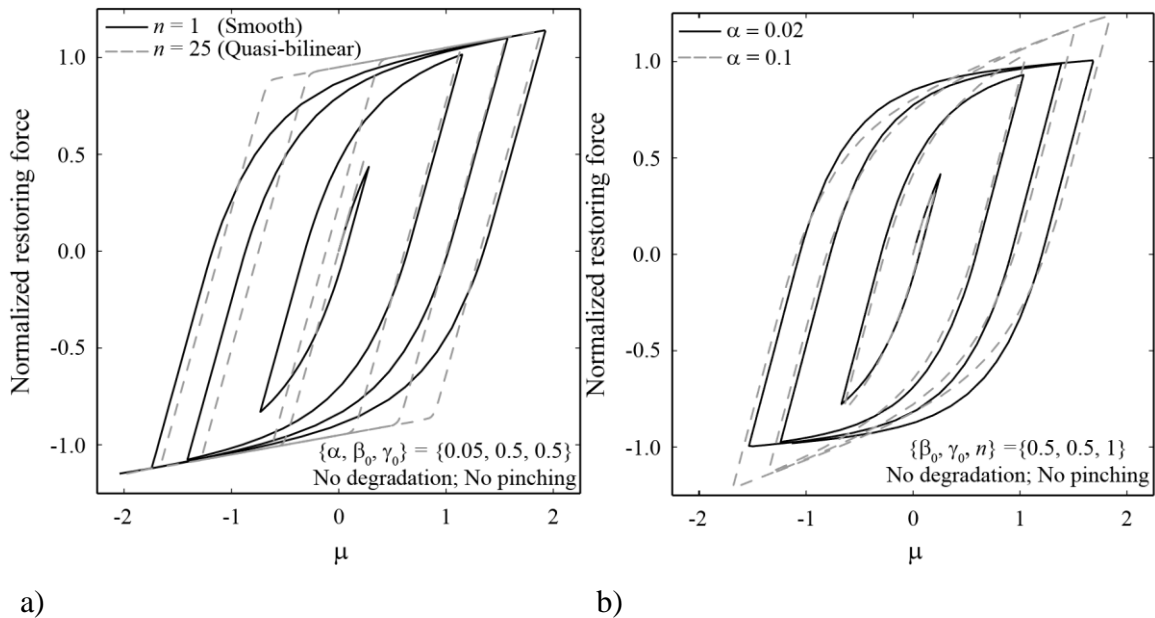


Figure 3.4. Illustration of force-deformation curve of the Bouc-Wen hysteretic models subjected to harmonic excitations with increasing amplitude: a) smooth hysteretic and quasi-bilinear models; b) smooth hysteretic models with different post-yield and unloading slopes.

In general, the identification of the model parameters of Bouc-Wen model for a given response time history can be estimated based on optimization algorithms (Sues et al. 1988; Maruyama et al. 1989; Ma et al. 2004). However, for the model adopted in this study which

contains only four model parameters $\{\alpha, \beta_0, \gamma_0, n\}$ (see Eqs. (3.7) and (3.8)) and with β_0 and γ_0 that are already assumed to be equal to 0.5, α and n can be assigned with relatively ease. First, the ratio of post-yield stiffness to initial stiffness α can be obtained through bilinear approximation. The parameter n can then be adjusted by minimizing the difference between predicted capacity curve using the equivalent SDOF system and the curves shown in Figures 3.1 to 3.3.

Using the procedure described above, the obtained α and n values for the responses along two structural axes are shown in Table 3.2 for the three designed wood buildings. The adequacy of the predicted capacity curve by using the estimated model parameters is illustrated in Figure 3.5.

Table 3.2. Estimated model parameters for the equivalent SDOF systems along two horizontal orthogonal structural axes.

Design	Direction	Bouc-Wen model parameters	
		α	n
10-Storey	E-W	0.34	2.2
	N-S	0.54	3.0
15-Storey	E-W	0.54	3.9
	N-S	0.50	3.6
20-Storey	E-W	0.36	4.0
	N-S	0.37	4.1

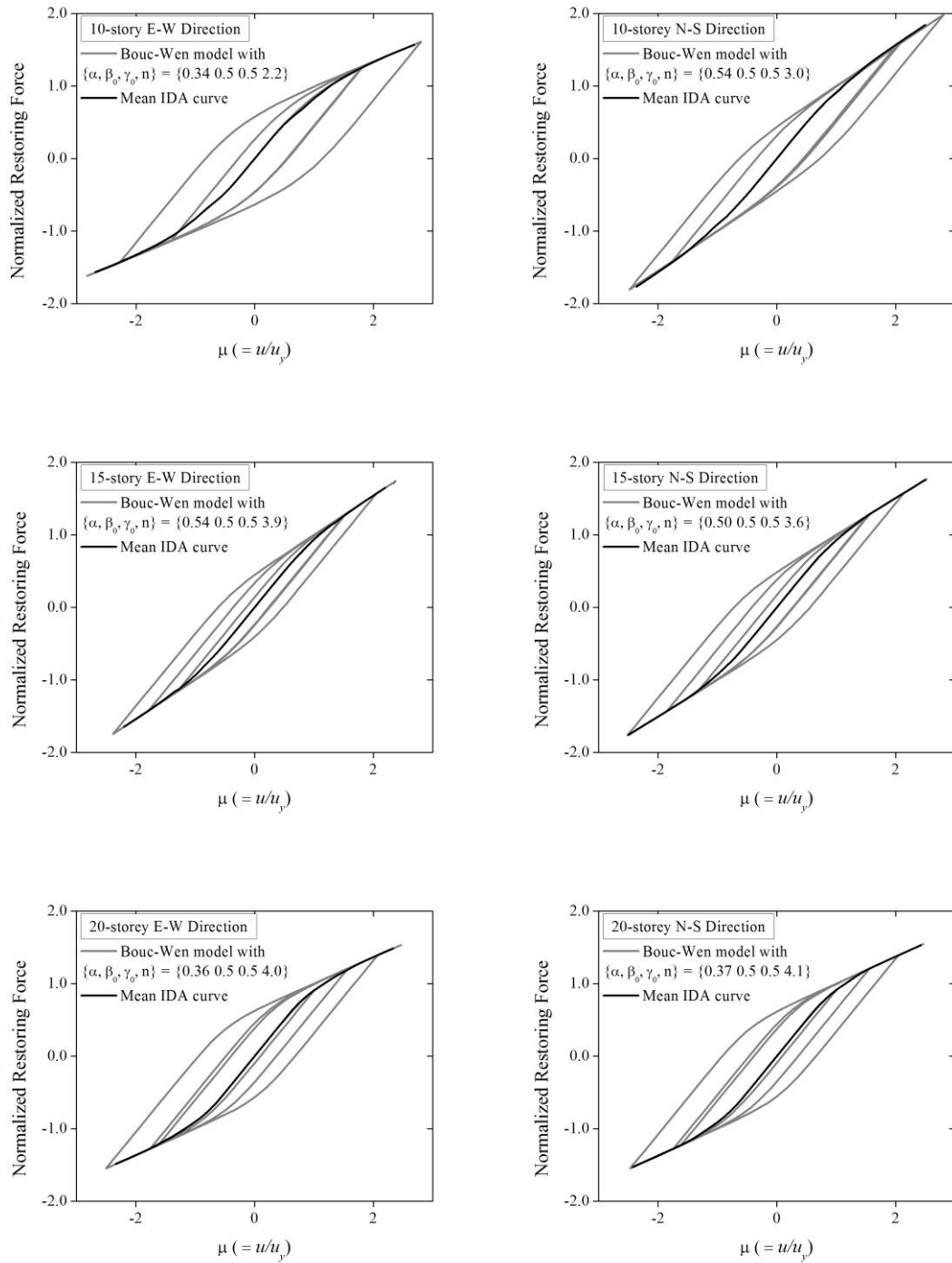


Figure 3.5. Hysteresis curves of equivalent SDOF systems and capacity curves of designed three wood buildings along two horizontal orthogonal structural axes.

3.4 Seismic demand, reliability evaluation procedure and results

3.4.1 Seismic demand and reliability evaluation procedure

For Canadian sites, the annual maximum $S_A(T_n, \xi)$ could be considered to be a lognormal variate, at least in the upper tail region. Based on the results given in Hong et al. (2006), the coefficient of variation (cov) of $S_A(T_n, \xi)$, v_s , for the considered construction site is estimated and shown in Table 3.1. Since $S_A(T_n, \xi)$ is a lognormal variate, it can be shown that L is also lognormal variate with the cov equal to v_s and the mean m_L given by,

$$m_L = \sqrt{1 + v_s^2} \exp\left(-\beta_T \sqrt{\ln(1 + v_s^2)}\right), \quad (3.12)$$

where $\beta_T = \Phi^{-1}(1 - \chi)$ and $\Phi^{-1}(\bullet)$ is the inverse standard normal distribution function.

Based on this, since L_m , R_o and R_d are deterministic quantities, if R_n is a lognormal variate (or deterministic quantity), it can be shown that $\ln(\zeta)$ is a normal variate with the mean

$m_{\ln(\zeta)}$ and standard deviation $\sigma_{\ln(\zeta)}$ given by,

$$m_{\ln(\zeta)} = \ln\left(\frac{m_{R_n}}{\sqrt{1 + v_{R_n}^2}}\right) + \ln\left(\frac{L_m}{R_o R_d}\right) - \ln\left(\frac{m_L}{\sqrt{1 + v_s^2}}\right), \quad (3.13)$$

and,

$$\sigma_{\ln(\zeta)} = \sqrt{\ln(1 + v_{R_n}^2) + \ln(1 + v_L^2)}, \quad (3.14)$$

where m_{R_n} and v_{R_n} denote the mean and cov of R_n , respectively. The values of L_m , m_{R_n} and v_{R_n} for each building are given in Table 3.1.

For the equivalent nonlinear inelastic SDOF system, the condition that ζ is less than 1 implies that the response of the system is within nonlinear inelastic range, therefore, the probability of incipient damage of designed structure, P_D is,

$$P_D = \text{Pr ob}(\zeta < 1) = \Phi\left(-m_{\ln(\zeta)} / \sigma_{\ln(\zeta)}\right), \quad (3.15)$$

The probability of incipient collapse, P_C , for a structure with the displacement ductility capacity, μ_R , can be evaluated based on the limit state, g_C , defined by,

$$g_C = \mu_R / \mu_{\max} - 1, \quad (3.16)$$

in which μ_R is the ductility capacity of the structure; μ_{\max} represents the peak ductility demand (i.e., the maximum normalized yield displacement) for an SDOF system governed by Eqs. (3.8) and (3.10) during an earthquake event. This leads to,

$$P_C = \Pr \text{ob}(\mu_R / \mu_{\max} < 1 | \zeta < 1) \Pr \text{ob}(\zeta < 1), \quad (3.17)$$

Note that that μ_R for steel structures could be considered as a lognormal variate with the mean and cov of μ_R , denoted by m_{μ_R} and v_{μ_R} , respectively (Diaz-Lopez and Esteva 1991). This probabilistic model is also adopted for the considered wood buildings. The statistical characterizations of μ_{\max} for a nonlinear equivalent SDOF system (Hong and Hong 2007; Goda et al. 2009) can be carried out by using a set of selected ground motion records. In particular, for the present study, the statistical characterizations of μ_{\max} for the considered equivalent SDOF systems are carried out by solving Eqs. (3.8) and (3.10) for a set of 762 horizontal record components from 31 California earthquakes is considered. This set of records is a subset of records considered in Hong and Goda (2007) which is used in Goda et al. (2009). The records are obtained from NGA database (<http://peer.berkeley.edu/nga/index.html>). As the low-cut filter corner frequency used in processing the raw record affects the calculated elastic and inelastic peak responses of SDOF systems (Akkar and Bommer 2006; Tothong and Cornell 2006), a low-cut filter corner frequency of 0.2 Hz is considered in selecting the considered records. The use of such a low-cut filter corner frequency is based on the trade-off between the adequacy of strong ground motions for relatively long vibration period of ground motions and the number of available records. For a range of ζ values, the obtained samples of μ_{\max} are presented in Figure 3.6.

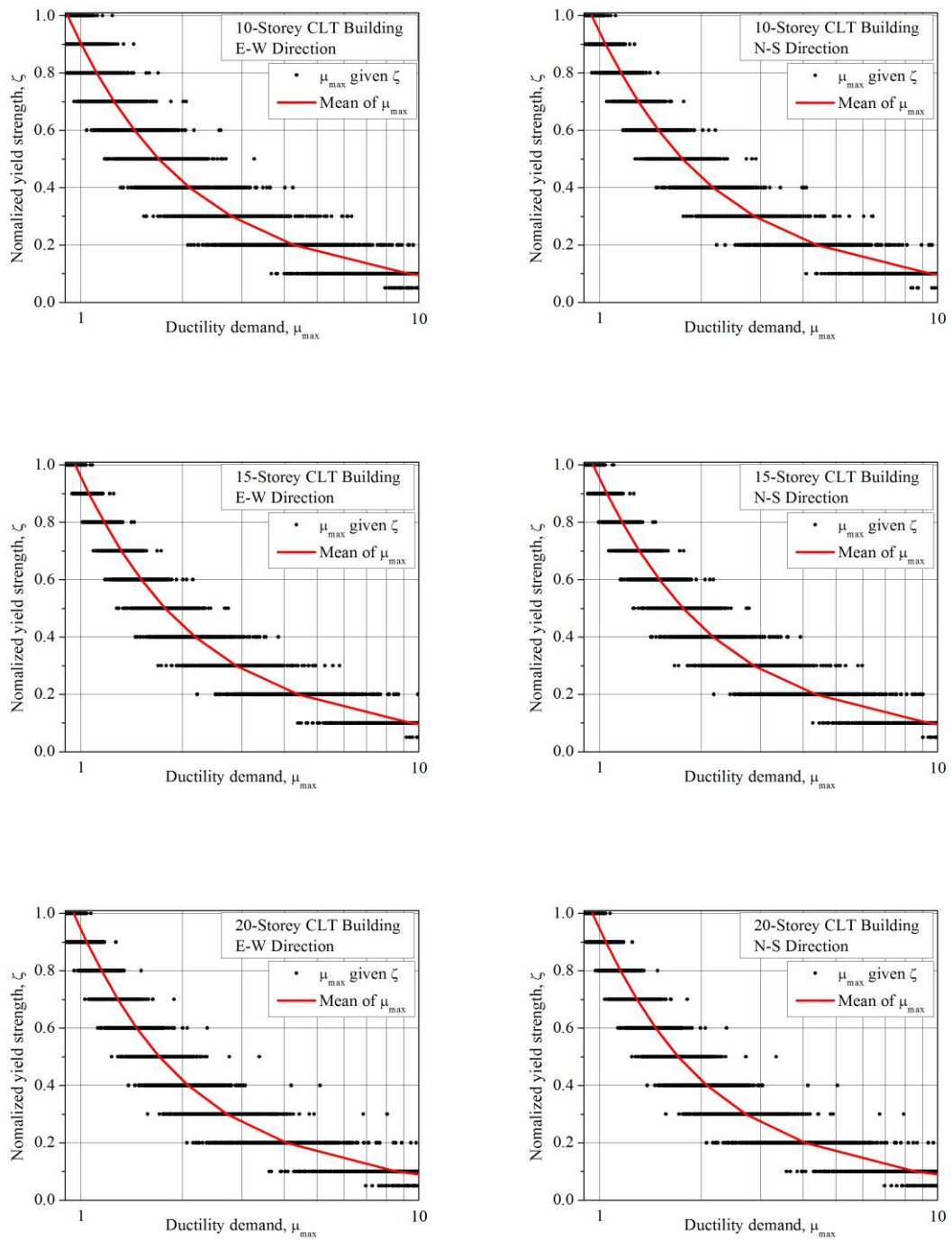


Figure 3.6. Estimated ductility demand for the equivalent SDOF systems.

Probability distribution fitting exercise is carried out using the obtained samples of μ_{\max} conditioned on ζ . For the fitting, the (shifted) lognormal, Frechet, Weibull, and gamma distributions with a shift to limit $\mu_{\max} \geq 1.0$ are considered. The use of the maximum likelihood criterion (or the Akaike information criterion (AIC)) indicates that the Frechet distribution is preferred among the considered distribution types. Also, a visual inspection of the samples of μ_{\max} conditioned on ζ presented in Figure 3.7 in the (shifted) Frechet probability paper indicates that the use of such a probabilistic model is adequate.

Based on the above formulation, P_C shown in Eq. (3.17) can be evaluated using Monte Carlo technique according to the following steps:

- 1) Sample ζ , according to the probability distribution function of ζ ;
- 2) For $\zeta < 1$, do the following:
 - 2.1) Calculate the mean and cov of μ_{\max} according to the developed relations from the samples of μ_{\max} shown Figure 3.6, and find the Frechet distribution parameters for μ_{\max} ;
 - 2.2) Sample μ_{\max} and μ_R , and calculate $g_C = \mu_R / \mu_{\max} - 1$;
- 3) Repeat Steps 1) and 2) sufficient cycles and estimate P_C as the ratio of the number of times that $g_C < 0$ to the total number of cycles.

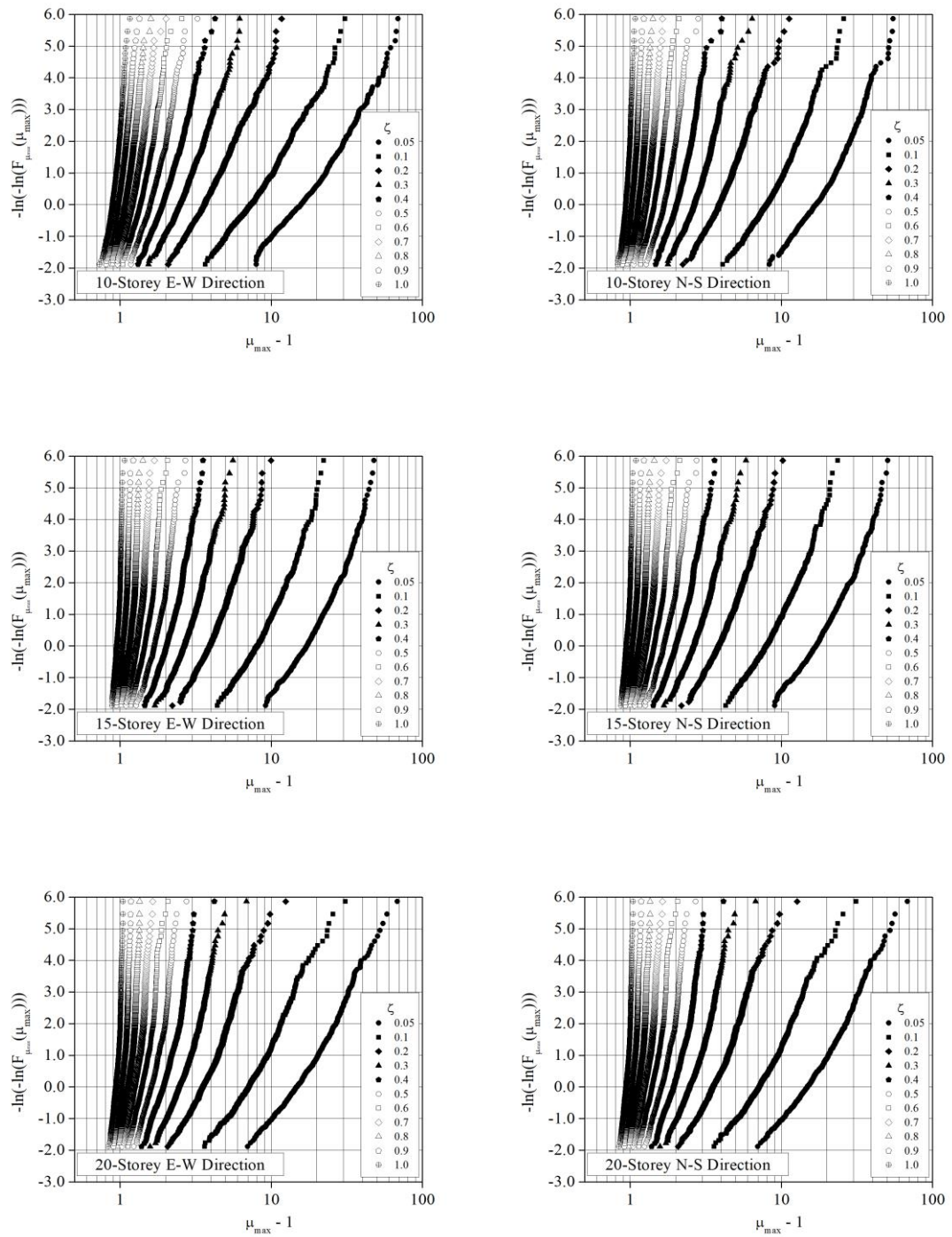


Figure 3.7. Samples of maximum ductility demand presented in the (shifted) Fréchet distribution paper.

3.4.2 Analysis results

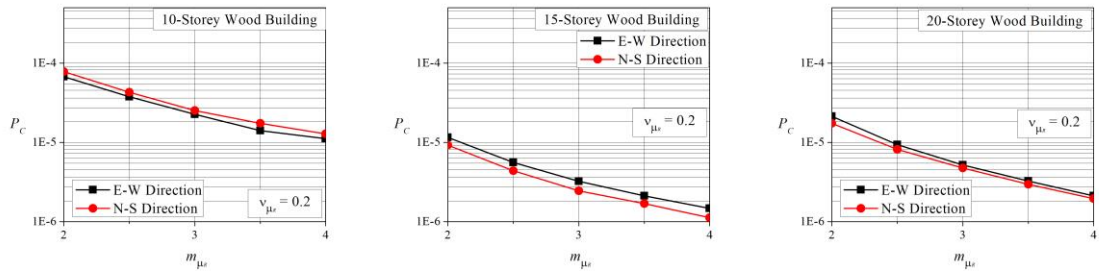
An evaluation of P_D and P_C for the designed 10-, 15-, and 20-storey wood buildings is carried out based on the formulation and evaluation procedure given in the previous section. The estimated P_D and the corresponding reliability index $\beta_{P_D} = -\Phi^{-1}(P_D)$ are shown in Table 3.3. In all cases, the estimated P_D values are in the order of 10^{-4} . Note that there is no guideline on the tolerable P_D for the code development.

Table 3.3. Estimated probabilities of the incipient damage P_D .

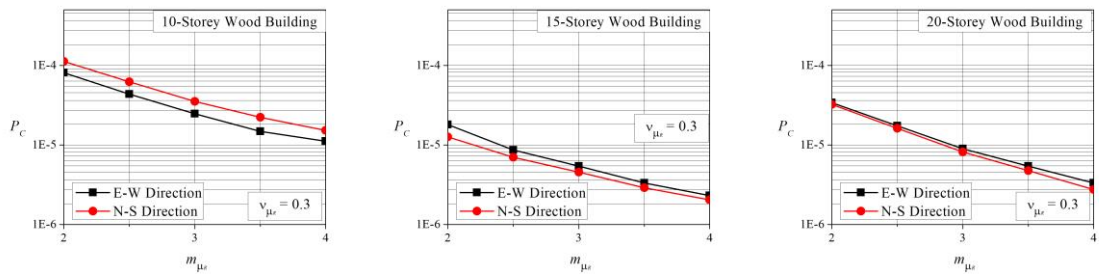
Design	Direction	P_D	β_{P_D}
10-Storey	E-W	7.05E-04	3.19
	N-S	7.66E-04	3.17
15-Storey	E-W	8.83E-05	3.75
	N-S	5.53E-05	3.87
20-Storey	E-W	3.02E-04	3.43
	N-S	2.99E-04	3.43

The calculated P_C for the mean of μ_R range from 2 to 4 and a cov of 0.3 (inferred from the behaviour of CLT panels) (Popovski et al. 2011; Gavric et al. 2015a, 2015b) are shown in Figure 3.8. It can be observed that in all cases the estimated P_C is below 2.5×10^{-4} . This value is slightly lower than or equal to that associated with steel frames designed according to NBCC subjected to earthquake load given in Hong et al. (2010). It is also comparable to the system reliability of steel frames subjected to permanent and live loads (Zhou and Hong 2004). As the failure probability of the overall system is about one order of magnitude lower than the failure probability of the most critically loaded member (Zhou and Hong 2004), and a tolerable annual failure probability of about 2.7×10^{-5} is adopted to calibrate load factors implemented in NBCC based on structural member performance (Bartlett et al. 2013), the results obtained in this section indicates that the use of the current approach in the NBCC and the wood design practice is adequate if the ultimate limit state under seismic load is of concern. The fact that the P_C values for the wood buildings are lower

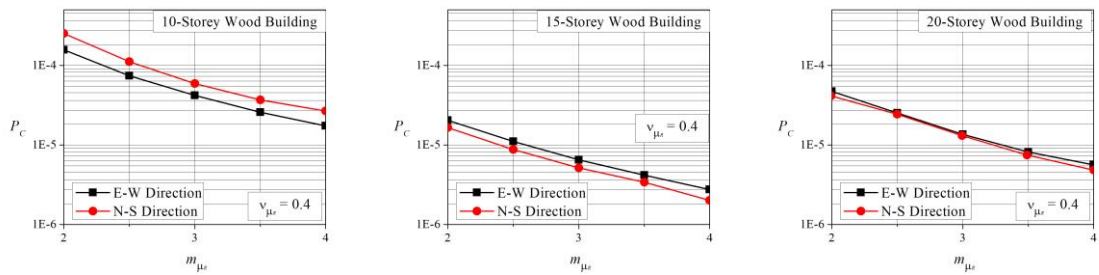
than those for the steel frame structures can be explained by noting that the design of the considered wood buildings are governed by drift or serviceability requirement under wind or earthquake load which resulted significant overstrengthening. In addition, the results shown in Figure 3.8 indicates that the estimated P_C varies significantly for the range of the considered mean of the ductility capacity value. For example, P_C decreases by one order of magnitude for m_{μ_R} varying from 2 to 4. Furthermore, since the considered cov of μ_R is inferred from the behaviour of CLT panels rather the structural system, a sensitivity analysis of P_C to the cov of μ_R is carried out by considering the cov of μ_R equal to 0.2 and 0.4. The estimated P_C for these cases are also shown in Figure 3.8. Comparison of the results shown in the figure indicates that the cov of μ_R does influence the estimated P_C . The above results suggest that there is need and incentive to carry out experimental or detailed numerical investigation to gather sufficient statistical data on the ductility capacity of mid- and high-rise wood buildings to narrow the range of the estimated P_C values.



a) $v_{\mu_R} = 0.2$



b) $v_{\mu_R} = 0.3$



c) $v_{\mu_R} = 0.4$

Figure 3.8. Estimated annual failure probability P_c : a) $v_{\mu_R} = 0.2$; b) $v_{\mu_R} = 0.3$; c)

$v_{\mu_R} = 0.4$.

3.5 Conclusions

Reliability analysis is carried out for three wood buildings that are designed to satisfy requirements in applicable structural design codes in Canada. The analysis considers that the response of the wood buildings under seismic excitations can be approximated by the response of an equivalent nonlinear inelastic single-degree-of-freedom (SDOF) system, where the nonlinear behaviour is represented by Bouc-Wen model. The procedure to identify the parameters of this simple equivalent model is given based on the capacity curve obtained from nonlinear static pushover analysis or the incremental dynamic analysis.

By considering the equivalent nonlinear inelastic SDOF system and the effect of record-to-record variability on the seismic ductility demand and, by incorporating the design considerations, the probabilities of the incipient damage and of incipient collapse are estimated. The results indicate that the estimated probability of incipient collapse is similar to or lower than that obtained for steel frame structures designed according to codified Canadian design practice. This suggests that the use of the heavy timber as mid- and high-rise building construction material is adequate for earthquake load.

It must be emphasized that the ductility capacity of the wood building system is unknown and the use of the assumed values serves as a parametric investigation. To gain further support in using heavy timber as building construction material, there is need and incentive to carry out experimental investigation to gather sufficient statistical data on the ductility capacity of mid- and high-rise wood building systems so to further validate the estimated failure probability.

3.6 References

Akkar, S., and Bommer, J. J. (2006). Influence of long-period filter cut-off on elastic spectral displacements. *Earthquake Engineering and Structural Dynamics*, 35(9), 1145-1166.

Ansys, (2012). ANSYS multiphasics version 14.5. *Ansys Inc., Canonsburg, PA.*

- Bartlett, F. M., Hong, H. P., and Zhou, W. (2003). Load factor calibration for the proposed 2005 edition of the National Building Code of Canada: Statistics of loads and load effects. *Canadian Journal of Civil Engineering*, 30(2), 429-439.
- Canadian Standard Association. (2009). Engineering Design of Wood. *Standard CSA O86-09*. Canadian Standards Association, Mississauga, ON, Canada.
- Canadian Wood Council. (2010). Wood Design Manual. CWC, Ottawa, ON, Canada
- Chopra, A. K. (2001). Dynamics of structures: Theory and applications.
- Cornell, C. A., Jalayer, F., Hamburger, R. O., and Foutch, D. A. (2002). Probabilistic basis for 2000 SAC federal emergency management agency steel moment frame guidelines. *Journal of Structural Engineering*, 128(4), 526-533.
- Díaz-López, O., and Esteva, L. (1991). Calibrating simplified models for computation of seismic reliability of multistory frames. *Proceeding of ICASP6 (eds. Esteva, L, and S Ruiz.)*, Institute of Engineering, Mexico, DF, Mexico, 328-337.
- Foliente, G. C. (1995). Hysteresis modeling of wood joints and structural systems. *Journal of Structural Engineering*, ASCE, 121(6), 1013-1022.
- Foliente, G. C., Paevere, P., Saito, T., and Kawai, N. (2000). Reliability assessment of timber shear walls under earthquake loads. In *Proc., 12th World Conf. Earthquake Engineering*.
- FPIinnovations. (2011). CLT Handbook – Cross-Laminated Timber, *FPIinnovations*, Quebec, Quebec, Canada.
- Gavric, I., Fragiaco, M., and Ceccotti, A. (2015a). Cyclic behaviour of typical screwed connections for cross-laminated (CLT) structures. *European Journal of Wood and Wood Products*, 73(2), 179-191.

- Gavric, I., Fragiacomio, M., and Ceccotti, A. (2015b). Cyclic behaviour of typical metal connectors for cross-laminated (CLT) structures. *Materials and structures*, 48(6), 1841-1857.
- Goda, K., Hong, H. P., and Lee, C. S. (2009). Probabilistic characteristics of seismic ductility demand of SDOF systems with Bouc-Wen hysteretic behaviour. *Journal of Earthquake Engineering*, 13(5), 600-622.
- Hong, H. P., Goda, K., and Davenport, A. G. (2006). Seismic hazard analysis: a comparative study. *Canadian Journal of Civil Engineering*, 33(9), 1156-1171.
- Hong, H. P., and Goda, K. (2007). Orientation-dependent ground-motion measure for seismic-hazard assessment. *Bulletin of the Seismological Society of America*, 97(5), 1525-1538.
- Hong, H. P., and Hong, P. (2007). Assessment of ductility demand and reliability of bilinear single-degree-of-freedom systems under earthquake loading. *Canadian Journal of Civil Engineering*, 34(12), 1606-1615.
- Hong, H. P., Hong, P., and Wang, W. (2010). Reliability of steel frames designed in accordance with the National Building Code of Canada seismic provisions and its implication in codified design. *Engineering Structures*, 32(5), 1284-1291.
- Koduru, S. D., and Haukaas, T. (2010). Feasibility of FORM in finite element reliability analysis. *Structural Safety*, 32(2), 145-153.
- Lee, K. H., and Rosowsky, D. V. (2006). Fragility analysis of woodframe buildings considering combined snow and earthquake loading. *Structural Safety*, 28(3), 289-303.
- Ma, F., Zhang, H., Bockstedte, A., Foliente, G. C., and Paevere, P. (2004). Parameter analysis of the differential model of hysteresis. *Journal of Applied Mechanics*, 71(3): 342-349.
- Madsen, H. O., Krenk, S., and Lind, N. C. (2006). Methods of structural safety. *Courier Corporation*.

- Maruyama, O., Shinozuka, M., and Daigaku, M. K. (1989). Program EXKAL2 for identification of structural dynamic systems. *National Center for Earthquake Engineering Research*.
- MGB Architecture and Design. (2012). Tall Wood Report. *MGB Architecture and Design*.
- NEWBuilds. (2015). Application of Analysis Tools from NEWBuildS Research Network in Design of a High-Rise Wood Building, *Network on Innovative Wood Products and Building Systems (NEWBuildS)*, University of New Brunswick, Fredericton, New Brunswick, Canada.
- NGA database. Next Generation Attenuation <http://peer.berkeley.edu/nga/index.html>. 325 *Davis Hall, University of California, Berkeley, CA 94720-1792*
- NRC Canada (2010a). National Building Code of Canada, *NRC Canada*, Ottawa, Ontario, Canada.
- NRC Canada (2010b). *User's Guide – NBC 2010, Structural Commentaries (Part 4 of Division B)*, NRC Canada, Ottawa, Ontario, Canada.
- Pang, W., Rosowsky, D. V., Ellingwood, B. R., and Wang, Y. (2009). Seismic fragility analysis and retrofit of conventional residential wood-frame structures in the central United States. *Journal of structural engineering*, 135(3), 262-271.
- Pei, S., van de Lindt, J. W., and Popovski, M. (2012). Approximate R-factor for cross-laminated timber walls in multistory buildings. *Journal of Architectural Engineering*, 19(4), 245-255.
- Popovski, M., Karacabeyli, E., and Ceccotti, A. (2011). Seismic Performance of Cross-Laminated Timber Buildings. *Chapter 4 of the Handbook on Cross-Laminated Timber. FPInnovations Special Publication SP-528E*, ISBN 978-0-86488-547-0.
- Rosowsky, D. V., and Ellingwood, B. R. (2002). Performance-based engineering of wood frame housing: Fragility analysis methodology. *Journal of Structural Engineering*, 128(1), 32-38.

- Sues, R. H., Mau, S. T., and Wen, Y. K. (1988). Systems identification of degrading hysteretic restoring forces. *Journal of Engineering Mechanics*, 114(5), 833-846.
- Tothong, P., and Cornell, C. A. (2006). An empirical ground-motion attenuation relation for inelastic spectral displacement. *Bulletin of the Seismological Society of America*, 96(6), 2146-2164.
- Vamvatsikos, D., and Cornell, C. A. (2002). Incremental dynamic analysis. *Earthquake Engineering and Structural Dynamics*, 31(3), 491-514.
- van de Lindt, J. W., and Walz, M. A. (2003). Development and application of wood shear wall reliability model. *Journal of Structural Engineering*, 129(3), 405-413.
- Zhou, W., and Hong, H. P. (2004). System and member reliability of steel frames. *Steel and Composite Structures*, 4(6), 419-435.

Chapter 4

4 Assessing the Capacity Surface of Mid- and High-rise Wood Buildings under Bidirectional Seismic Excitations

4.1 Introduction

The performance-based procedure to evaluate existing or designed new buildings under seismic loading is well accepted. A main component of the evaluation is focused on the structural capacity to sustain seismic demand, such as the displacement or drift demand. The estimation of the capacity is frequently carried out for structures subjected to unidirectional excitations, and both nonlinear static or dynamic analyses can be used. Reviews of the practical nonlinear methods for such a purpose are given in Fajfar (2002) and Aydinoglu (2003), indicating that many of the procedures are associated with the concept of capacity spectrum method (Freeman et al. 1975), and with the use of an equivalent nonlinear inelastic single-degree-of-freedom (SDOF) system to approximate the nonlinear behaviour of multi-degree-of-freedom (MDOF) system (Saiidi and Sozen 1981). The adequacy of the use of the nonlinear inelastic SDOF system in such a context was extensively discussed by many, including Fajfar and Fischinger (1988), Vidic et al. (1994), and Fajfar (2000). These methods, in one form or another, formed the basis for some of the recommended design requirements implemented in codes and standards. The most frequently used procedures to identify the structural capacity curve are the nonlinear static pushover analysis (NSPA) and the incremental dynamic analysis (IDA).

For the NSPA, a displacement independent or invariate along height load pattern needs to be selected; commonly used patterns are the inverted triangle, or first (sway) vibration mode shape. However, the use of any invariate load pattern is not consistent with the progressive yielding of the structure during pushover analysis, and cannot capture the higher mode effects. To overcome the former and potentially improve the accuracy, the analysis could be carried out by applying the adaptive load patterns at each pushover step defined using the results from response spectrum method with the modes calculated based on the tangent stiffness matrix (Elnashai 2002; Antoniou et al. 2002). To overcome the latter, the modal pushover analysis (MPA) procedure (Paret et al. 1996; Sasaki et al. 1998;

Chopra and Goel 2001) could be used. The MPA is similar to the single-mode pushover analysis but it is extended to multiple-mode; the peak responses of the structure are then obtained by applying the modal combination rules using the responses calculated from the pushover analysis for each mode. However, a theoretical foundation to use the modal combination rules for inelastic responses is not clear. Additional analysis procedures by incorporating these concepts are also developed in Gupta and Kunnath (2000), Kalkan and Kunnath (2004, 2006) and Aydinoglu (2003). Furthermore, the direct use of IDA to evaluate the capacities of the structures in sustaining engineering demand is also advanced (Vamvatsikos and Cornell 2002; Giovenale et al. 2004), although it can be computationally intensive task and the selection of the optimum ground motion measure to be used to scale the records is not trivial. A comparison of results from simple inelastic pushover analysis and dynamic analysis for a set of reinforced concrete buildings indicated their good correlation, verifying the usefulness of the nonlinear static pushover analysis for practical applications (Mwafy and Elnashai 2001).

The above-mentioned studies are focused on the structures under unidirectional seismic excitations. Rosenblueth and Contreras (1977) investigated the structural responses under multi-component earthquake ground motions. The subject of structural responses under multi-component seismic excitations was also investigated by other, including Lopez and Terres (1997), Menun and Der Kiureghian (1998), and Athanatopoulou (2005). These studies are focused on linear elastic responses.

An early experimental work by Takizawa and Aoyama (1976) showed that structural members subjected to bidirectional loading have deformation larger than that under unidirectional loading. Similar observation was made by Zeris and Mahin (1991) indicating that the deteriorations of the strength and stiffness of reinforced concrete members under biaxial bending are greater than those under uniaxial response. In fact, the bidirectional cyclic loads will lead to the reduction of the capacity of the structure because of the biaxial interaction effects on the lateral load resisting system. Analysis procedures to calculate the nonlinear inelastic responses under multi-component seismic excitations were also reported in the literature. For example, Reyes and Chopra (2011) extended MPA to analyze asymmetric-plan buildings subjected to multi-component ground motions, where the

responses subjected to each of the three ground motion components is obtained from MPA independently, the responses are then combined by using a modal combination rule considering multi-component excitations. This approach is also considered by others (Manoukas et al. 2012; Poursha et al. 2014; Shakeri and Ghorbani 2015). Again, theoretical justifications of using the modal combination rule to nonlinear inelastic responses are not elaborated.

Furthermore, the application of the IDA is extended to estimate the capacity curve under bidirectional horizontal ground motions (Vamvatsikos 2006; Lagaros 2010). In such a case, a set of ground motion records is selected for the time history analysis; the two horizontal orthogonal components for each selected record are scaled equally by the same scaling factors. Similar to the case of uniaxial excitations, the maximum responses of interest and the intensity measures are then used to form the IDA curve for each considered ground motion record. However, unlike the case of the uniaxial excitations, the incidence angle for the excitation in the horizontal plan needs to be considered. Also, the selection of the response of interest to define the capacity curve is not a trivial task. For example, by using the maximum drift ratio or the maximum (roof) horizontal displacement as the response of interest, the IDA curve may not necessarily fall within the same vertical plan because the maximum roof horizontal displacements for a series of scaling factors projected on the horizontal plane may not fall on a straight line due to inelastic behaviour. Also, the ductility capacity within different vertical planes could differ. Therefore, the consideration of the capacity surface rather than capacity curve is preferred, especially in the context of reliability analysis (Mara and Hong 2013; Yang et al. 2017).

In addition to the above, the application of wood laminating technique has led to wood composites with improved properties as compared to sawn lumber. Engineered wood composites such as structural composite lumber (SCL), laminated veneer lumber (LVL) and cross-laminated timber (CLT) can be used to construct tall wood buildings (Pang et al. 2010; Gagnon et al. 2010; MGB 2012; NEWBuildS 2015). However, the characteristics of seismic behaviour of such buildings subjected to bidirectional seismic ground motions are unknown, and could discourage practicing engineers in using wood or composite wood material in design and construction of tall buildings.

The main objectives of the present chapter are: to evaluate the responses of wood buildings designed to satisfy the requirements in the National Building Code of Canada (NBCC) (NRCC 2010) and CAN/CSA O86-09 (CSA 2009) under bidirectional seismic excitations, to characterize the capacity surface under bidirectional seismic excitations, and to discuss the major differences between the capacity curve and capacity surface under seismic loading. The evaluation of the responses needed to define the capacity surface is carried out by using IDA considering bidirectional orthogonal horizontal ground motions. Also, the use of NSPA is considered as a simple practical alternative. To account for the effect of the incidence angle of bidirectional excitations on the structural capacity, the analysis is carried out by rotating the axes of the bidirectional horizontal excitations relative to the structural axis. The obtained responses from IDA and NSPA for each incidence angle are used to form the capacity surface, which is defined as the total base shear versus the maximum roof displacements decomposed in the two orthogonal axes in the horizontal plan of the structure. Furthermore, the implication from the obtained capacity surface on the performance-based design procedures of the mid- and high-rise wood buildings is discussed.

4.2 Response characteristics of designed wood buildings under bidirectional horizontal seismic load

4.2.1 Designed tall wood buildings

This section is similar to Section 3.2; it is presented in here to facilitate the reader. The design of the wood building includes the consideration of appropriate design methodology, reasonable assumptions, and common practice in structural engineering and architecture. Details on the design procedures and the designed 10-, 15- and 20-storey buildings with footprint of 24 m × 23.2 m are given in Chapter 2. The essential considerations of the design and modeling are:

- 1) The height of first storey is 4.4 m, and upper storeys are 3.2 m; the CLT panels are used for floors, roof, shear walls, elevator shaft; the glulam is used for beams and columns;
- 2) The design was carried out for seismic load and checked for wind load. It was concluded that the design is governed by inter-storey drift limits due to earthquake or wind, or vibration limit under wind load (NRCC 2010b); and

3) Finite element models are developed for the designed wood building by considering the nonlinear behaviour of connectors among the panels.

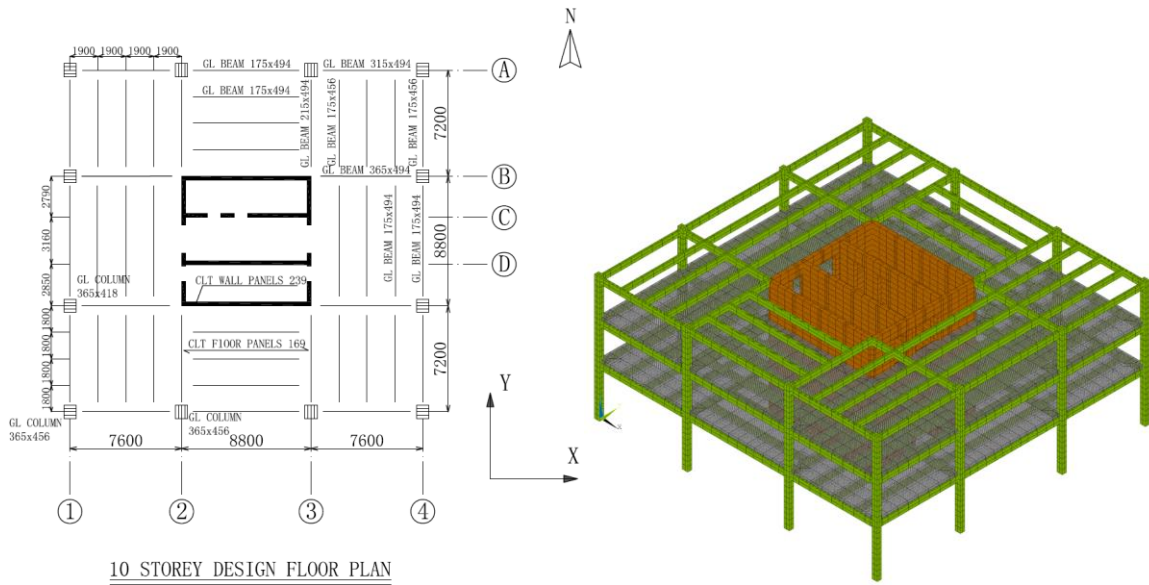


Figure 4.1. Designed 10-Storey wood building

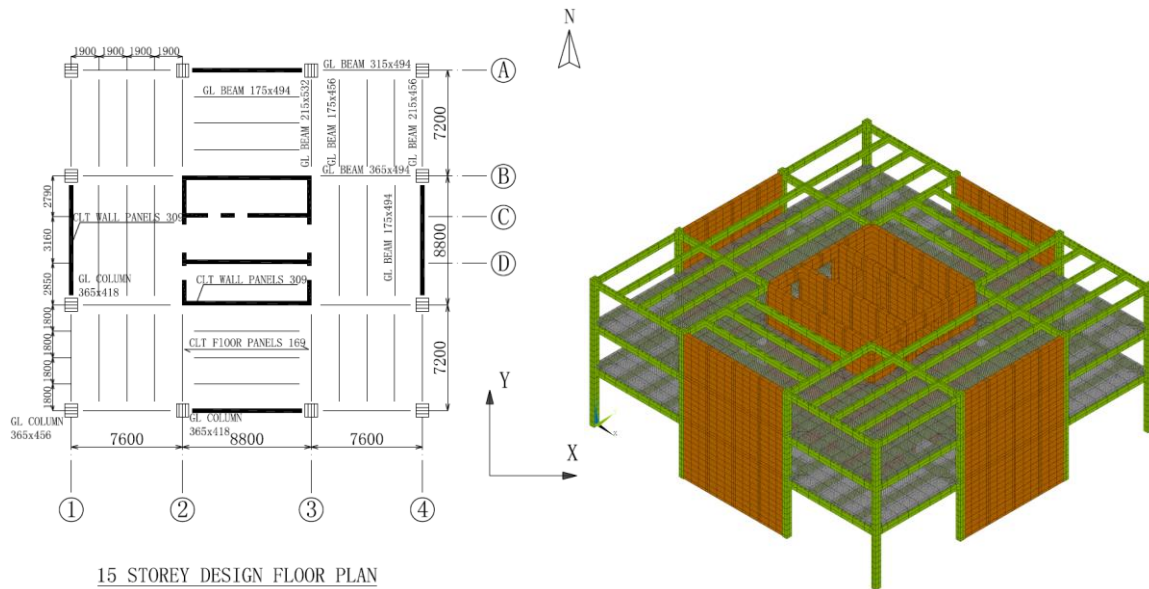


Figure 4.2. Designed 15-Storey wood building.

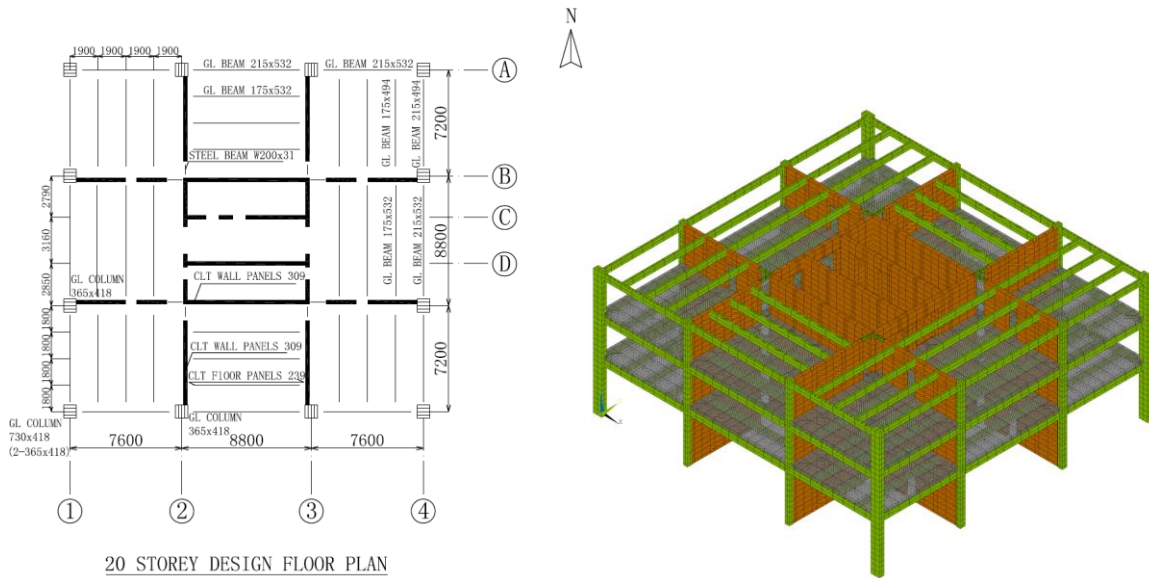


Figure 4.3. Designed 20-Storey wood building.

4.2.2 Evaluation of the capacity surface under bidirectional horizontal ground motions

To evaluate the capacity of the designed wood buildings under bidirectional seismic excitations, the IDA can be used (Vamvatsikos and Cornell 2002; Vamvatsikos 2006; Lagaros 2010). This analysis consists of carrying out a series of nonlinear dynamic analyses by applying the scaled ground motion records with increased ground motion intensities. The study by Vamvatsikos and Cornell (2002) is focused on the response subjected to unidirectional ground motion component while those by Vamvatsikos (2006) and Lagaros (2010) consider the bidirectional horizontal ground motions. In the latter, the two horizontal record components are scaled equally (i.e., by the same scaling factor), and the series of the scaled record components are associated with increased intensities. This procedure is used in the following numerical analysis.

For the IDA with bidirectional excitations, 11 ground motion records, each with two horizontal orthogonal component, are selected from the NGA database (<http://peer.berkeley.edu/nga/index.html>) as shown in Table 4.1. The criteria used to select the records are already given in Chapter 2.

Table 4.1. Selected ground motion records.

No.	NGA #	Event	Station	Moment Magnitude
1	31	Parkfield	Cholame - Shandon Array #8	6.19
2	36	Borrego Mtn	El Centro Array #9	6.63
3	62	San Fernando	Colton - So Cal Edison	6.61
4	165	Imperial Valley-06	Chihuahua	6.53
5	463	Morgan Hill	Hollister Diff Array #1	6.19
6	718	Superstition Hills-01	Wildlife Liquef. Array	6.22
7	721	Superstition Hills-02	El Centro Imp. Co. Cent	6.54
8	744	Loma Prieta	Bear Valley #12, Williams Ranch	6.93
9	841	Landers	Boron Fire Station	7.28
10	960	Northridge-01	Canyon Country - W Lost Cany	6.69
11	1762	Hector mine	Amboy	7.13

For the time history analysis, first, consider the 10-storey building shown in Figure 4.1 and No. 4 ground motion record listed in Table 4.1. By aligning the first and second horizontal record components with the X - and Y -axes of the structure (see Figure 4.3 and 4.4), the IDA is carried out for a series of increasing scaling factors. The incidence angle equals α if the two ground motion components are oriented in the X' - and Y' -axes as shown in Figure 4.4. Due to the complexity of the 3D finite element model, the time history analysis for a single record and one scaling factor (i.e., a single run) is about 7 hours by using a desktop computer (Intel Core i7, 8G RAM). The IDA analysis is stopped if the roof drift ratio exceeds 2%. The consideration of this drift ratio is consistent with those suggested by Filiatrault and Folz (2002), Ellingwood et al. (2008) and Pei et al. (2015).

For each considered scaling factor, the following quantities are obtained or extracted from nonlinear time history analysis:

- 1) The maximum of the spectral acceleration by considering each of the horizontal ground motion components, $S_{2A}(T_1, \xi)$, where T_1 denotes the fundamental vibration of the structure, and ξ is the damping ratio which is taken equal to 0.05;
- 2) The maximum base shear V ,

$$V = \max_t \left(V_x(t)^2 + V_y(t)^2 \right)^{1/2} \quad (4.1)$$

where $V_x(t)$ and $V_y(t)$ are the base shears along the X - and Y -axes at time t , respectively;

3) The maximum roof displacement,

$$D = \max_t \left(D_x(t)^2 + D_y(t)^2 \right)^{1/2} \quad (4.2)$$

where $D_x(t)$ and $D_y(t)$ are the roof displacements along the X - and Y -axes at time t , respectively. The time leading to D is denoted as t_{\max} ;

4) The displacements along the X - and Y -axes at time t_{\max} , are denoted as D_x and D_y . The trajectory of (D_x, D_y) is presented in Figure 4.5a while the relation between V and D is shown in Figure 4.5b.

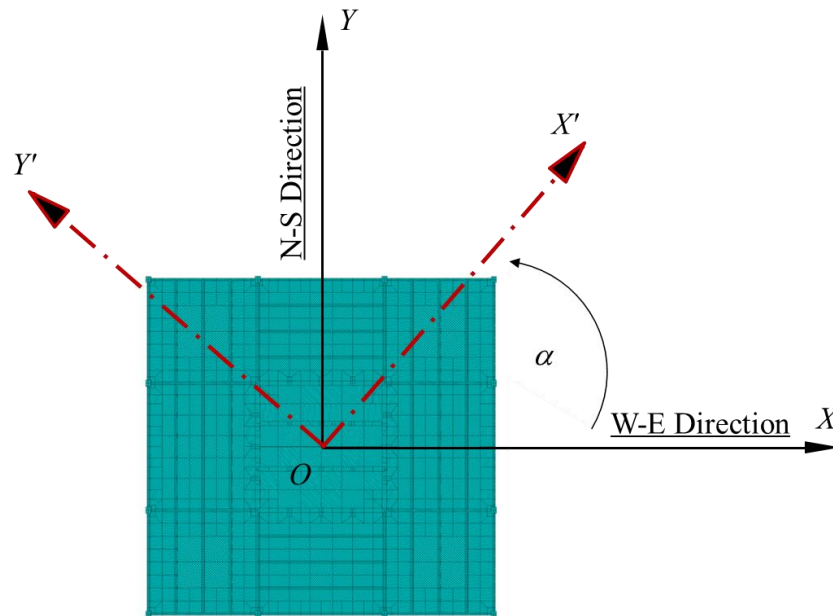


Figure 4.4. Definition of the earthquake incidence angle α .

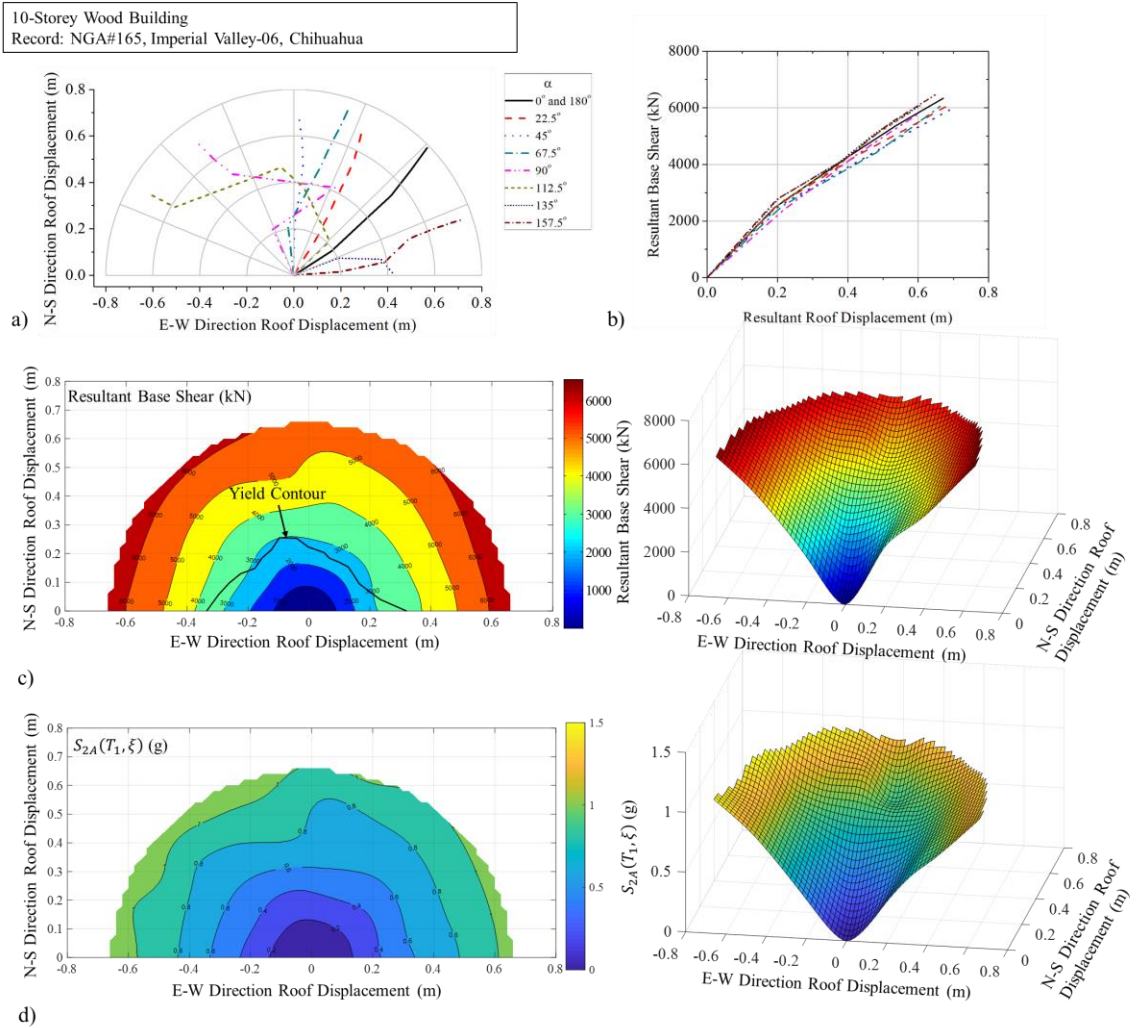


Figure 4.5. Capacity of the 10-storey wood building under bidirectional horizontal orthogonal ground motions by considering Record # 4 listed in Table 4.1: a) Trajectory of the maximum displacement projected in the horizontal plane; b) capacity curve; c) capacity surface considering the base shear; d) capacity surface using $S_{2A}(T_1, \xi)$ as the ground motion measure.

Figure 4.5a shows that the values of (D_x, D_y) do not fall on the X -axis is expected since bidirectional ground motions are considered. The trajectory of (D_x, D_y) does not follow a straight line, indicating that the values of (D_x, D_y) do not fall in the same vertical plane. Figure 4.5b shows that the capacity curve represented by V and D resembles the shape of a typical curve that could be obtained for a 2D structure under unidirectional ground motions.

To take into account the influence of the incidence angle on the seismic response of the structure, the IDA analysis is carried out by rotating the directions of the two horizontal orthogonal ground motion components with respect to the X -axis as shown in Figure 4.4. Since the considered structural is bisymmetric, the responses obtained based on incidence angle equal to $\alpha + 180^\circ$ are the same but opposite sign as those obtained by using incidence angle equal to α . The trajectory of (D_x, D_y) obtained for the incidence angle equals to α is identical to the trajectory of (D_x, D_y) obtained for the incidence angle equals to $\alpha + 180^\circ$. Therefore, the assessment of the effect of incidence angle will be carried out by varying α from 0° to 180° only to reduce the computation. If the trajectory of (D_x, D_y) obtained for an incidence angle falls in the third and fourth quadrates, at least based on the linear elastic responses, the whole trajectory of (D_x, D_y) is rotated by 180° counterclockwise and plotted. To emphasize this, the notation (D_x, D_y) is replaced (D_{px}, D_{py}) .

For the analysis, α varying from 0° to 180° with an increment of 22.5° is carried out. This makes that the total computing time remains manageable for all the numerical analysis to be carried out in this chapter and, that the sensitivity of structural capacity to the incidence angle under seismic load can still be appreciated.

The analysis results for cases with α greater than zero, are also shown in Figures 4.5a and Figure 4.5b. Figure 4.5a shows that the trajectories of (D_{px}, D_{py}) for different values of α can intersect. Therefore, a value of (D_{px}, D_{py}) may correspond to several ground motion intensities or base shears. The capacity curves (each may not necessarily fall in the same vertical plane) shown in Figure 4.5b are similar. However, this does not mean that the use of a nonlinear inelastic single-degree-of-freedom (SDOF) system as a proxy for the considered building under bidirectional ground motions is adequate. This is because that

the values of (D_{px}, D_{py}) leading to V for a capacity curve do not fall within the same vertical plane, and that the inelastic displacement capacity of the building along different direction may differ.

To better appreciate the structural response under bidirectional horizontal orthogonal ground motions, a plot of the capacity surface defined by V, D_{px} and D_{py} is shown in Figure 4.5c while that defined by $S_{2A}(T_1, \xi), D_{px}$ and D_{py} is shown in Figure 4.5d. In the plots, the yield points are identified. In general, it can be observed that the curve associated with the yield points do not follow a circle for this considered building. Also, the points for a given base shear value or $S_{2A}(T_1, \xi)$ follows an irregular line; the capacity surface obtained for a record is not very smooth, especially for the region where the displacements are beyond the yield.

The above procedure to assess the capacity surface for bisymmetric building can be summarized as follows:

- 1) Select an appropriate ground motion record with two horizontal orthogonal components;
- 2) For $\alpha = 0$, carry out IDA using equally scaled record components and extract the base shear, D_{px} and D_{py} for each considered record scaling factor;
- 3) For a series of α values ranging from 0° to 180° , repeat the analysis in Steps 2) and 3);
and
- 4) Plot the triplets (base shear, D_{px} and D_{py} ; or $S_{2A}(T_1, \xi), D_{px}$ and D_{py}).

For cases where symmetry cannot be accounted for, α ranging from 0° to 360° needs to be considered, and the capacity surface can be defined based on the base shear, D_x and D_y .

To appreciate the impact of the record-to-record variability on the estimated capacity surface, the above analysis is repeated for Record # 8 listed in Table 4.1. The obtained results are shown in Figure 4.6. Comparison of the results shown in Figures 4.5 and 4.6 indicates that the capacity surface and the seismic response characteristics under bidirectional horizontal orthogonal ground motions are influenced by the selected record. This record-to-record variability on the statistics of capacity surface will be considered in the next section.

The analysis that is carried out for the 10-storey building is repeated for the 15-storey and 20-storey buildings. The obtained results are shown in Figures 4.7 to 4.10. Inspection of the results shown in Figures 4.7 to 4.10 indicates that the observations drawn from Figure 4.5 and 4.6 are equally applicable to Figures 4.7 to 4.10, except that the shape of the curve corresponds to the yield points differs for different buildings.

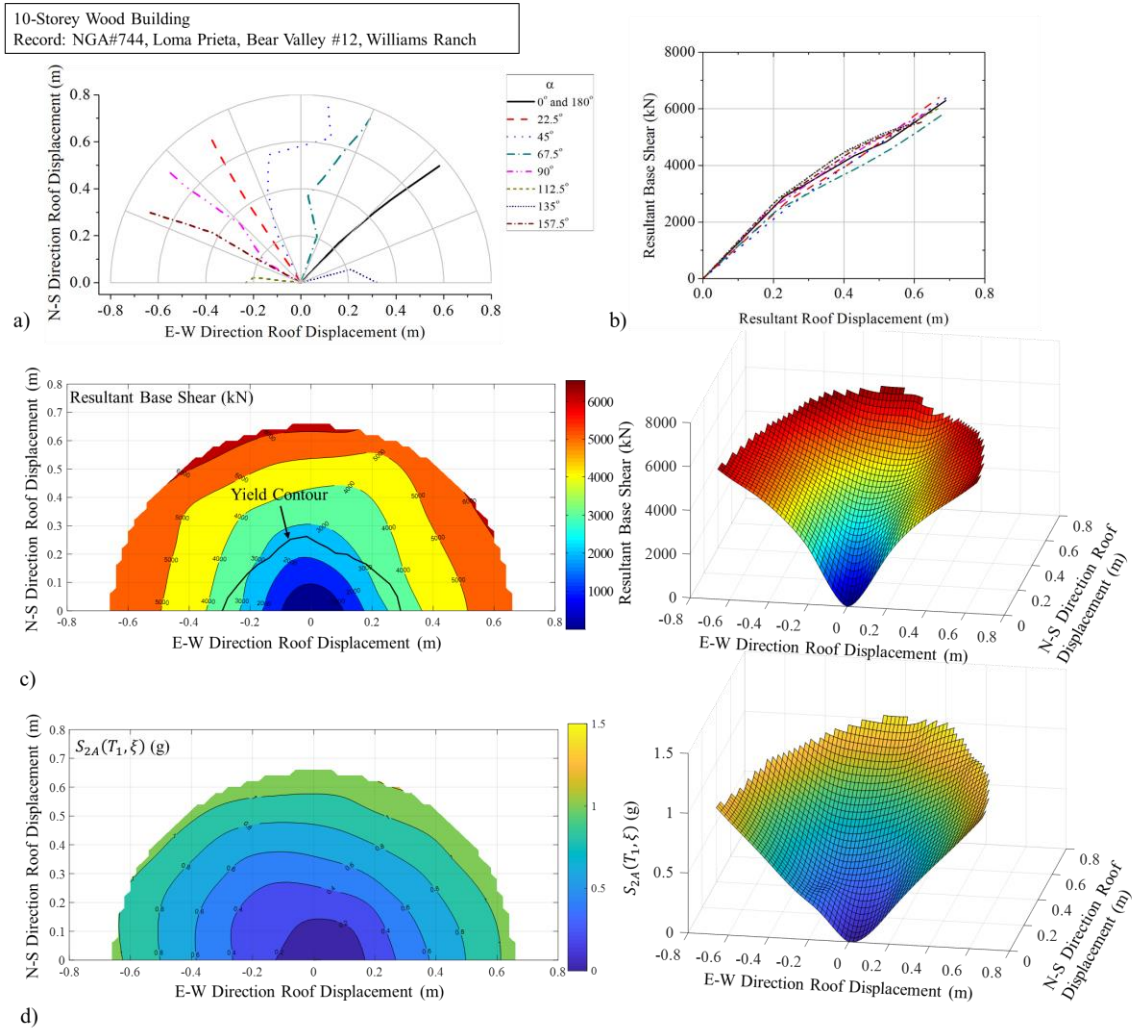


Figure 4.6. Capacity of the 10-storey wood building under bidirectional horizontal orthogonal ground motions by considering Record # 8 listed in Table 4.1: a) Trajectory of the maximum displacement projected in the horizontal plane; b) capacity curve; c) capacity surface considering the base shear; d) capacity surface using $S_{2A}(T_1, \xi)$ as the ground motion measure.

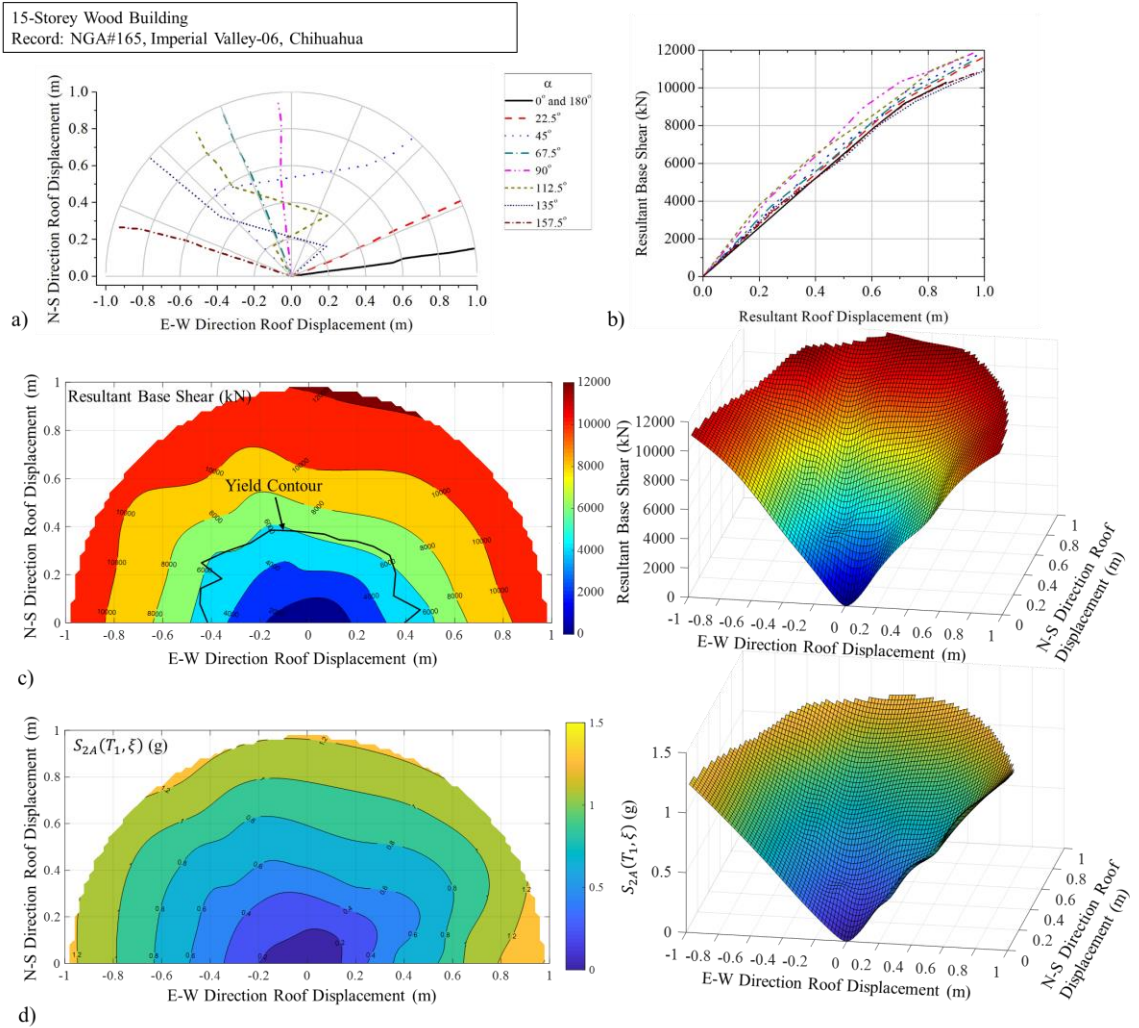


Figure 4.7. Capacity of the 15-storey wood building under bidirectional horizontal orthogonal ground motions by considering Record # 4 listed in Table 4.1: a) Trajectory of the maximum displacement projected in the horizontal plane, b) capacity curve, c) capacity surface considering the base shear, d) capacity surface using $S_{2A}(T_1, \xi)$ as the ground motion measure.

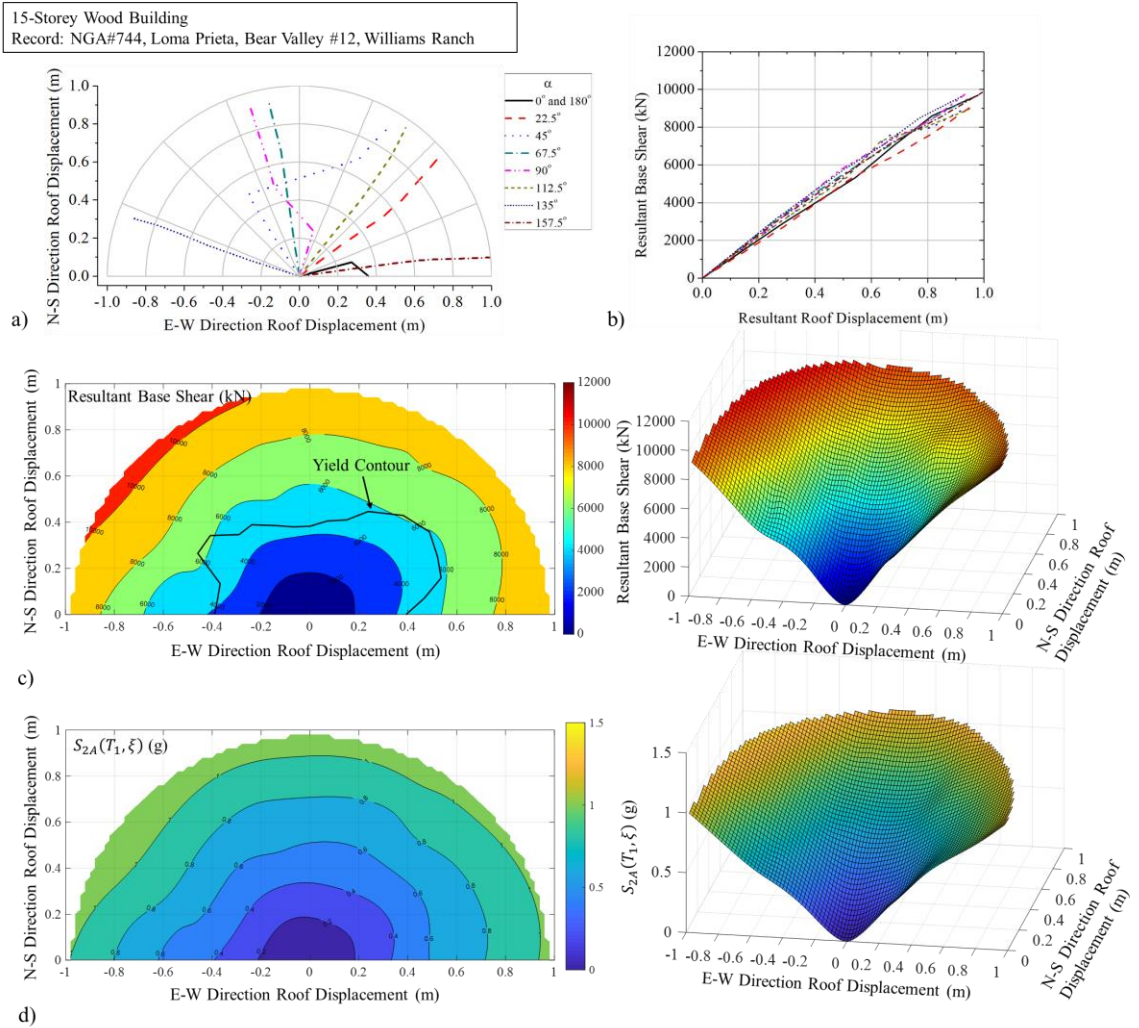


Figure 4.8. Capacity of the 15-storey wood building under bidirectional horizontal orthogonal ground motions by considering Record # 8 listed in Table 4.1: a) Trajectory of the maximum displacement projected in the horizontal plane; b) capacity curve; c) capacity surface considering the base shear; d) capacity surface using $S_{2A}(T_1, \xi)$ as the ground motion measure.

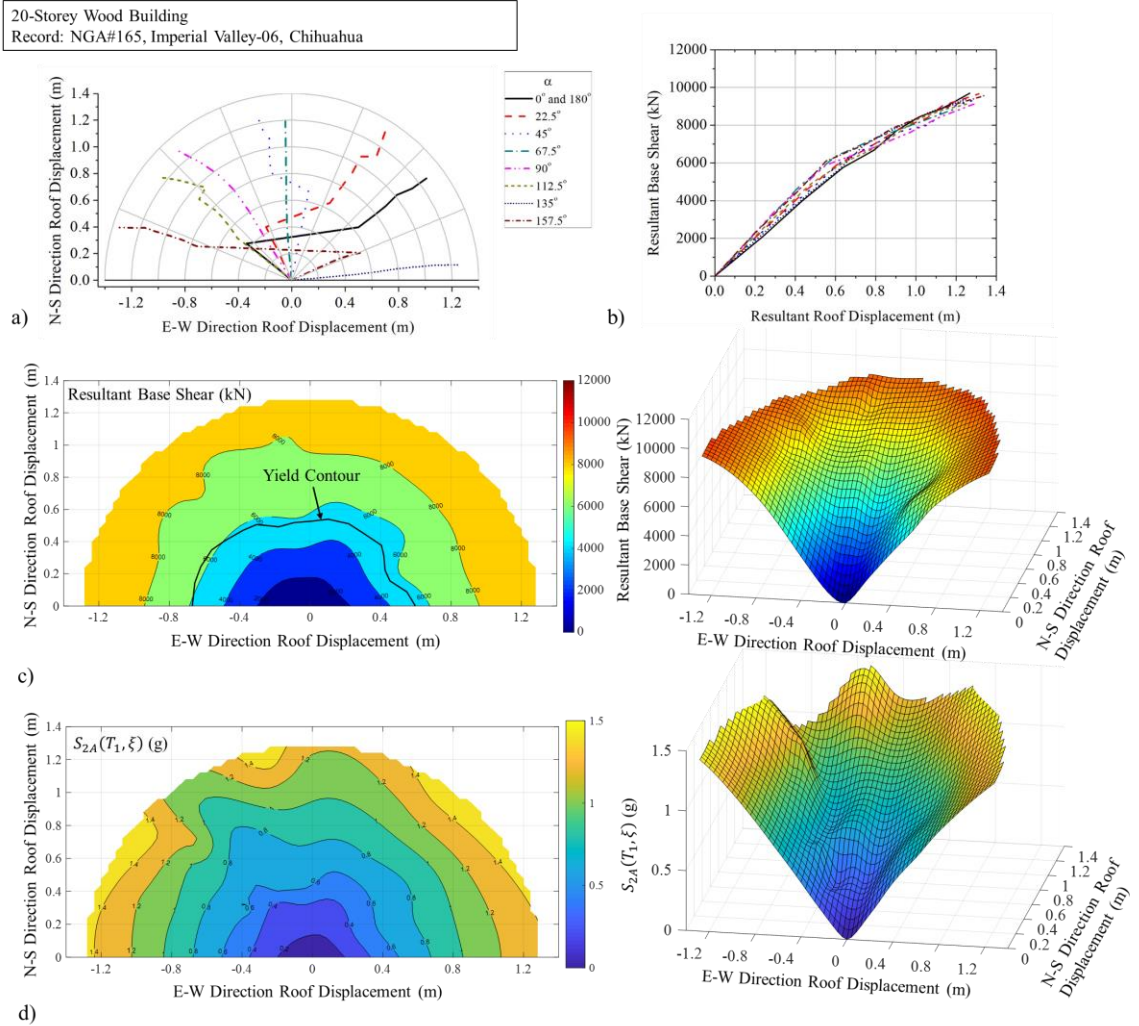


Figure 4.9. Capacity of the 20-storey wood building under bidirectional horizontal orthogonal ground motions by considering Record # 4 listed in Table 4.1: a) Trajectory of the maximum displacement projected in the horizontal plane; b) capacity curve; c) capacity surface considering the base shear; d) capacity surface using $S_{2A}(T_1, \xi)$ as the ground motion measure.

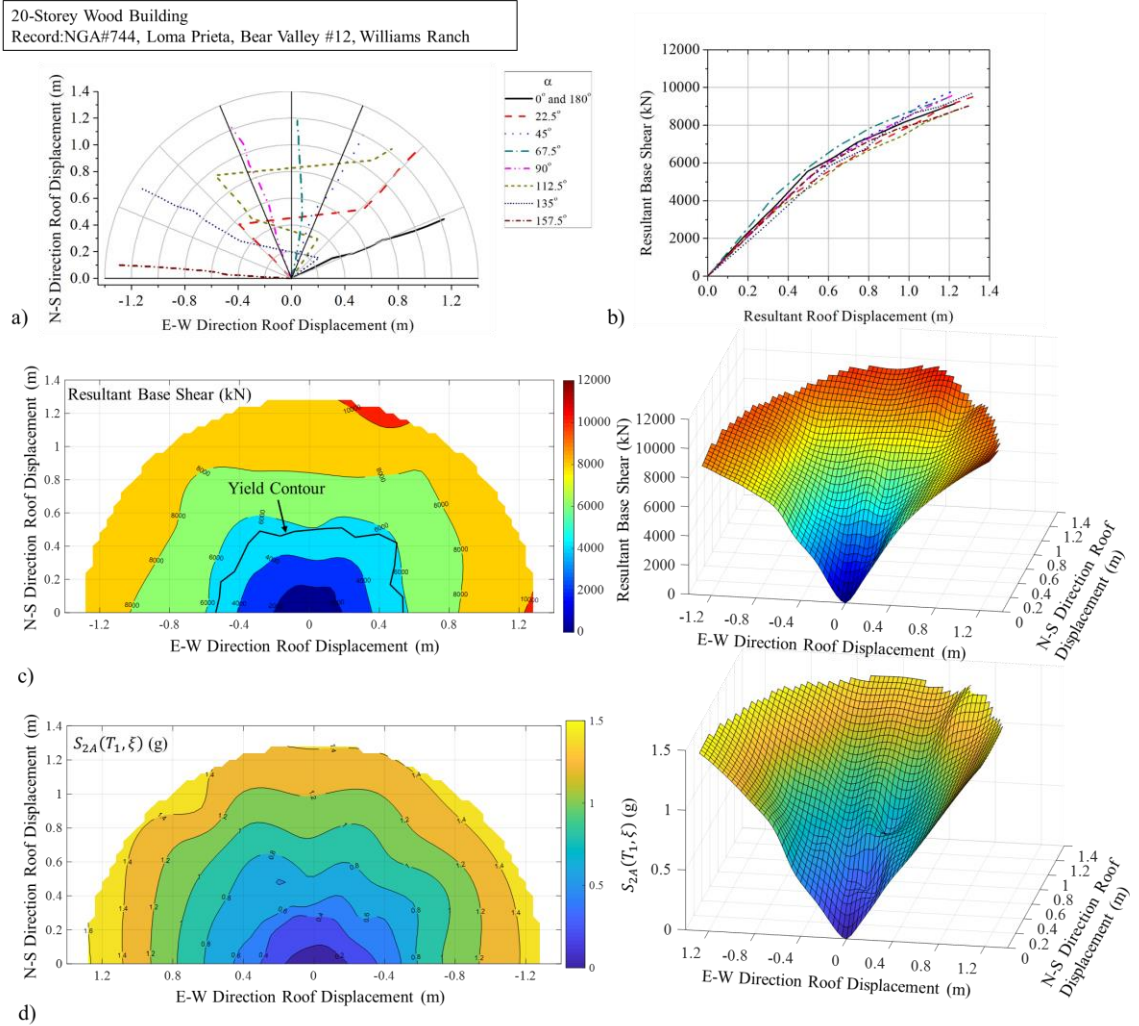
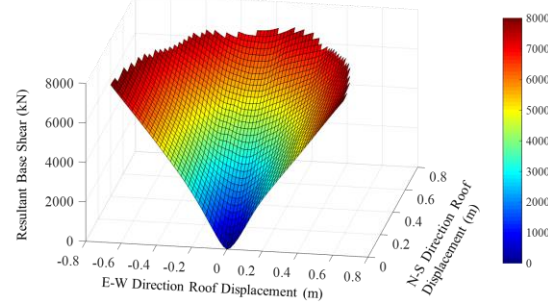


Figure 4.10. Capacity of the 20-storey wood building under bidirectional horizontal orthogonal ground motions by considering Record # 8 listed in Table 4.1: a) Trajectory of the maximum displacement projected in the horizontal plane; b) capacity curve; c) capacity surface considering the base shear; d) capacity surface using $S_{2A}(T_1, \xi)$ as the ground motion measure.

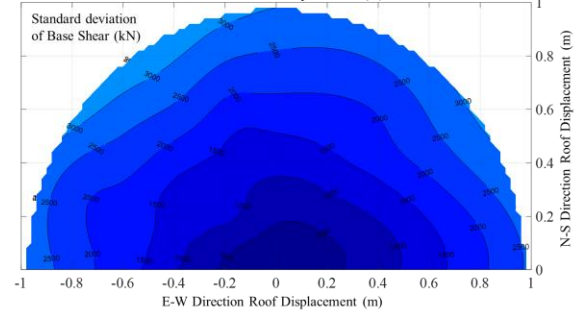
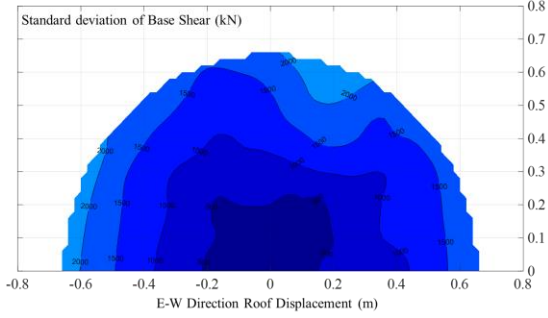
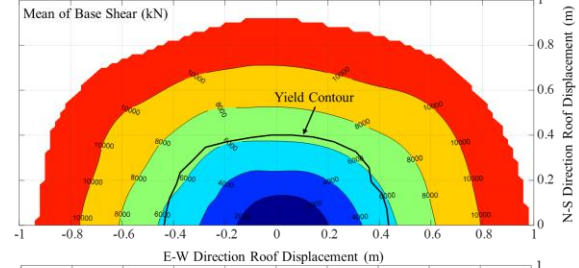
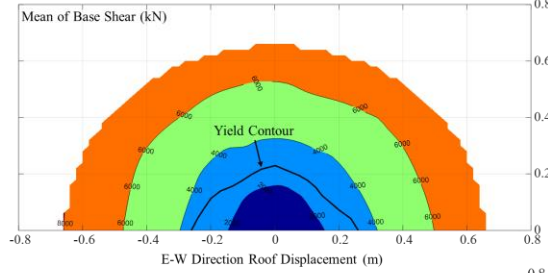
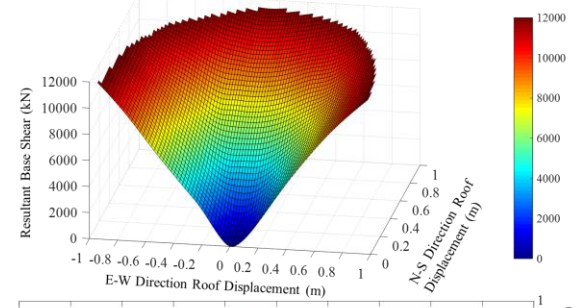
4.2.3 Effect of record-to-record variability on the response surface

To investigate the record-to-record variability, the analysis carried out in the previous section was repeated by considering all the records listed in Table 4.1. The mean and standard deviation of seismic demand (i.e., base shear or $S_{2A}(T_1, \xi)$) conditioned on the roof displacements (D_{px}, D_{py}) are shown in Figures 4.11 and 4.12. The mean IDA surface shown in Figure 4.11 indicates that the lines associated with the yield points for the 10-, 15- and 20-storey buildings follow a triangle, rectangular and semi-circle, respectively. The standard deviation of the IDA surface, shown in Figures 4.11 and 4.12 reflects the effect of the record-to-record variability on the capacity surface. In general the values of standard deviation increase as the displacements (D_{px}, D_{py}) increase. This is consistent with the observation made for 2D structural model under unidirectional ground motions (Hong and Jiang 2004). Also, for a given value of base shear or $S_{2A}(T_1, \xi)$, the estimated standard deviation is influenced by the considered axis Γ or orientation, which is defined by rotating the X -axis counterclockwise γ degrees.

10-Storey Wood Building
Mean Capacity Surface using Base Shear

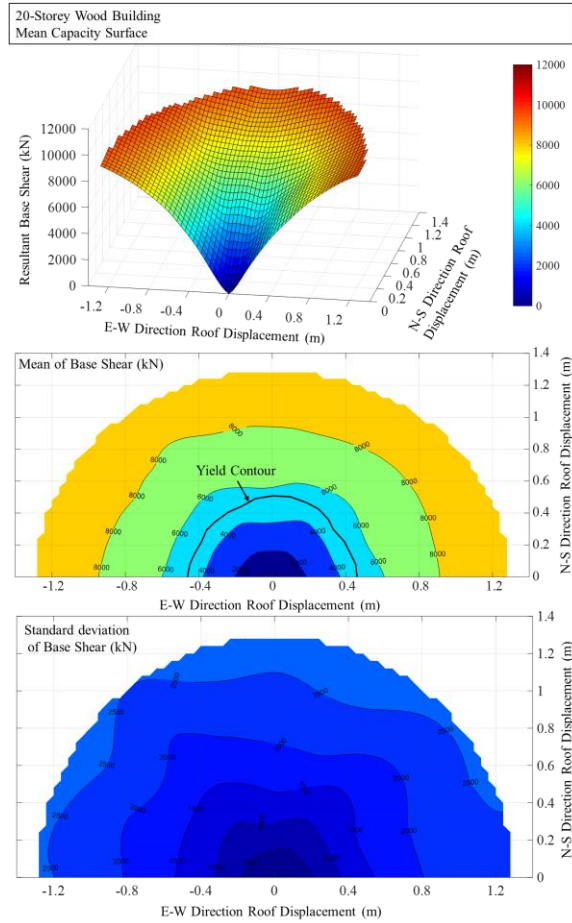


15-Storey Wood Building
Mean Capacity Surface using Base Shear



a)

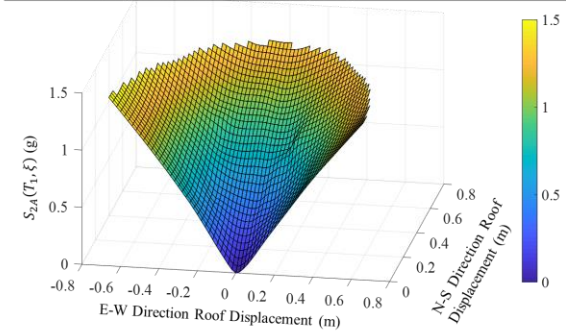
b)



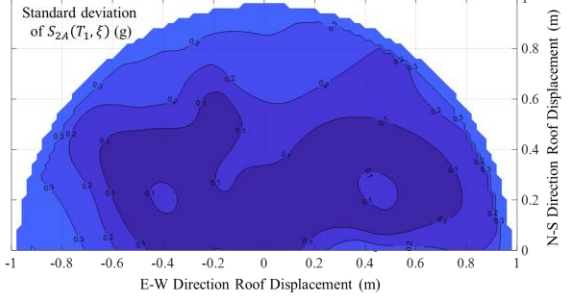
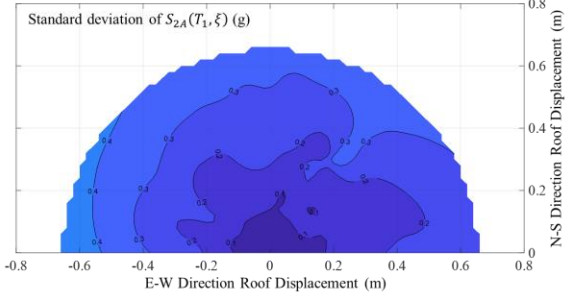
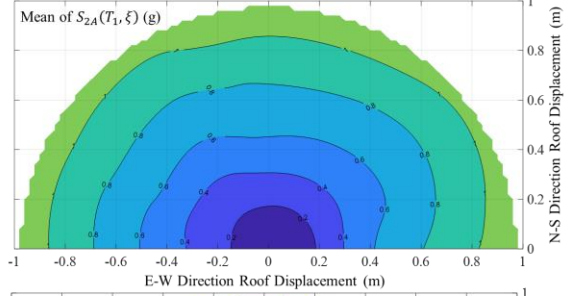
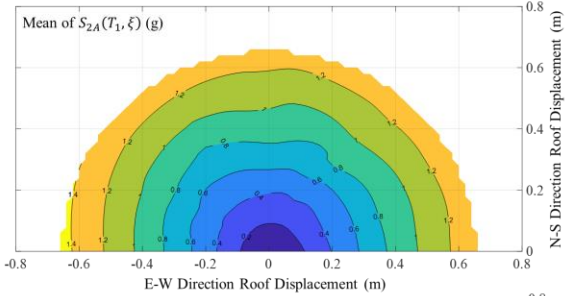
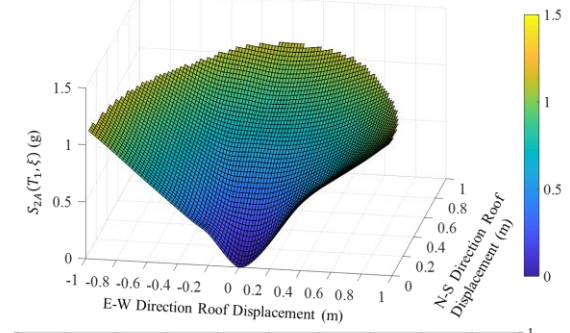
c)

Figure 4.11. The obtained mean and standard deviation of capacity surfaces by using base shear for wood buildings: a) 10-storey; b) 15-storey; c) 20-storey.

10-Storey Wood Building
Mean Capacity Surface using $S_{2A}(T_1, \xi)$

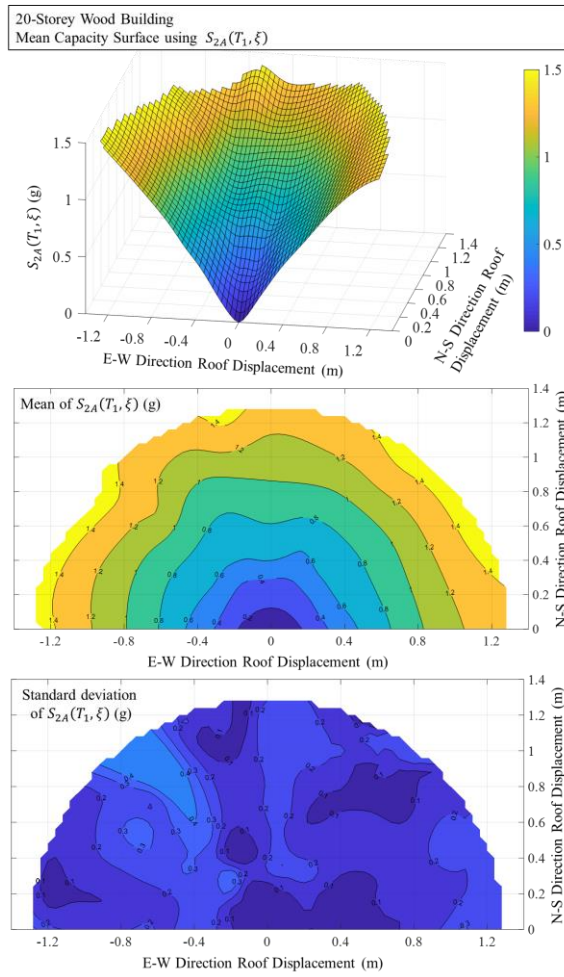


15-Storey Wood Building
Mean Capacity Surface using $S_{2A}(T_1, \xi)$



a)

b)



c)

Figure 4.12. The obtained mean and standard deviation of capacity surfaces by using $S_{2A}(T_1, \xi)$ for wood buildings: a) 10-storey; b) 15-storey; c) 20-storey.

4.2.4 Comparison of the mean IDA surface and nonlinear static pushover analysis results

The IDA is computing time consuming. To simplify the analysis, it is noted that for a bisymmetric structure subjected to bidirectional horizontal orthogonal ground motions, following Chopra (2006), and Reyes and Chopra (2011), it can be shown that the effective earthquake forces can be expressed as,

$$p_{effx}(t) = -\Gamma_x M_x \ddot{u}_{gx}(t), \quad (4.3a)$$

for the first sway vibration mode along the X -axis, ψ_x , and,

$$p_{effy}(t) = -\Gamma_y M_y \ddot{u}_{gy}(t), \quad (4.3a)$$

for the first sway vibration mode along the Y -axis ψ_y , where M_x and Γ_x are the modal mass and modal participation factor for the sway mode along the X -axis, respectively; M_y and Γ_y are defined similarly but along the Y -axis; and $\ddot{u}_{gx}(t)$ and $\ddot{u}_{gy}(t)$ represents the ground motions along the X - and Y -axes, respectively.

In particular, if the uniaxial ground excitation $\ddot{u}_g(t)$ is acting along the X' -axis (see Figure 4.4), $\ddot{u}_{gx}(t) = \ddot{u}_g(t) \cos(\alpha)$ and $\ddot{u}_{gy}(t) = \ddot{u}_g(t) \sin(\alpha)$. Therefore, by considering that an acceleration is acting along the X' -axis, and by applying NSPA procedure, one is applying the forces $P \cos(\alpha) \Gamma_x \eta_x$ and $P \sin(\alpha) \Gamma_y \eta_y$ along the X - and Y -axes, respectively, where P is an intensity factor; the elements of the vectors η_x and η_y are $\eta_{x,i} = m_i \psi_{x,i}$, $\eta_{y,i} = m_i \psi_{y,i}$; and m_i is the mass associated with the i -th element of ψ_x , $\psi_{x,i}$, (and the i -th element of ψ_y , $\psi_{y,i}$). This implies that the NSPA is carried out by considering bidirectional horizontal but height varying loadings ($P \cos(\alpha) \Gamma_x \eta_x$, $P \sin(\alpha) \Gamma_y \eta_y$).

More specifically, the NSPA for the 3D bisymmetric building under bidirectional horizontal force can be carried out by:

- 1) Perform the free vibration analysis to obtain the first sway mode along the X -axis, ψ_x , and the first sway mode along the Y -axis, ψ_y ;
- 2) Perform nonlinear static analysis by applying a series of loads $P \cos(\alpha) \Gamma_x \eta_x$ along the X -axis and $P \sin(\alpha) \Gamma_y \eta_y$ along the Y -axis with increased P value; and,

3) Present the results in a form similar to those shown in Figures 4.5a to 4.5c.

By following these steps, the results obtained from NSPA is presented in Figure 4.11a for the 10-storey building, in Figure 4.11b for the 15-storey building and in Figure 4.11c for the 20-storey building.

Inspection of the results shown in this figure and those shown in Figures 4.8 to 4.10, indicates that the former approximates well the latter. To quantify their differences, the relative difference between the capacity surfaces obtained by using the NSPA and by using the mean of IDA surface is estimated and shown in Figures 4.13 to 4.15. The results shown in the figure indicates that the maximum (absolute) differences in terms of the predicted roof displacements are 17.2%, 15.8% and 15.1% for the designed 10-, 15- and 20-storey buildings, respectively; the maximum (absolute) differences in terms of the base shear (conditioned on the same roof displacement) are 16.2%, 14.6%, and 11.7% for the designed 10-, 15- and 20-storey buildings, respectively. In particular, by considering the base shear equal to the seismic design force (see Chapter 2), or twice of the seismic design force, the obtained relative error (respect to the mean of IDA surface) are shown in Table 4.2 by considering response along different directions of the structure, where the direction is defined as the counterclock rotation from the structural X -axis. The relative error is calculated using,

$$\text{Relative error} = \frac{\text{Value from the mean IDA surface} - \text{Value from the NSPA surface}}{\text{Value from the mean IDA surface}} \quad (4.4)$$

This comparison suggests that the use of NSPA could lead to acceptable capacity surface, except in such a case, the quantification of the record-to-record variability is unavailable.

Table 4.2. Characterizing of capacities for designed CLT buildings considering different directions.

Building	10-Storey			15-Storey			20-Storey		
	Resultant Roof displacement (m) given $2V_d$ total applied load and the relative differences								
Direction (°)	Mean IDA	NSPA	Relative error	Mean IDA	NSPA	Relative error	Mean IDA	NSPA	Relative error
0	0.254	0.252	0.4%	0.352	0.397	-12.8%	0.557	0.556	0.2%
22.5	0.243	0.239	1.2%	0.359	0.388	-8.1%	0.517	0.512	1.0%
45	0.242	0.265	-9.5%	0.330	0.352	-6.7%	0.573	0.552	3.5%
67.5	0.252	0.281	-11.5%	0.304	0.333	-9.5%	0.561	0.604	-5.7%
90	0.268	0.307	-14.6%	0.305	0.332	-8.9%	0.572	0.598	-4.5%
112.5	0.252	0.282	-11.9%	0.301	0.328	-9.0%	0.560	0.605	-5.9%
135	0.241	0.264	-9.5%	0.330	0.351	-6.4%	0.570	0.553	3.0%
157.5	0.241	0.236	2.1%	0.359	0.391	-8.9%	0.519	0.515	0.8%
180	0.250	0.252	-0.8%	0.349	0.397	-13.8%	0.553	0.555	-0.4%

Note: The relative error = (Mean IDA surface – NSPA surface) / Mean IDA surface.

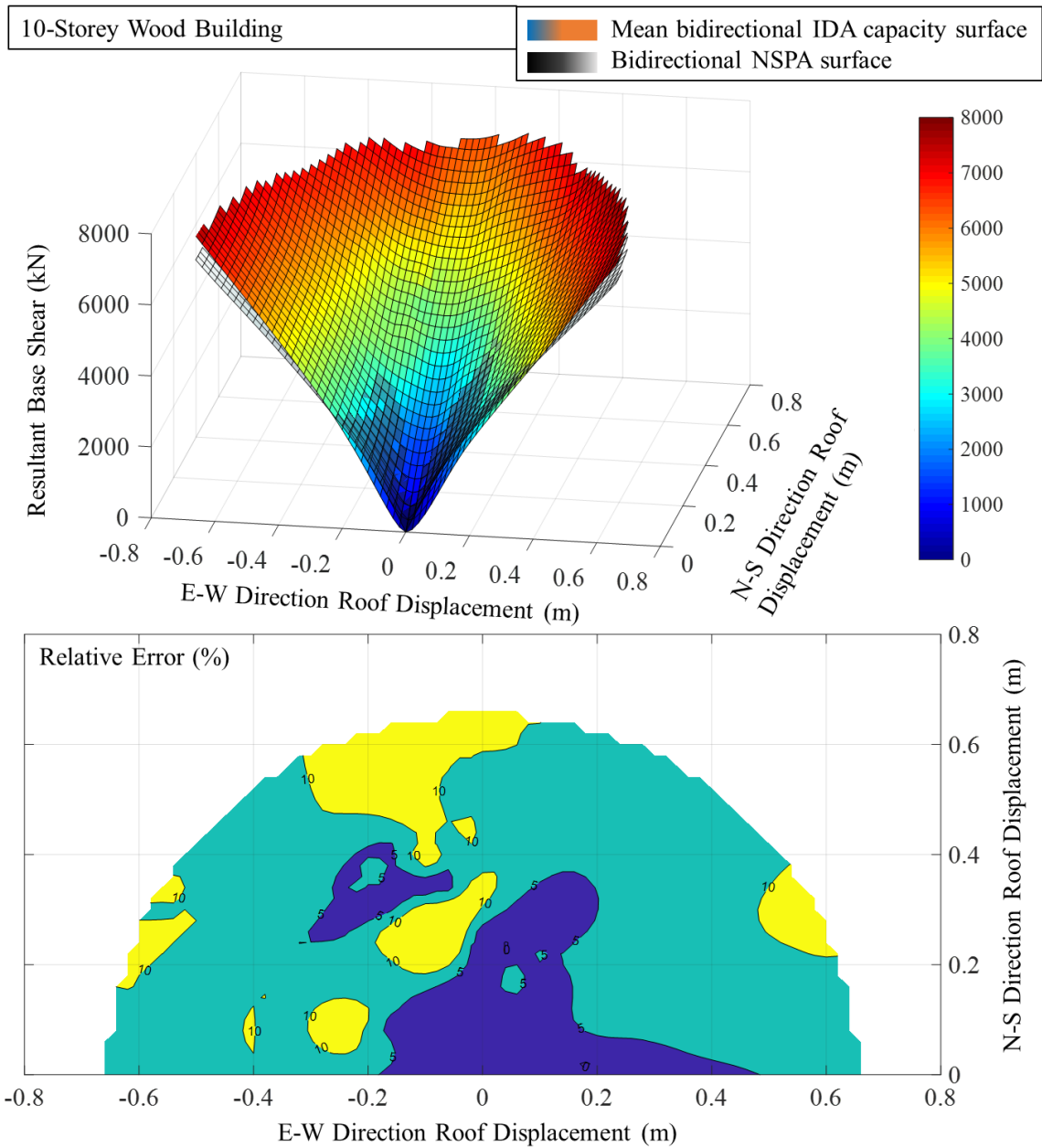


Figure 4.13. Capacity surfaces obtained by using the NSPA and by using the mean of IDA surface and the relative difference respect to the mean of IDA surface (conditioned on the same roof displacement) for the 10-storey building.

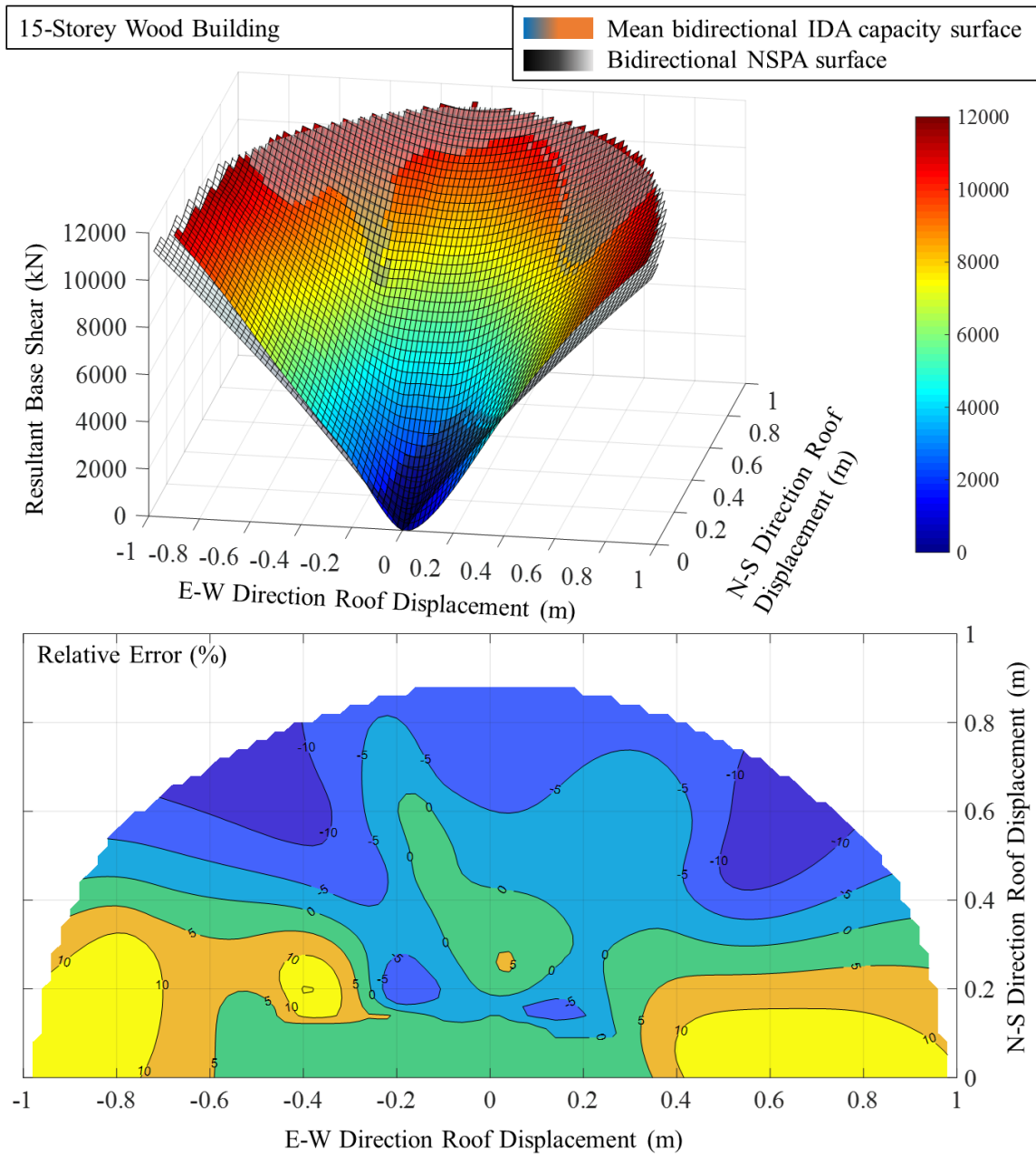


Figure 4.14. Capacity surfaces obtained by using the NSPA and by using the mean of IDA surface and the relative difference respect to the mean of IDA surface (conditioned on the same roof displacement) for the 15-storey building.

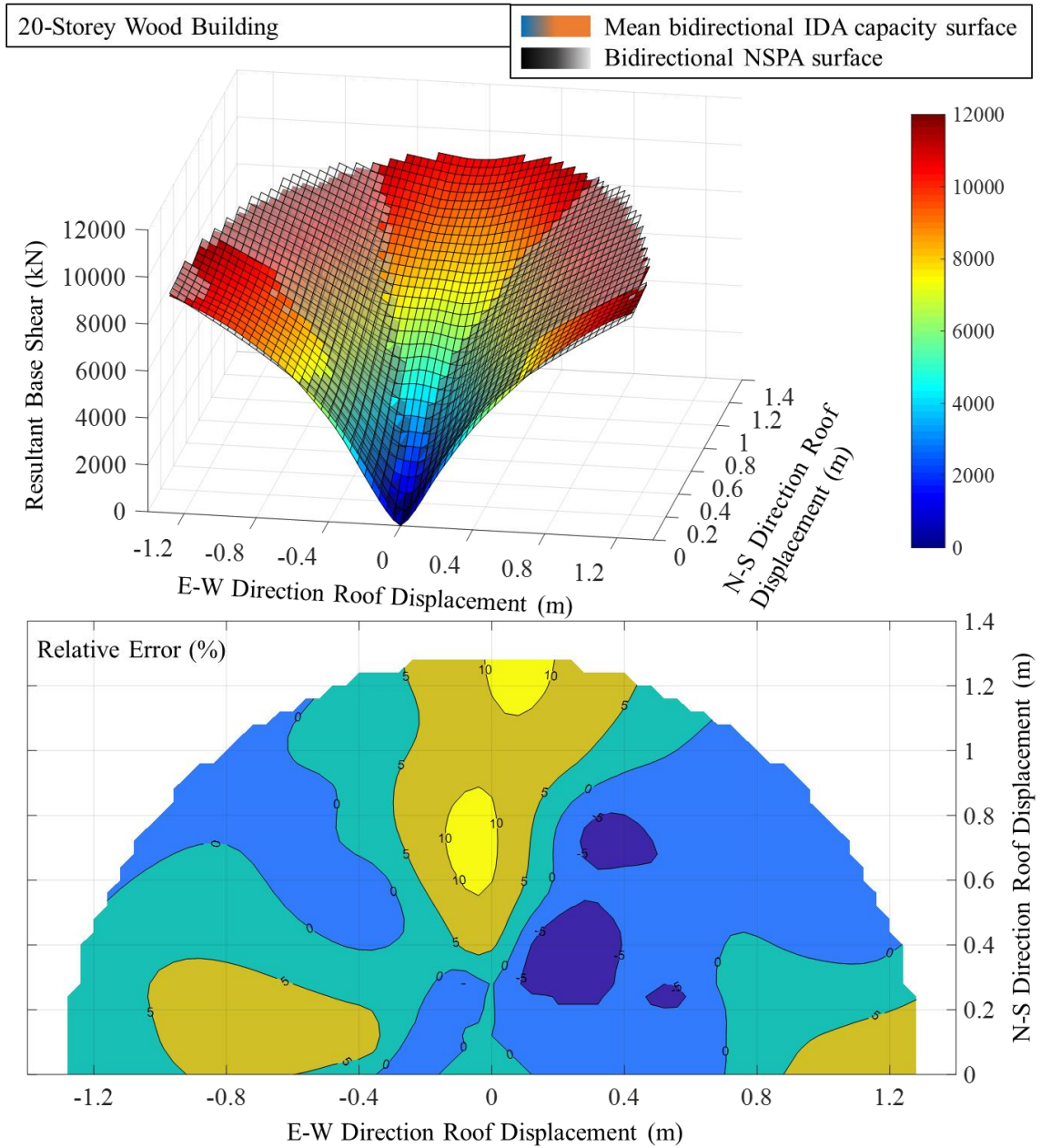


Figure 4.15. Capacity surfaces obtained by using the NSPA and by using the mean of IDA surface and the relative difference respect to the mean of IDA surface (conditioned on the same roof displacement) for the 20-storey building.

4.3 Conclusions

This chapter is focused on the investigation of the building capacity subjected to bidirectional horizontal orthogonal ground motions. It is shown that such a capacity can be expressed in terms of capacity surface, where the capacity in terms of base shear or ground motion measure is expressed as a function of the displacement defined by two horizontal displacements components along the X - and Y -axes. The capacity surface is a direct extension of the capacity curve for a structure subjected to unidirectional ground motions.

A procedure to evaluate the capacity surface is presented by using the incremental dynamic analysis (IDA) as well as the nonlinear static pushover analysis (NSPA). By using this procedure, the numerical analysis results obtained for three mid- and high-rise wood buildings indicate that the record-to-record variability is significant for the capacity surface, and that the yield capacity contour depends on the displacement path and the considered building. Therefore, the use of the capacity curve as opposed to capacity surface, for 3D building subjected to the bidirectional ground motions may not be appropriate. Comparison of the capacity curve obtained from the IDA and NSPA indicates that the results obtained from the latter could be considered to be a good approximation for the mean IDA surface. However, the use of NPSA does not provide information on the record-to-record variability on the estimated capacity surface.

4.4 References

- Antoniou, S., Rovithakis, A., and Pinho, R. (2002, September). Development and verification of a fully adaptive pushover procedure. In *Proceedings of the Twelfth European Conference on Earthquake Engineering*.
- Athanatopoulou, A. M. (2005). Critical orientation of three correlated seismic components. *Engineering Structures*, 27(2), 301-312.
- Aydinoğlu, M. N. (2003). An incremental response spectrum analysis procedure based on inelastic spectral displacements for multi-mode seismic performance evaluation. *Bulletin of Earthquake Engineering*, 1(1), 3-36.

- Chopra, A. K., and Goel, R. K. (2001). Direct displacement-based design: use of inelastic vs. elastic design spectra. *Earthquake Spectra*, 17(1), 47-64.
- Ellingwood, B. R., Rosowsky, D. V., and Pang, W. (2008). Performance of light-frame wood residential construction subjected to earthquakes in regions of moderate seismicity. *Journal of structural engineering*, 134(8), 1353-1363.
- Elnashai, A. S. (2002). Do we really need inelastic dynamic analysis?. *Journal of Earthquake Engineering*, 6(spec01), 123-130.
- Fajfar, P. (2000). A nonlinear analysis method for performance-based seismic design. *Earthquake spectra*, 16(3), 573-592.
- Fajfar, P. (2002, September). Structural analysis in earthquake engineering—a breakthrough of simplified non-linear methods. In *12th European conference on earthquake engineering*.
- Fajfar, P., and Fischinger, M. (1988). N2-A method for non-linear seismic analysis of regular buildings. In *Proceedings of the ninth world conference in earthquake engineering* (Vol. 5, pp. 111-116).
- Filiatrault, A., and Folz, B. (2002). Performance-based seismic design of wood framed buildings. *Journal of Structural Engineering*, 128(1), 39-47.
- Freeman, S. A. (1975). Evaluations of existing buildings for seismic risk—A case study of Puget Sound Naval Shipyard. In *Proc. 1st US Nat. Conf. on Earthquake Engrg., Bremerton, Washington*, (pp. 113-122).
- Gagnon, S., Munoz, W., Mohammad, M., and Below, K. D. (2010, July). Design guidelines for an 8-storey hybrid wood-concrete multi-family building. In *Structures and Architecture (Proceedings of the First International Conference on Structures and Architecture, Guimaraes, Portugal, 21-23 July 2010)*, CRC Press, Leiden, The Netherlands (pp. 109-110).

- Giovenale, P., Cornell, C. A., and Esteva, L. (2004). Comparing the adequacy of alternative ground motion intensity measures for the estimation of structural responses. *Earthquake engineering and structural dynamics*, 33(8), 951-979.
- Gupta, B., and Kunnath, S. K. (2000). Adaptive spectra-based pushover procedure for seismic evaluation of structures. *Earthquake spectra*, 16(2), 367-392.
- Kalkan, E., and Kunnath, S. K. (2004). Method of modal combinations for pushover analysis of buildings. In *Proc. of the 13th World Conference on Earthquake Engineering*, (pp. 1-6).
- Kalkan, E., and Kunnath, S. K. (2006). Adaptive modal combination procedure for nonlinear static analysis of building structures. *Journal of Structural Engineering*, 132(11), 1721-1731.
- Lagaros, N. D. (2010). Multicomponent incremental dynamic analysis considering variable incident angle. *Structure and Infrastructure Engineering*, 6(1-2), 77-94.
- López, O. A., and Torres, R. (1997). The critical angle of seismic incidence and the maximum structural response. *Earthquake engineering and structural dynamics*, 26(9), 881-894.
- Manoukas, G., Athanatopoulou, A., and Avramidis, I. (2012). Multimode pushover analysis for asymmetric buildings under biaxial seismic excitation based on a new concept of the equivalent single degree of freedom system. *Soil Dynamics and Earthquake Engineering*, 38, 88-96.
- Mara, T. G., and Hong, H. P. (2013). Effect of wind direction on the response and capacity surface of a transmission tower. *Engineering structures*, 57, 493-501.
- Menun, C., and Der Kiureghian, A. (1998). A replacement for the 30%, 40%, and SRSS rules for multicomponent seismic analysis. *Earthquake Spectra*, 14(1), 153-163.
- Mwafy, A. M., and Elnashai, A. S. (2001). Static pushover versus dynamic collapse analysis of RC buildings. *Engineering structures*, 23(5), 407-424.

- NEWBuilds. (2015). Application of Analysis Tools from NEWBuildS Research Network in Design of a High-Rise Wood Building, *Network on Innovative Wood Products and Building Systems (NEWBuildS)*, University of New Brunswick, Fredericton, New Brunswick, Canada.
- NRCC (2010). *National Building Code of Canada*, NRC Canada, Ottawa, Ontario, Canada.
- Pang, W., Rosowsky, D. V., Ellingwood, B. R., and Wang, Y. (2009). Seismic fragility analysis and retrofit of conventional residential wood-frame structures in the central United States. *Journal of structural engineering*, 135(3), 262-271.
- Paret, T. F., Sasaki, K. K., Eilbeck, D. H., and Freeman, S. A. (1996). Approximate inelastic procedures to identify failure mechanisms from higher mode effects. In *Proceedings of the eleventh world conference on earthquake engineering* (Vol. 2).
- Pei, S., van de Lindt, J. W., and Popovski, M. (2012). Approximate R-factor for cross-laminated timber walls in multistory buildings. *Journal of Architectural Engineering*, 19(4), 245-255.
- Poursha, M., Khoshnoudian, F., and Moghadam, A. S. (2014). The extended consecutive modal pushover procedure for estimating the seismic demands of two-way unsymmetric-plan tall buildings under influence of two horizontal components of ground motions. *Soil Dynamics and Earthquake Engineering*, 63, 162-173.
- Reyes, J. C., and Chopra, A. K. (2011). Three-dimensional modal pushover analysis of buildings subjected to two components of ground motion, including its evaluation for tall buildings. *Earthquake Engineering and Structural Dynamics*, 40(7), 789-806.
- Rosenblueth, E., and Contreras, H. (1977). Approximate design for multicomponent earthquakes. *Journal of the Engineering Mechanics Division*, 103(5), 881-893.
- Saiidi, M., and Sozen, M. A. (1981). Simple nonlinear seismic analysis of R/C structures. *Journal of structural Engineering (ASCE)*, Vol. 107, pp. 937-952.

- Sasaki, K. K., Freeman, S. A., and Paret, T. F. (1998). Multimode pushover procedure (MMP)—a method to identify the effects of higher modes in a pushover analysis. In *Proceedings of the 6th US National Conference on Earthquake Engineering, Seattle, Washington*.
- Shakeri, K., and Ghorbani, S. (2015). A pushover procedure for seismic assessment of buildings with bi-axial eccentricity under bi-directional seismic excitation. *Soil Dynamics and Earthquake Engineering*, 69, 1-15.
- Takizawa, H., and Aoyama, H. (1976). Biaxial effects in modelling earthquake response of R/C structures. *Earthquake Engineering and Structural Dynamics*, 4(6), 523-552.
- Vamvatsikos, D., and Cornell, A. (2006). Incremental dynamic analysis with two components of motion for a 3D steel structure. In *Proceedings of the 8th US National Conference on Earthquake Engineering*.
- Vamvatsikos, D., and Cornell, C. A. (2002). Incremental dynamic analysis. *Earthquake Engineering and Structural Dynamics*, 31(3), 491-514.
- Vidic, T., Fajfar, P., and Fischinger, M. (1994). Consistent inelastic design spectra: strength and displacement. *Earthquake Engineering and Structural Dynamics*, 23(5), 507-521.
- Yang, S. C., Liu, T. J., and Hong, H. P. (2017). Reliability of Tower and Tower-Line Systems under Spatiotemporally Varying Wind or Earthquake Loads. *Journal of Structural Engineering*, 143(10), 04017137.
- Zeris, C. A., and Mahin, S. A. (1991). Behaviour of reinforced concrete structures subjected to biaxial excitation. *Journal of structural engineering*, 117(9), 2657-2673.

Chapter 5

5 Reliability Assessment of the Mid- and High-rise Wood Buildings under Bidirectional Seismic Excitations

5.1 Introduction

Structural reliability analysis results for buildings subjected to earthquake load are used to aid the design code calibration, risk management and decision-making under uncertainty. Reliability analysis methods are well developed (Madsen et al. 1986; Melchers 1999); and the commonly employed methods include the first-order reliability method, second-order reliability method, response surface method and simulation techniques. The first-order or second-order reliability methods are extremely efficient and are adequate for problems with smooth limit state functions or performance functions; they could breakdown for cases where the derivatives of the considered limit state function are discontinuous. The application of simulation techniques to estimate structural reliability can be accurate but often computing time consuming, especially if a 3D nonlinear inelastic complex structural model is considered. The use of the response surface method can be efficient and adequate, especially if the response surface provides a good fit to the actual system behaviour near the design point (Madsen et al. 1986), which is unknown a priori.

To avoid some of these mentioned drawbacks, and to simplify the estimation of the structural reliability by considering seismic hazard, several approaches have been developed and employed (Yeh and Wen 1990; Han and Wen 1997; Shome and Cornell 1999; Cornell et al. 2000). In these approaches, often the probabilistic assessment of structural capacity to sustain seismic loads and seismic hazard assessment are first decoupled. For example, in Shome and Cornell (1999) and Cornell et al. (2000), the probabilistic structural capacity of a 2D structural system is evaluated based on the incremental dynamic analysis; the probabilistic capacity curve in terms of a ground motion measure (e.g., spectral acceleration (SA)) together with the probabilistic model of the ground motion measure obtained from seismic hazard assessment are then used to estimate the structural reliability. Alternatively, the 2D nonlinear structural system could be approximated by an equivalent nonlinear inelastic single-degree-of-freedom (SDOF)

system based on the results from the nonlinear static pushover analysis (NSPA), and the reliability analysis is then carried out based on probabilistic ductility demand model for the equivalent SDOF system and the probabilistic model of the SA (Hong and Hong 2007; Hong et al. 2010). However, it seems that an extension of these approaches to 3D structural models under bidirectional horizontal excitations has not been elaborated in the literature.

The consideration of the 3D structural model under bidirectional horizontal orthogonal ground motions can be important since both horizontal record components affect the estimated elastic and inelastic displacements. Statistics of inelastic responses of simple hysteretic systems under bidirectional seismic excitations was investigated in Lee and Hong (2010, 2012).

The main objectives of this chapter are to establish a simple procedure to estimate reliability of 3D bisymmetric buildings subjected to bidirectional orthogonal ground motions, to apply the procedure to estimate the reliability of mid- and high-rise wood buildings under bidirectional ground motions, and to compare the estimated reliabilities by considering uni- and bi-directional ground motions. The procedure considers that the bisymmetric buildings can be approximated by an equivalent nonlinear inelastic two-degree-of-freedom (2DOF) system. The equivalent systems are used to represent three designed mid-rise and tall wood buildings in the present chapter. Statistics of the ductility demand for the equivalent nonlinear inelastic 2DOF systems are assessed based on 381 selected ground motion records.

In the following, first, the characteristics of the designed wood buildings and their responses under bidirectional ground motions are summarized. The summary provides the needed information to be used for their approximations by using the equivalent 2DOF systems. The seismic reliability evaluation procedure is then proposed considering the equivalent 2DOF system. This is followed by the analysis results and discussion.

5.2 Seismic response characteristics of designed prototype wood buildings

The 10-, 15- and 20-storey buildings with footprint of $24 \text{ m} \times 23.2 \text{ m}$ designed to satisfy applicable design codes and standards in Canada (see Chapter 2 for detail) are considered. The buildings are shown in Figure 5.1 to 5.3. The essential design consideration includes:

- 1) The height of first storey is 4.4 m, and upper storeys are 3.2 m; the CLT panels are used for floors, roof, shear walls, and elevator shaft; the glulam is used for beams and columns;
- 2) The design was carried out for seismic load and checked for wind load. It was concluded that the design is governed by inter-storey drift limits due to wind or earthquake, or wind induced vibration; and
- 3) Finite element models are developed for the buildings by considering the nonlinear inelastic behaviour of fasteners among the panels.

Capacity surfaces of the buildings subjected to bidirectional horizontal orthogonal ground motions are assessed using the incremental dynamic analysis (IDA) procedure and nonlinear static pushover analysis (see Chapter 4). The IDA analysis is carried out using 11 records so to reduce the computing time to a manageable level. The effect of incidence angle on the response is considered by varying incidence angles from 0° to 180° as the considered buildings are bisymmetric. Comparison of the capacity surface represented by the mean of the IDA surface and by the NSPA surface indicates that the use of the latter provides good approximation to the former.

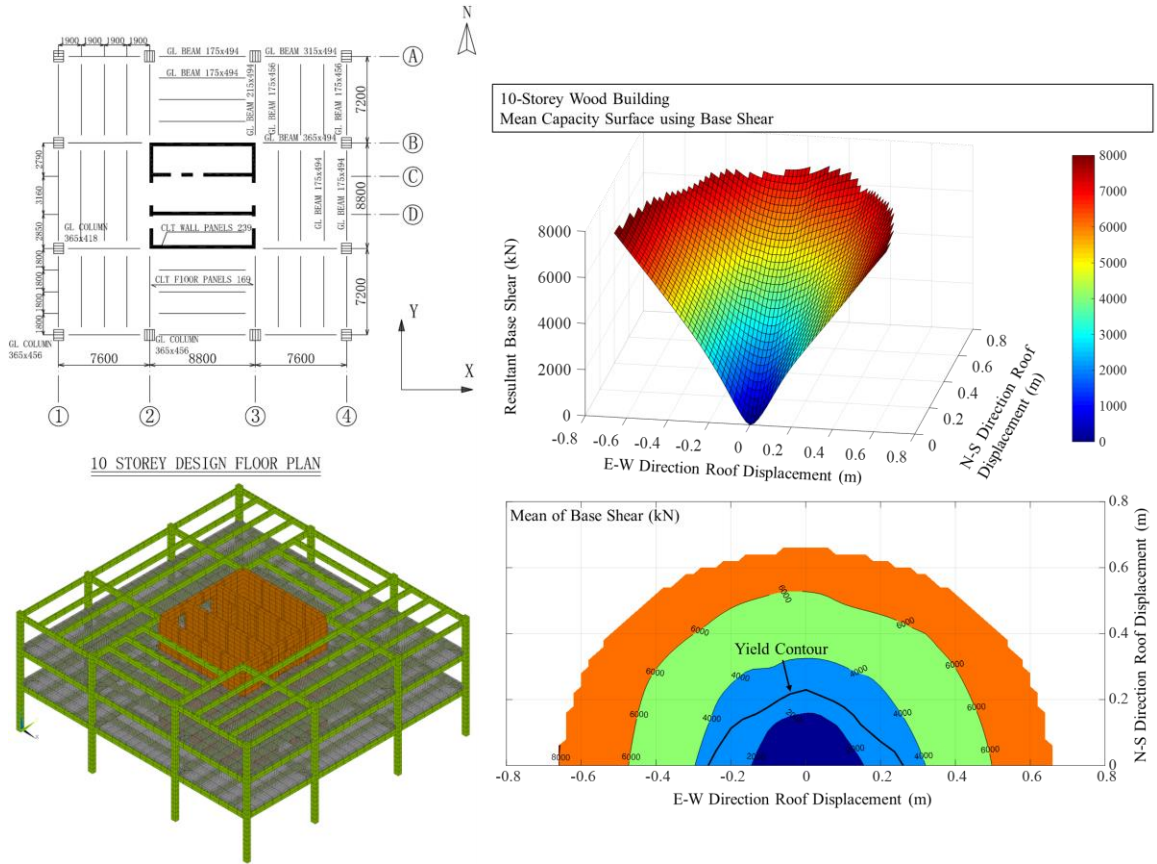


Figure 5.1. Designed 10-storey wood building and its mean capacity surface by considering bidirectional ground motions.

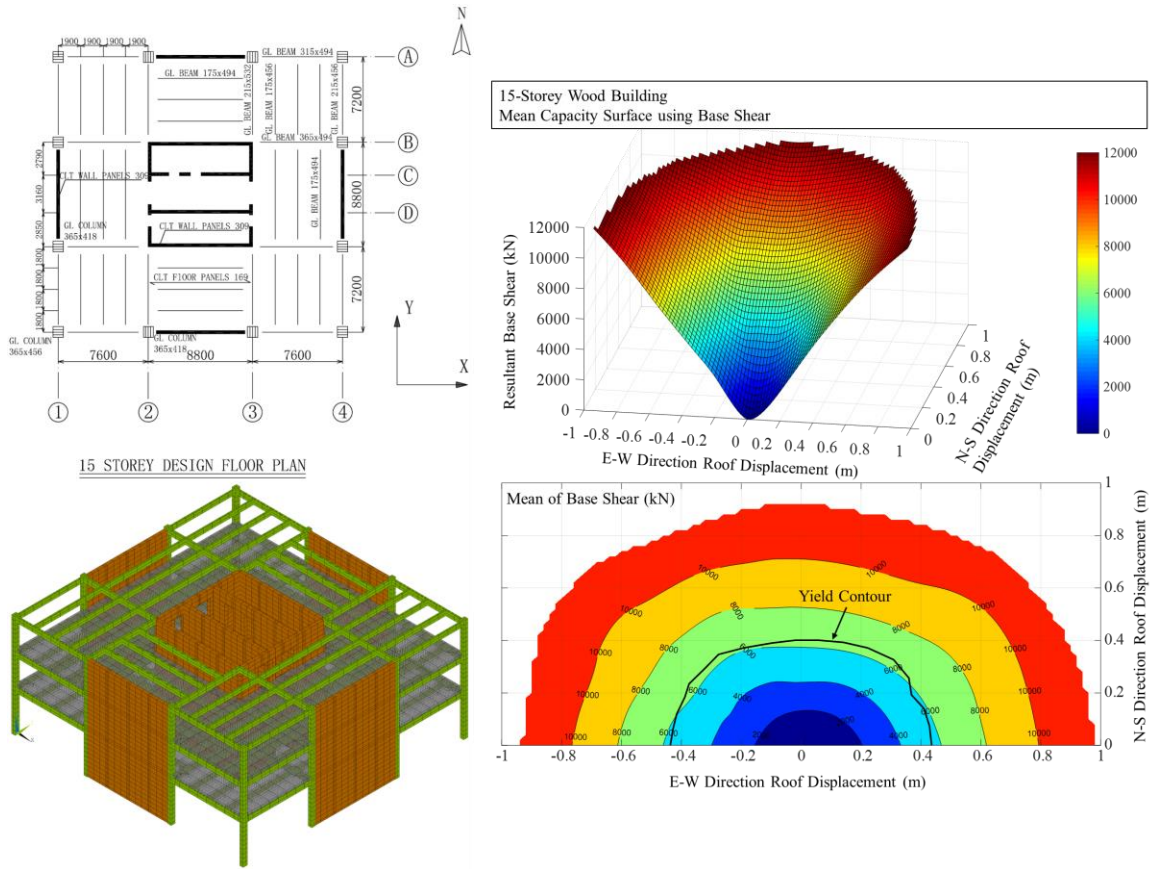


Figure 5.2. Designed 15-storey wood building and its mean capacity surface by considering bidirectional ground motions.

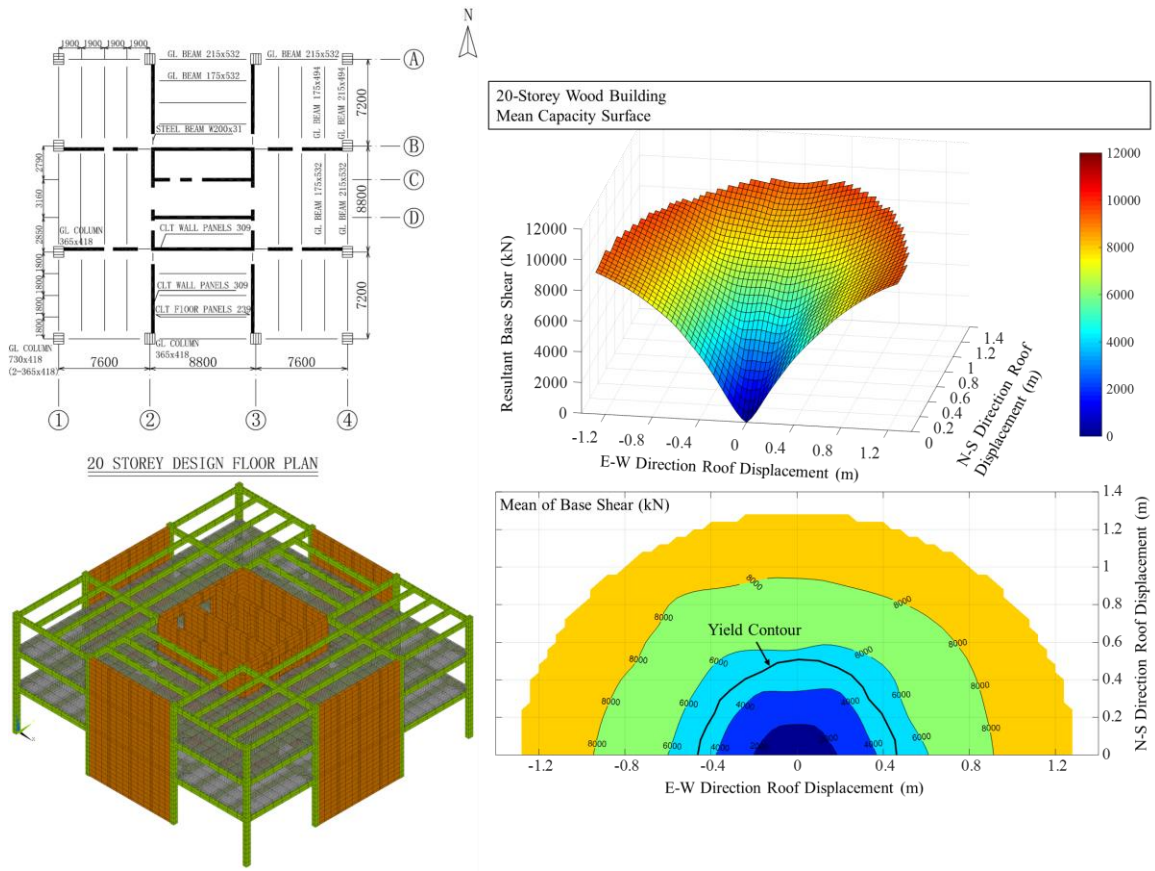


Figure 5.3. Designed 20-storey wood building and its mean capacity surface by considering bidirectional ground motions.

5.3 Approximating bisymmetric buildings using equivalent 2DOF system

5.3.1 Equation of motion

It is considered that the behaviour of a buildings shown in Figures 5.1 to 5.3 under bidirectional ground motions can be approximated by an equivalent nonlinear inelastic 2DOF system; the equivalent system is then employed to assess the structural reliability. This is akin to the approach used to evaluate reliability of a 2D structure under unidirectional ground motions (Shome and Cornell 1999; Cornell et al. 2000; Hong and Hong 2007, Hong et al. 2010).

The nonlinear inelastic 2DOF systems with Bouc-Wen hysteretic behaviour are adopted as a proxy to model the buildings in the following. The equations of motion for the 2DOF system subjected to two horizontal orthogonal components of ground motions, \ddot{u}_{gx} and \ddot{u}_{gy} , can be expressed as (Yeh and Wen 1990; Wang and Wen 2000; Lee and Hong 2010),

$$m\ddot{u}_x + c_x\dot{u}_x + \alpha k_x u_x + (1 - \alpha)k_x z_x = -m\ddot{u}_{gx} \quad (5.1)$$

and,

$$m\ddot{u}_y + c_y\dot{u}_y + \alpha k_y u_y + (1 - \alpha)k_y z_y = -m\ddot{u}_{gy} \quad (5.2)$$

where the subscripts x and y denote that they represent the quantities associated with the structural X - and Y -axes shown in Figure 5.4; u , \dot{u} , and \ddot{u} are the translational displacement, velocity, and acceleration, respectively; m is the mass, c is the viscous damping coefficient, k is the stiffness; α is the ratio of post-yield stiffness to initial stiffness; and z is the hysteretic displacement (Foliente 1995; Ma et al. 2004). In the above, it is implicitly assumed that the values of α along the X - and Y -axes are the same.

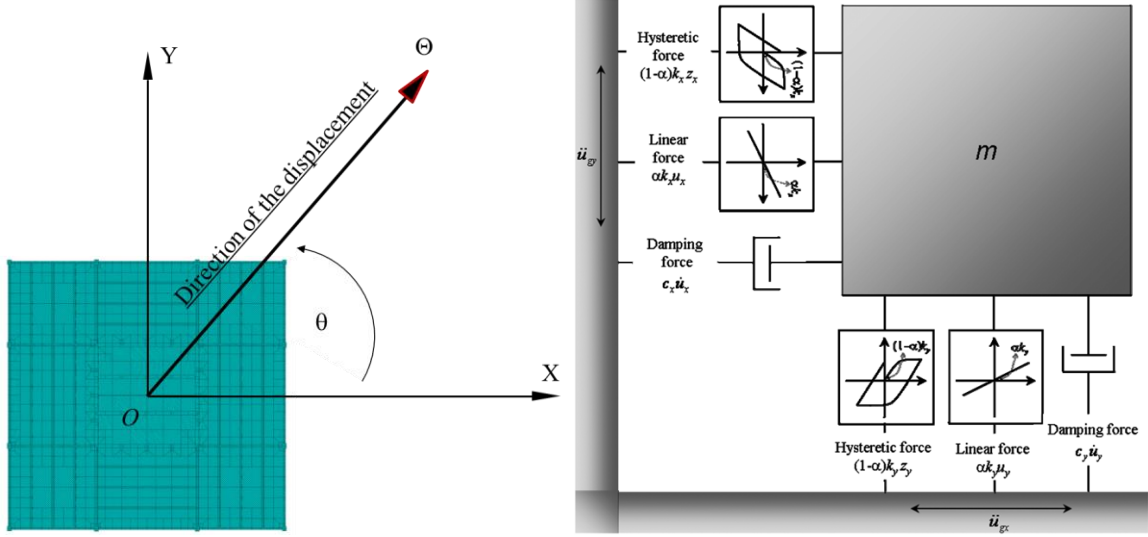


Figure 5.4. Structural axes and definition of the Θ -axis and illustration of the inelastic 2DOF system (from Lee and Hong 2010).

The hysteretic displacements z_x and z_y are governed by the following equations (Park et al. 1986; Wang and Wen 2000; Lee and Hong 2010),

$$\dot{z}_x = \frac{1}{\eta} [\dot{u}_x - \nu z_x I] \quad (5.3)$$

and,

$$\dot{z}_y = \frac{1}{\eta} [\dot{u}_y - \nu z_y I] \quad (5.4)$$

where

$$I = |\dot{u}_x| |z_x|^{n-1} [\beta + \gamma \operatorname{sgn}(\dot{u}_x z_x)] + \frac{\Delta_x^n}{\Delta_y^n} |\dot{u}_y| |z_y|^{n-1} [\beta + \gamma \operatorname{sgn}(\dot{u}_y z_y)] \quad (5.5)$$

Δ_x and Δ_y are the yield displacements along the X -axis and Y -axis; β , γ , and n are shape parameters; η and ν are the parameters related to the degradation, which can be calculated by using,

$$\eta = 1 + \delta_\eta E_{n,b} \quad (5.6)$$

and,

$$\nu = 1 + \delta_\nu E_{n,b} \quad (5.7)$$

in which δ_η and δ_ν are the parameters controlling the stiffness degradation and strength

degradation, respectively; $E_{n,b}$ represents the normalized dissipated hysteretic energy for biaxial response, which is defined as a quantity proportional to the integral of the product of the normalized hysteretic displacement and the normalized velocity.

The system is orthotropic if Δ_x is not equal to Δ_y . By letting $u_{y1} = (\Delta_x / \Delta_y) u_y$, $z_{y1} = (\Delta_x / \Delta_y) z_y$ and the restoring force along the YI -axis $q_{y1} = (Q_x / Q_y) q_y$, where $q_y = \alpha k_y u_y + (1 - \alpha) k_y z_y$, Q_x and Q_y are the yield forces along the X -axis and Y -axis, the system is translated to an equivalent isotropic system (Park et al. 1986; Wang and Wen 2000; Lee and Hong 2010). In such a case, if the systems are without the stiffness degradation and strength degradation (i.e., $\delta_\eta = 0$ and $\delta_\nu = 0$), the yield displacement for a rectilinear displacement passing through the origin in the $X-YI$ plane with a counterclockwise rotation θ , Δ , is given by,

$$\Delta = \left[(\beta + \gamma) \left(|\cos^n \theta| + |\sin^n \theta| \right) \right]^{-1/n} \quad (5.8)$$

The normalized dissipated hysteretic energy $E_{n,b}$ can be expressed as,

$$E_{n,b} = (1 - \alpha) \int_0^t \frac{z_x \dot{u}_x + z_{y1} \dot{u}_{y1}}{\Delta^2} dt \quad (5.9)$$

To facilitate the evaluation the ductility demand of the system under bidirectional horizontal orthogonal ground motions, one can introduce the normalized displacements $\mu_x = u_x / \Delta_x$, $\mu_y = u_y / \Delta_y$, $\mu_{zx} = z_x / \Delta_x$ and $\mu_{zy} = z_y / \Delta_y$. The substitution of these into Eqs. (5.1) to (5.4) results in,

$$\ddot{\mu}_x + 2\xi_x \omega_{nx} \dot{\mu}_x + \alpha \omega_{nx}^2 \mu_x + (1 - \alpha) \omega_{nx}^2 \mu_{zx} = -\ddot{u}_{gx} / (\phi_x d_x) \quad (5.10)$$

$$\ddot{\mu}_y + 2\xi_y \omega_{ny} \dot{\mu}_y + \alpha \omega_{ny}^2 \mu_y + (1 - \alpha) \omega_{ny}^2 \mu_{zy} = -\ddot{u}_{gy} / (\phi_y d_y) \quad (5.11)$$

$$\dot{\mu}_{zx} = \frac{1}{\eta} [\dot{\mu}_x - \nu \mu_{zx} I] \quad (5.12)$$

and,

$$\dot{\mu}_{zy} = \frac{1}{\eta} [\dot{\mu}_y - \nu \mu_{zy} I] \quad (5.13)$$

where $\xi_x = c_x / (2m\omega_{nx})$ and $\xi_y = c_y / (2m\omega_{ny})$ are the damping ratios associated with the X - and Y -axes, respectively; ω_{nx} and ω_{ny} are vibration frequency corresponding to the fundamental sway vibration mode along the X - and Y -axes; $\omega_{nx} = \sqrt{k_x / m}$ and $\omega_{ny} = \sqrt{k_y / m}$, in rad/s, respectively; ϕ_x and ϕ_y are the normalized yield strength defined by,

$$\phi_x = \Delta_x / d_x = F_{y,x} / F_{Ex}, \quad (5.14)$$

and,

$$\phi_y = \Delta_y / d_y = F_{y,y} / F_{Ey}, \quad (5.15)$$

where d_x and d_y are the earthquake-induced displacements in the corresponding linear elastic system along the X - and Y -axes, respectively; the forces corresponding to d_x and d_y are denoted by F_{Ex} and F_{Ey} , respectively; and $F_{y,x}$ and $F_{y,y}$ denote the yield forces with the corresponding yield displacements Δ_x and Δ_y , respectively. The values of d_x and d_y can be obtained by solving Eqs. (5.1) and (5.2) with α equal to unity for given ground motion components \ddot{u}_{gx} and \ddot{u}_{gy} , respectively. Further, I shown in Eq. (5.5) which is needed in Eqs. (5.12) and (5.13) can be re-written as,

$$I = |\dot{\mu}_x| |\mu_{zx}|^{n-1} [\beta_0 + \gamma_0 \operatorname{sgn}(\dot{\mu}_x \mu_{zx})] + |\dot{\mu}_y| |\mu_{zy}|^{n-1} [\beta_0 + \gamma_0 \operatorname{sgn}(\dot{\mu}_y \mu_{zy})] \quad (5.16)$$

where $\beta_0 + \gamma_0 = 1$, $\beta_0 = \beta \Delta_x^n$ and $\gamma_0 = \gamma \Delta_x^n$. The yield displacement Δ shown in Eq. (5.8) and the normalized dissipated hysteretic energy, $E_{n,b}$, shown in Eq. (5.9) become,

$$\Delta = \Delta_x \left(|\cos^n \theta| + |\sin^n \theta| \right)^{-1/n} \quad (5.17)$$

and,

$$E_{n,b} = (1 - \alpha) \int_0^t (\mu_{zx} \dot{\mu}_x + \mu_{zy} \dot{\mu}_y) \left(|\cos^n \theta| + |\sin^n \theta| \right)^{2/n} dt \quad (5.18)$$

Eq. (5.17) indicates that depending on the value of n the yield displacement in different directions can differ as shown in Lee and Hong (2010). For $n = 1, 2, 3, 4$ and 5 , the contours for the incipient yield are depicted in Figure 5.5. For $n = 1$, the contour becomes a rhombus, implying a very significant interaction for the biaxial yield responses. For $n = 2$, the contour is a circle, representing the isotropic behaviour. As n increases, the contour approaches to

a square, and the yield strength in one axis is independent of the displacement in its orthogonal axis. The plot depicted in Figure 5.5 indicates that the nonlinear inelastic 2DOF system considered in this section is not true isotropic system except for $n = 2$. Moreover, it must be noted that for convenience the ratio of the post-yield stiffness to initial stiffness along the X- and Y-axes is the same as mentioned earlier. This is a limitation of the adopted model.

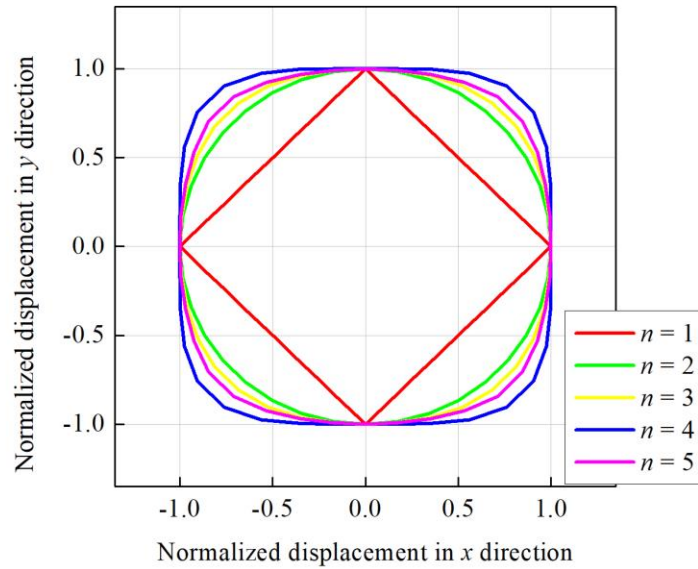


Figure 5.5. Contour for the incipient yield defined by the biaxial Bouc–Wen model.

5.3.2 Incorporating design consideration

To incorporate the seismic design requirements in the equivalent 2DOF system shown in the previous section, let $V_{yield,x}$ and $V_{yield,y}$ denote the base shears in the X- and Y-axes at incipient yield of a designed structure, respectively; and let V_{dx} and V_{dy} denote the design base shears, in the X- and the Y-axes, respectively. According to NBCC 2010 (NRCC 2010), the design base shear V_d is to be calculated using,

$$V_d = S_{A-\chi}(T_n, \xi) M_V I_E W / (R_o R_d), \quad (5.19)$$

in which $S_{A-\chi}(T_n, \xi)$ denotes the design spectral acceleration (for a system with the natural vibration period T_n and a damping ratio ξ), representing $(1-\chi)$ -fractile of SA with $\chi =$

1/2475; M_V is the higher mode factor that equals 1.0 for the considered structural systems; I_E is the importance factor that equals 1.0 if the ultimate limit state (ULS) is considered; W represents the building weight plus 25% of snow load; and R_o and R_d denote the overstrengthening related factor and ductility related factor, respectively. Therefore, V_{dx} equals V_d calculated by considering T_n and ξ equal to the first sway vibration period T_{nx} and the damping ratio for the first sway vibration mode along X-axis, ξ_x , respectively. Similarly, V_{dy} can be calculated with the subscript x replaced by y .

Since often the structures are overdesigned due to available member size, or due to that the design is governed by serviceability rather than ultimate limit state function, let $R_{nx} = V_{yield,x}/V_{dx}$ and $R_{ny} = V_{yield,y}/V_{dy}$. By considering this and following Hong and Hong (2007), ϕ_x in Eq. (5.10) is replaced by

$$\phi_x = \zeta_x = \frac{V_{yield,x}}{F_{Ex}} = \frac{R_{nx} V_{dx}}{F_{Ex}} = \frac{R_{nx}}{R_o R_d} \frac{L_{mx}}{L_x}, \quad (5.20)$$

and,

$$\phi_y = \zeta_y = \frac{V_{yield,y}}{F_{Ey}} = \frac{R_{ny} V_{dy}}{F_{Ey}} = \frac{R_{ny}}{R_o R_d} \frac{L_{my}}{L_y}, \quad (5.21)$$

in which $L_{mx} = M / \Lambda_x$ and $L_x = S_{Ax}(T_{nx}, \xi_x) / S_{A-\chi}(T_{nx}, \xi_x)$; and $L_{my} = M / \Lambda_y$ $L_y = S_{Ay}(T_{ny}, \xi_y) / S_{A-\chi}(T_{ny}, \xi_y)$; M is the total mass of the structure and Λ_x and Λ_y represent the effective modal mass in the X- and Y-axes, respectively; $S_{Ax}(T_{nx}, \xi_x)$ and $S_{Ay}(T_{ny}, \xi_y)$ represents the spectral acceleration for the considered record component in the X- and Y-axes, respectively. For the design of the wood buildings, the product of the reduction factors, $R_d R_o$, equal to 3.0 was employed (see Chapter 2); the calculated values for the parameters associated with the above equations for the designed buildings are shown in Table 5.1. The use of ζ_x and ζ_y , rather than ϕ_x and ϕ_y is to make the distinction that the design yield forces and the seismic demand based on linear elastic responses are incorporated in the formulation.

Table 5.1. Parameters used to calculate the design based shear for and the characteristics of the designed wood buildings in X-axis and Y-axis.

Design	10-Storey		15-Storey		20-Storey	
Parameters	X-axis	Y-axis	X-axis	Y-axis	X-axis	Y-axis
T_n (s)	1.30	1.63	1.92	1.66	1.97	2.11
V_d (kN)	1715	1394	2005	2481	3010	2788
v_s	2.29	2.35	2.45	2.36	2.47	2.71
L_m	1.81	2.05	1.74	1.98	1.77	1.91
Mean of R_n , m_{R_n}	1.87	1.85	2.90	2.21	1.76	1.75
Coefficient of variation of R_n , v_{R_n}	0.23	0.28	0.20	0.29	0.17	0.12
Coefficient of variation of SA, v_s	2.29	2.35	2.45	2.36	2.47	2.71

Based on the above consideration, Eqs. (5.10) and (5.11) are replaced by,

$$\ddot{u}_x + 2\xi_x \omega_{nx} \dot{u}_x + \alpha \omega_{nx}^2 u_x + (1-\alpha) \omega_{nz}^2 u_x = -\ddot{u}_{gx} / (\zeta_x d_x) \quad (5.22)$$

and,

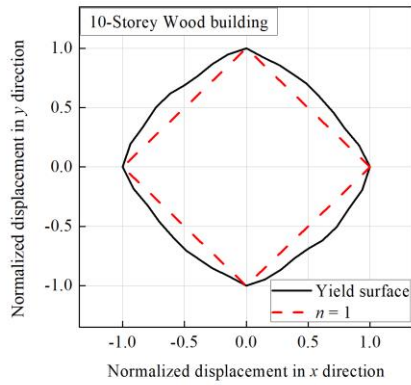
$$\ddot{u}_y + 2\xi_y \omega_{ny} \dot{u}_y + \alpha \omega_{ny}^2 u_y + (1-\alpha) \omega_{ny}^2 u_y = -\ddot{u}_{gy} / (\zeta_y d_y) \quad (5.23)$$

5.3.3 Fitting the equivalent model based on the capacity surface

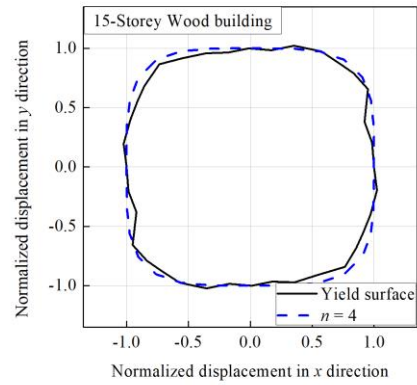
The assessment of α for the equivalent model is carried out similar to the case of analysis of a 2D structure under unidirectional ground motions. More specifically, the bilinear approximation is used to fit two capacity curves: the capacity curve obtained based on the response surface where the displacement in the Y-axis equals zero, and the capacity curve obtained based on the capacity surface where the displacement in the X-axis equal to zero. For each building, the average value of the ratio of the post-yield stiffness to initial stiffness obtained from these two fitting is assigned to α , which is shown in Table 5.2. From the table, it can be observed that α values for the considered three structures range from about 0.4 to 0.6. These values are much greater than those considered for steel frame structures due to post-yield behaviour of steel that is significantly different than the timber and timber connection. It is also noted that these values differ from those obtained by considering unidirectional ground motion (see Chapter 3). This is partly due to that the differences in

the obtained capacity surfaces or curves and, that the average value of α for the responses along the X - and along the Y -axes is used to calculate α for the equivalent 2DOF model.

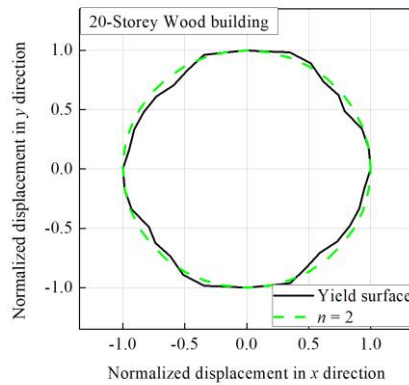
The parameters β_0 and γ_0 are considered equal to 0.5 as these values could be considered to be acceptable for most structures (Goda et al. 2009). The identification of n for the 2DOF systems to represent the designed wood buildings is carried out using the contour for incipient yield of the design buildings obtained from the capacity surface. The identified contours from the capacity surfaces shown in Figures 5.1 to 5.3 are plotted in Figure 5.5. Figure 5.5a indicates that the use of $n = 1$ could be appropriate for the 10-storey building; Figure 5.5b indicates that the use of $n = 4$ could be appropriate for the 15-storey building; and Figure 5.5c indicates that the use of $n = 2$ could be appropriate for the 20-storey building. The differences in the shape of the contours for incipient yield are attributed to how the shear walls are placed for the 10-, 15- and 20-storey buildings (see Figure 5.1 to 5.3). For example, the CLT panels are placed close to the center of the 10-storey building so the structural is relatively weak along its diagonal direction. For the 15-storey building, besides the CLT panels near the building center, several panels are placed along the perimeter of the building so the structural capacity in an axis is almost independent of less dependent on the displacement along its orthogonal axis. In the case of 20-storey building, the CLT panels are extended from the core outwards making the building's capacity less dependent on the orientation.



a)



b)



c)

Figure 5.6. Contours of incipient yield identified based on the mean of the IDA surface for the designed wood buildings: a) 10-storey wood building; b) 15-storey wood building; c) 20-storey wood building.

Table 5.2. Estimated model parameters.

Design	Bidirectional Bouc-Wen Model Parameters	
	α	n
10-Storey	0.53	1
15-Storey	0.59	4
20-Storey	0.39	2

5.4 Seismic demand, reliability evaluation procedure and results

5.4.1 Seismic demand and reliability evaluation procedure

The annual maximum $S_A(T_n, \xi)$ at a site is often developed based on the ground motion prediction equations (GMPEs) for a random orientation. Moreover, the SA values for the recorded horizontal orthogonal ground motion components are considered to be independent and identically distributed in develop such GMPEs (Boore et al. 1997). Therefore, it is reasonable to assume that $S_{Ax}(T_{nx}, \xi_x)$ and $S_{Ay}(T_{ny}, \xi_y)$ are independent and identically distributed as $S_A(T_{nx}, \xi_x)$ and $S_A(T_{ny}, \xi_y)$. For Canadian sites, $S_A(T_n, \xi)$ could be considered to be a lognormal variate, at least in the upper tail region (Hong et al. 2006). The probability distributions of $S_{Ax}(T_{nx}, \xi_x)$ and $S_{Ay}(T_{ny}, \xi_y)$ provide the probabilistic characterization of the seismic hazard for linear elastic system under bidirectional horizontal ground motions. However, they do not provide direct indication on the inelastic seismic demand for a hysteretic system such as the one shown in Eqs. (5.22) and (5.23).

To assess the inelastic seismic demand (i.e., μ_x and μ_y), it is noted that since $L_x = S_{Ax}(T_{nx}, \xi_x) / S_{A-\chi}(T_{nx}, \xi_x)$ and $L_y = S_{Ay}(T_{ny}, \xi_y) / S_{A-\chi}(T_{ny}, \xi_y)$, L_x and L_y are also lognormally distributed with their mean values m_{L_x} and m_{L_y} given by,

$$m_{L_x} = \sqrt{1 + v_{sx}^2} \exp\left(-\beta_T \sqrt{\ln(1 + v_{sx}^2)}\right), \quad (5.24)$$

and,

$$m_{L_y} = \sqrt{1 + v_{sy}^2} \exp\left(-\beta_T \sqrt{\ln(1 + v_{sy}^2)}\right), \quad (5.25)$$

where $\beta_T = \Phi^{-1}(1 - \chi)$ and $\Phi^{-1}(\bullet)$ is the inverse standard normal distribution function; v_{sx} denotes the cov of $S_{Ax}(T_{nx}, \xi_x)$; and v_{sy} denotes the cov of $S_{Ay}(T_{ny}, \xi_y)$. For the considered construction site, the estimated v_{sx} and v_{sy} based on the results reported in Hong et al. (2006) are also include in Table 5.1 that are applicable to the considered structures.

By considering that R_{nx} is lognormally distributed with mean $m_{R_{nx}}$ and cov $v_{R_{nx}}$, R_{ny} is

lognormally distributed with mean $m_{R_{ny}}$ and cov $v_{R_{ny}}$, $\ln(\zeta_x)$ and $\ln(\zeta_y)$ are normally distributed. Their means $m_{\ln(\zeta_x)}$ and $m_{\ln(\zeta_y)}$, and standard deviations denoted as $\sigma_{\ln(\zeta_x)}$ and $\sigma_{\ln(\zeta_y)}$ are given by,

$$m_{\ln(\zeta_x)} = \ln \left(\frac{m_{R_{nx}}}{\sqrt{1+v_{R_{nx}}^2}} \right) + \ln \left(\frac{L_{mx}}{R_o R_d} \right) - \ln \left(\frac{m_{L_x}}{\sqrt{1+v_{sx}^2}} \right), \quad (5.26)$$

$$m_{\ln(\zeta_y)} = \ln \left(\frac{m_{R_{ny}}}{\sqrt{1+v_{R_{ny}}^2}} \right) + \ln \left(\frac{L_{my}}{R_o R_d} \right) - \ln \left(\frac{m_{L_y}}{\sqrt{1+v_{sy}^2}} \right), \quad (5.27)$$

$$\sigma_{\ln(\zeta_x)} = \sqrt{\ln(1+v_{R_{nx}}^2) + \ln(1+v_{L_x}^2)}, \quad (5.28)$$

and,

$$\sigma_{\ln(\zeta_y)} = \sqrt{\ln(1+v_{R_{ny}}^2) + \ln(1+v_{L_y}^2)}, \quad (5.29)$$

The above probabilistic models completely characterize ζ_x and ζ_y . Given the values of ζ_x and ζ_y , the linear elastic demand for the considered equivalent 2DOF system is completely defined (see Eqs. (5.22) and (5.23)). However, the corresponding inelastic demand for the system, in terms of ductility demand, is unknown and need to be evaluated.

The inelastic seismic demand for the system, $\mu_{b,\max}$, can be expressed as (Lee and Hong 2010),

$$\mu_{b,\max} = \max_{\text{for all } t} \left(|u_x / \Delta_x|^n + |u_y / \Delta_y|^n \right)^{1/n} = \max_{\text{for all } t} \left(|\mu_x|^n + |\mu_y|^n \right)^{1/n} \quad (5.30)$$

which is a function of both ζ_x and ζ_y , (see Eqs. (5.20) and (5.21)). The evaluation of statistics of μ_x and μ_y conditioned on ζ_x and ζ_y , is presented shortly below for the considered equivalent 2DOF models.

The condition that $\mu_{b,\max}$ is greater than 1 implies that the system subjected a given ground motion record with two horizontal orthogonal components undergoes inelastic deformation. Therefore, the probability of incipient yield (or damage) of the system subjected to bidirectional seismic excitations, $P_{D,b}$, can be expressed as,

$$P_{D,b} = \text{Pr ob}(\mu_{b,\max} > 1), \quad (5.31)$$

The probability of incipient collapse, $P_{C,b}$, can be expressed as,

$$P_{C,b} = \text{Pr ob}(\mu_{b,\max} / \mu_{cap} > 1) \quad (5.32)$$

where $\mu_{cap} = (\mu_{x,cap}^n + \mu_{y,cap}^n)^{1/n}$, $\mu_{x,cap}$ and $\mu_{y,cap}$ are the ductility capacities of the structure along the X -axis and Y -axis, respectively. In addition, $\mu_{x,cap}$ and $\mu_{y,cap}$ could be considered as lognormal variates (Diaz-Lopez and Esteva 1991) with the mean and cov of $\mu_{x,cap}$, denoted by $m_{\mu_{x,cap}}$ and $v_{\mu_{x,cap}}$, and the mean and cov of $\mu_{y,cap}$, denoted by $m_{\mu_{y,cap}}$ and $v_{\mu_{y,cap}}$, respectively.

Rather than assessing $P_{C,b}$ based on ductility alone, one could also consider the application of the Park-Ang damage index under the biaxial excitations (Park et al. 1985; Lee and Hong 2010),

$$D_{b,PA} = D_{b,PA}^* / \mu_{cap} \quad (5.33)$$

where $D_{b,PA}^* = \mu_{b,\max} + \lambda E_{n,b}$ and $E_{n,b}$ is calculated from Eq. (5.18) and λ is the coefficient for cyclic loading ranging from 0.005 to 0.25 (Park and Ang 1985, Chung and Loh 2002), and $D_{b,PA} \geq 1$ implies collapse. Based on this consideration the probability of incipient collapse, denoted as $P_{C,PA}$, can be expressed as,

$$P_{C,PA} = \text{Pr ob}(D_{b,PA} \geq 1) \quad (5.34)$$

The statistical characterizations of $\mu_{b,\max}$ and $D_{b,PA}^*$ for a nonlinear equivalent 2DOF system needed to evaluate Eqs. (5.31), (5.32) and (5.34) can be carried out following the procedure used in Lee and Hong (2010). It involves in selecting a set of ground motion records, and estimating of μ_x , μ_y and $D_{b,PA}^*$ conditioned on ζ_x and ζ_y for each selected record by solving Eqs. (5.22) and (5.23) - the solution procedure requires the evaluation of $E_{n,b}$ shown in Eq. (5.18).

For the numerical analysis carried out in this chapter, a set of 381 ground motion records from 31 California earthquakes is considered. This set of records was considered in Hong and Goda (2007) and Lee and Hong (2010). An illustration of the time history of the

response, $\mu_{b,\max}$ and $D_{b,PA}^*$ for a single selected record is presented in Figures 5.7 to 5.9 for the equivalent 2DOF systems representing the 10-, 15- and 20-storey buildings.

To obtain the statistics of $\mu_{b,\max}$ and $D_{b,PA}^*$, the analysis carried out for the results shown in Figures 5.7 to 5.9 is repeated for the selected 381 records and a range of ζ_x and ζ_y values. The calculated mean and standard deviation (i.e., σ) of $\mu_{b,\max}$ and $D_{b,PA}^*$ (for $\lambda = 0.1$) from the samples are shown in Figures 5.10, and 5.11, respectively.

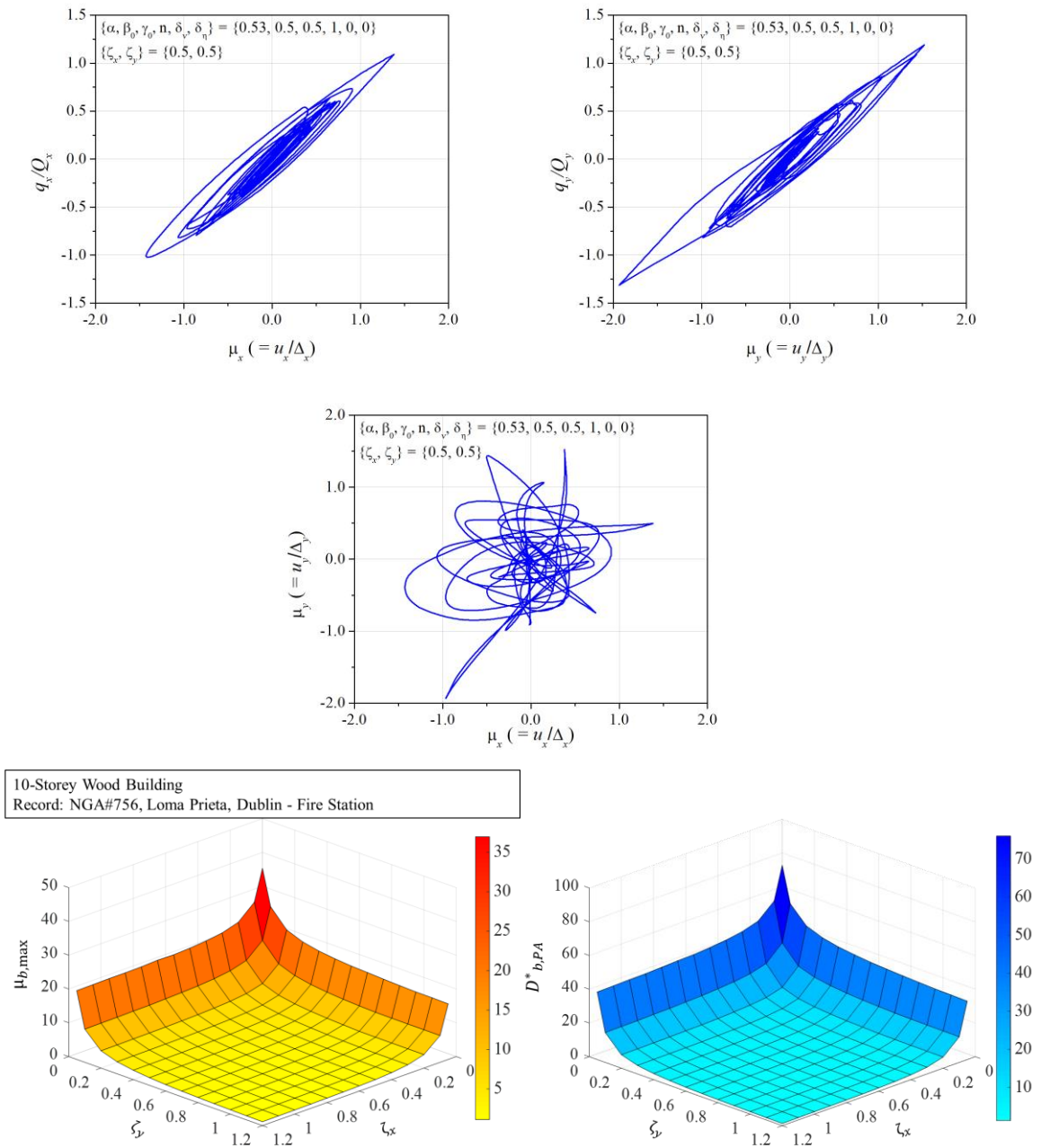


Figure 5.7. Calculated force-deformation curves along the X-axis and along the Y-axis, trajectory of displacement projected in the horizontal plane, $\mu_{b,max}$ and $D^*_{b,PA}$ (for $\lambda = 0.1$) for a selected record (NGA#756, Loma Prieta, Dublin - Fire Station) for the 2DOF system representing 10-storey wood building.

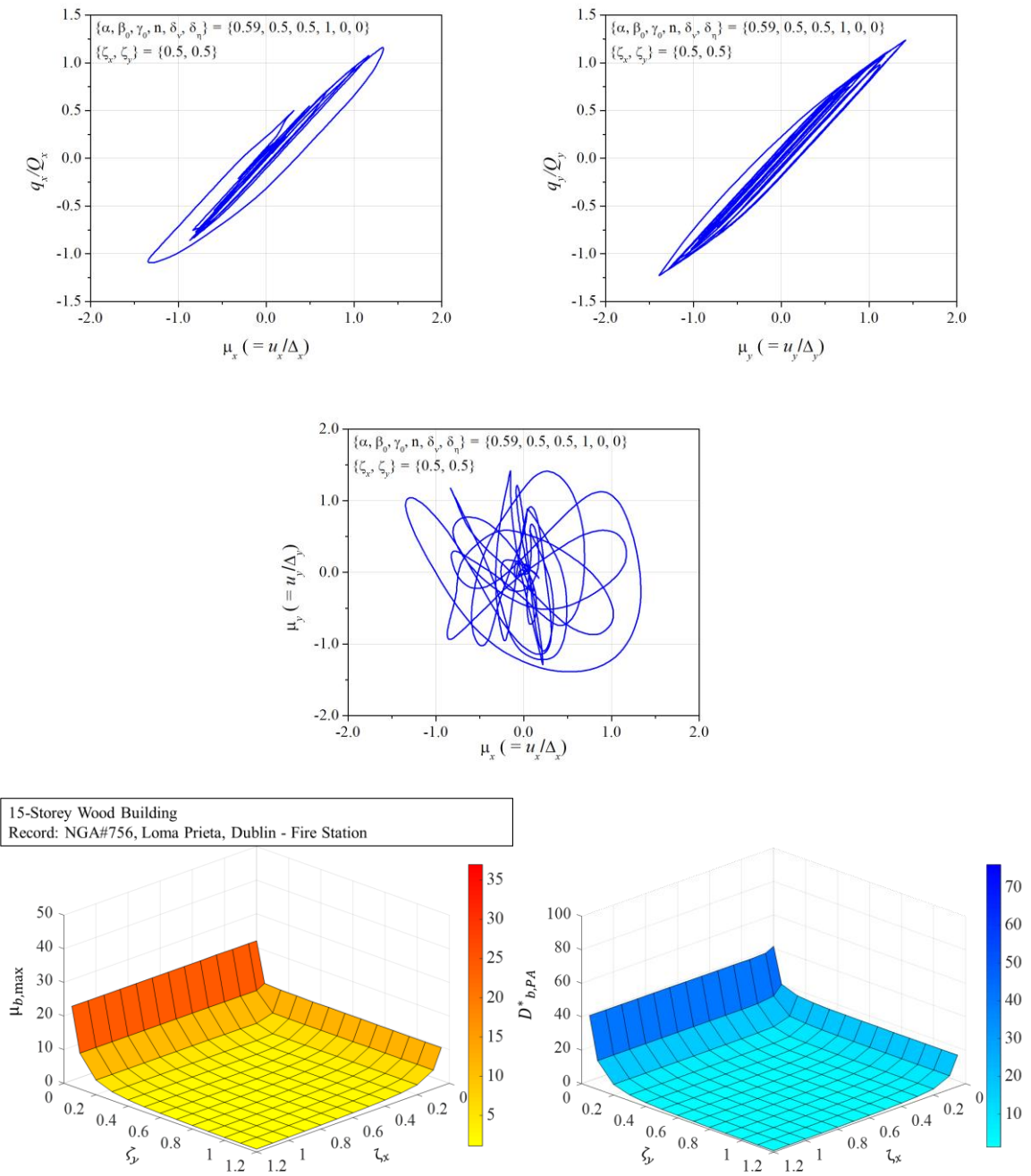


Figure 5.8. Calculated force-deformation curves along the X-axis and along the Y-axis, trajectory of displacement projected in the horizontal plane, $\mu_{b,max}$ and $D^*_{b,PA}$ (for $\lambda = 0.1$) for a selected record (NGA#756, Loma Prieta, Dublin - Fire Station) for the 2DOF system representing 15-storey wood building.

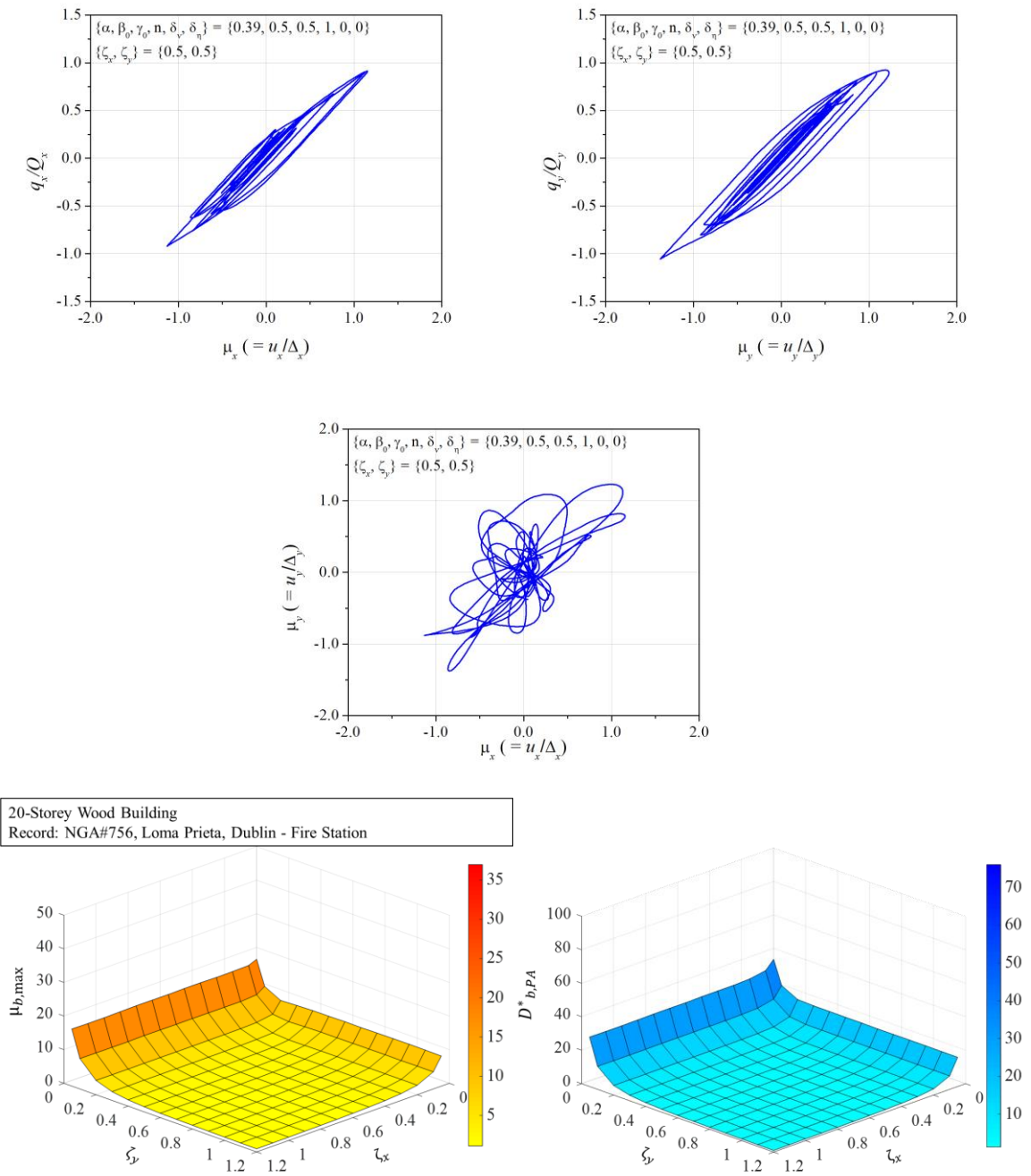


Figure 5.9. Calculated force-deformation curves along the X-axis and along the Y-axis, trajectory of displacement projected in the horizontal plane, $\mu_{b,max}$ and $D_{b,PA}^*$ (for $\lambda = 0.1$) for a selected record (NGA#756, Loma Prieta, Dublin - Fire Station) for the 2DOF system representing 20-storey wood building.

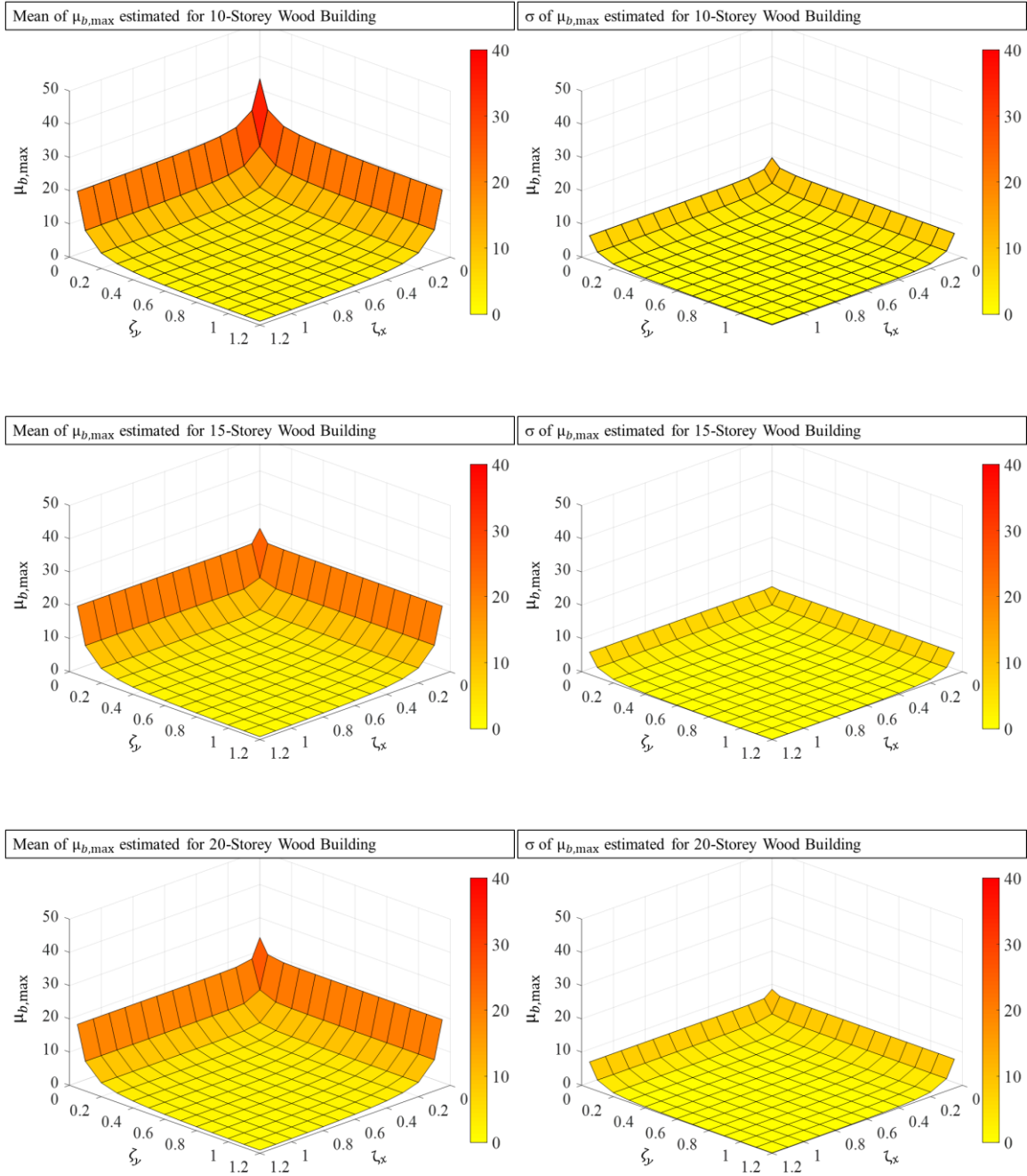


Figure 5.10. Estimated mean and standard deviation (σ) of $\mu_{b,max}$.

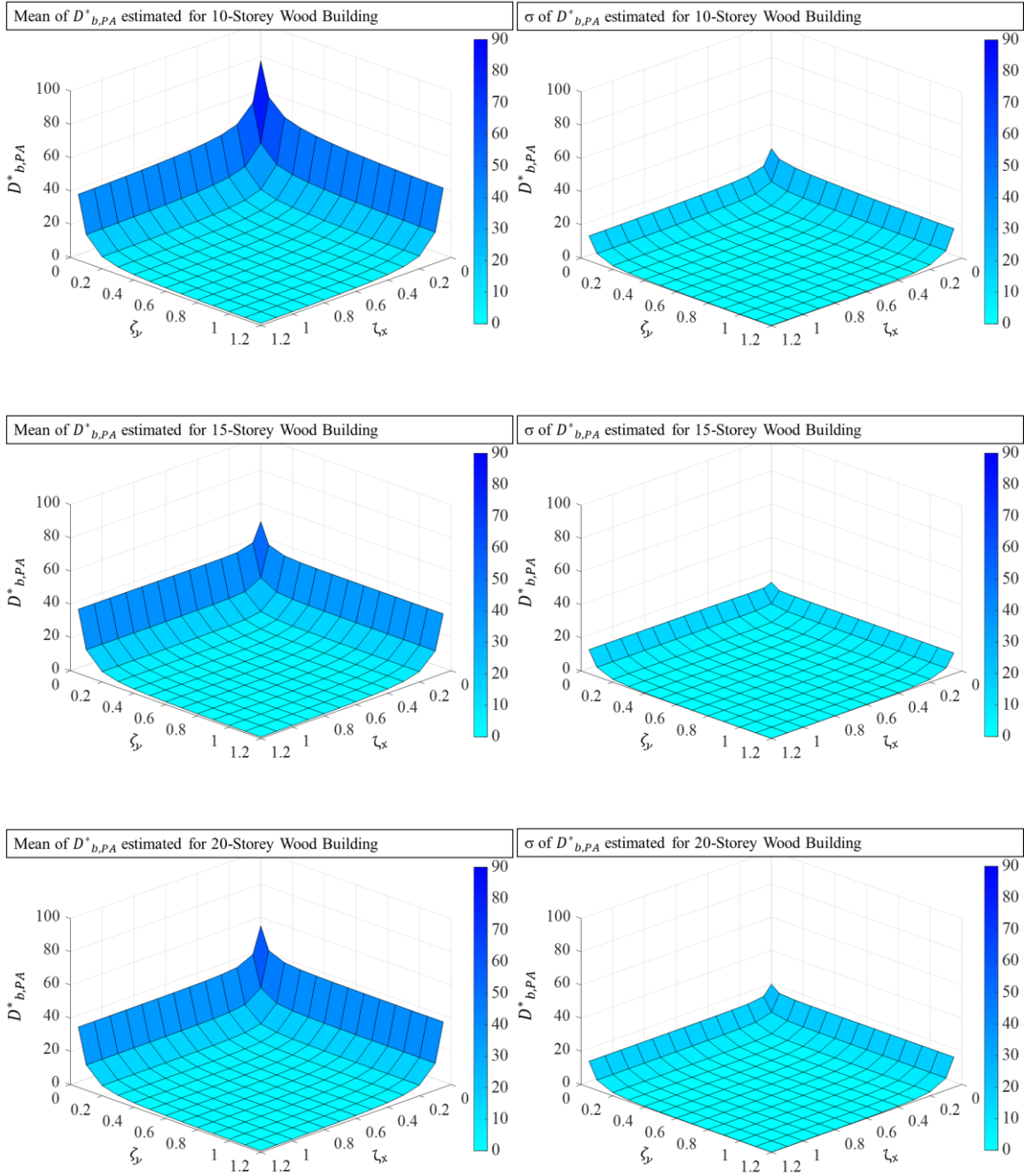


Figure 5.11. Estimated mean and standard deviation (σ) of $D_{b,PA}^*$.

Comparison of the results shown in Figures 5.10 and 5.11 and those given in Chapter 3 indicates that the ductility demand under bidirectional seismic excitations can be much greater than that obtained under unidirectional excitations (see Chapter 3) if the normalized yield strengths in both directions for the former are similar to that for the latter along a single direction. In addition, if the normalized yield strengths in both orthogonal directions differ significantly, the ductility demand under bidirectional ground motions is close to that obtained along unidirectional excitations for the smaller normalized yield strength. Furthermore, for the equivalent system representing the 10-storey building, the mean of $\mu_{b,\max}$ and $D_{b,PA}^*$ are greater than those for 15- and 20-storey buildings. This can be explained by noting that the differences between the yield displacements contours shown in Figures 5.5 and 5.6; the one associated with 10-storey building is within those associated with 15- and 20-storey buildings. As the yield contour associated with 15-storey building resembles a square, the effect of biaxial interaction on the ductility demand is much less significant than those associated with 10- and 20-storey buildings. In all cases, the standard deviation of the ductility demand (i.e., for cases with $\mu_{b,\max} > 1.0$) is significant. This is consistent with the results obtained under unidirectional ground motions (see Chapter 3).

To assign probabilistic models to $\mu_{b,\max}$, a probability distribution fitting exercise is carried out using several commonly used probability models, including the lognormal, Frechet, Weibull, and gamma distributions. Based on the maximum likelihood criteria (or Akaike information criterion (AIC)), it is concluded that the Frechet distribution is preferred for the models represent the 15- and 20-storey buildings, and that the lognormal distribution is preferred for the model representing the 10-storey building. The samples of $\mu_{b,\max}$ plotted in probability papers are illustrated in Figure 5.12. Similar analysis is carried out for $D_{b,PA}^*$. For λ equal to 0.1, the samples of $D_{b,PA}^*$ plotted in probability papers are also illustrated in Figure 5.12. The distribution fitting exercise indicates that the Frechet distribution is preferred for the models represent the 10-, 15- and 20- storey buildings.

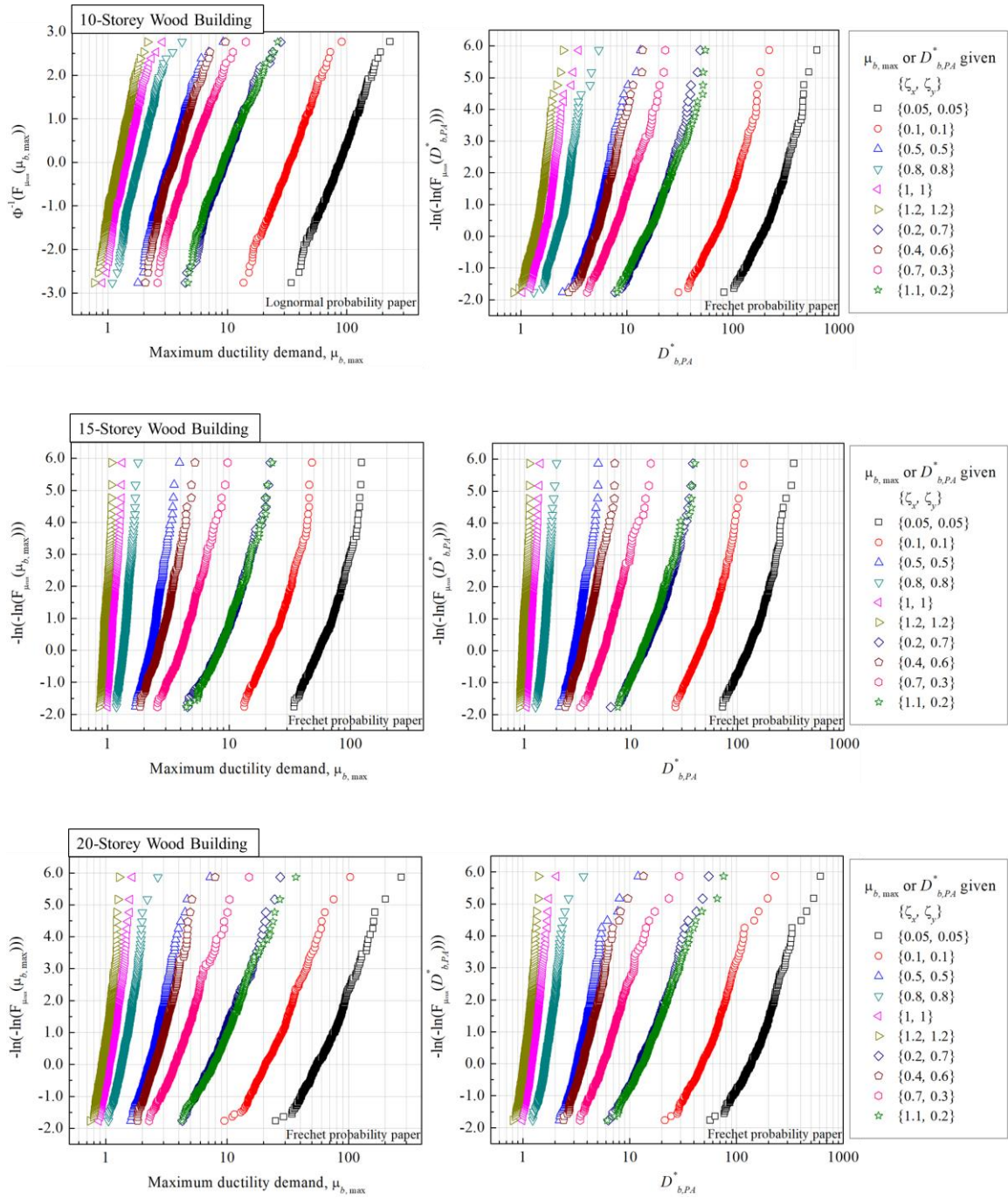


Figure 5.12. Plots of the samples of $\mu_{b,\max}$ and $D_{b,PA}^*$ in Frechet or lognormal probability papers for selected sets of (ζ_x, ζ_y) values.

Given the probabilistic models of SA, R_{nx} and R_{ny} (i.e., models of ζ_x and ζ_y shown in Eqs. (5.26) to (5.29)), ductility demand, and ductility capacity, the assessment of $P_{D,b}$, $P_{C,b}$ and $P_{C,PA}$ described in Eqs. (5.31), (5.32) and (5.34)) can be evaluated by using the following steps:

- 1) Sample ζ_x and ζ_y according to their probability distribution functions;
- 2.1) Calculate the mean and cov of $\mu_{b,max}$ according to the developed statistics of $\mu_{b,max}$ conditioned on ζ_x and ζ_y and through interpolation. Find the probability distribution parameters for $\mu_{b,max}$;
- 2.2) Similar to 2.1) calculate the mean and cov of $D_{b,PA}^*$, and find the probability distribution parameters for $D_{b,PA}^*$;
- 3) Sample $\mu_{b,max}$, $\mu_{x,cap}$ and $\mu_{y,cap}$, and $D_{b,PA}^*$ according to their distribution, calculate $g_D = \mu_{b,max} - 1$, $g_{C,b} = \mu_{b,max} / \mu_{cap} - 1$ and $g_{C,PA} = D_{b,PA}^* / \mu_{cap} - 1$;
- 4) Repeat Steps 1) and 3) n_T times and count the number of times that $g_D < 0$, $g_{C,b} < 0$ and $g_{C,PA} \leq 0$ to estimate $P_{D,b}$, $P_{C,b}$, and $P_{C,PA}$.

In all cases, for the numerical analysis to be carried out, n_T equals to 10^8 is considered.

5.4.2 Estimated failure probability

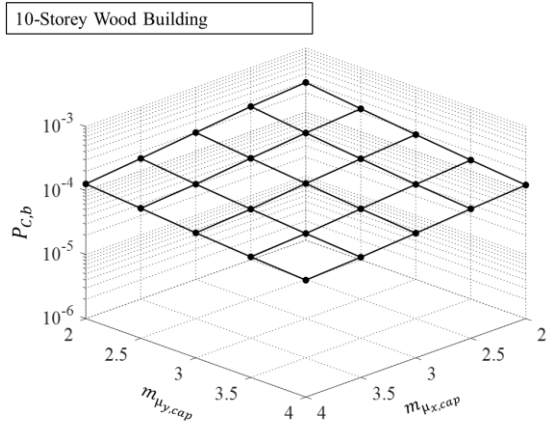
Using the procedure outlined in the previous section, the estimation of $P_{D,b}$, $P_{C,b}$, and $P_{C,PA}$ for the designed 10-, 15-, and 20-storey wood buildings is carried out. The estimated $P_{D,b}$ are 1.10×10^{-3} , 3.73×10^{-4} and 9.96×10^{-4} , for models representing the 10-, 15- and 20-storey buildings respectively. These values are greater but similar to those under unidirectional ground motions and agreed with those obtained for steel frame structures designed to satisfy requirements in the NBCC (Hong et al. 2010).

The calculated $P_{C,b}$, and $P_{C,PA}$ are shown in Figures 5.13, 5.14 and 5.15 for the models representing the 10-, 15- and 20-storey buildings, respectively. For the calculation, the mean of $\mu_{x,cap}$ and $\mu_{y,cap}$ range from 2 to 4 and a cov of 0.3 (inferred from the behaviour of CLT panels) (Popovski et al. 2011; Gavric et al. 2015) are considered.

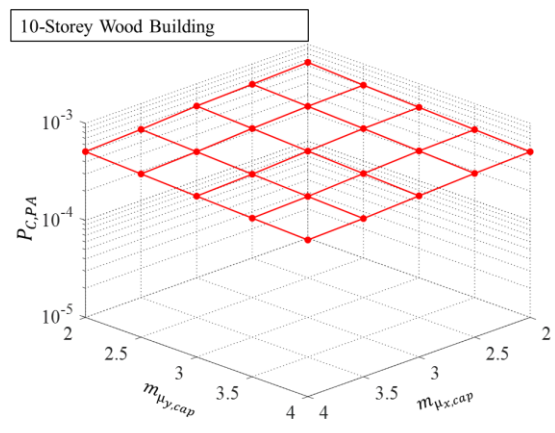
The results shown in the figures indicate that $P_{C,b}$ is consistently lower than $P_{C,PA}$, which is expected since the latter included the effect of accumulated damage. Also, as expected the estimated failure probability decreases for an increased ductility capacity. In all cases, the estimated failure probability $P_{C,b}$ is smaller than 10^{-4} , which is about one order of magnitude lower than the probability of incipient yield. The values of $P_{C,b}$ is the lowest for the model representing 15-storey wood building; this is followed by that for the 20-storey building. This observed low probability of incipient collapse can be explained is caused by both the over design (see overstrengthening factor R_n shown in Table 5.1) and the different shapes of the yield contours shown in Figures 5.4 and 5.5.

It must be emphasized that the values of $P_{C,b}$ shown in Figures 5.13 to 5.15 must not be compared directly with those corresponding cases under unidirectional ground motions shown in Chapter 3. This is partly because the ratio of post-yield stiffness to initial stiffness used in the equivalent 2DOF and in the equivalent SDOF systems differ. Furthermore, in general, the values of $P_{C,b}$ under bidirectional ground motions is greater than those under unidirectional ground motions.

In fact, by adopting the equivalent models but under unidirectional ground motions, the estimated probability of incipient yield along the X-axis are 7.06×10^{-4} , 8.81×10^{-5} and 3.02×10^{-5} for the models representing 10-, 15- and 20-storey buildings. These values become 7.68×10^{-4} , 5.54×10^{-5} and 3.01×10^{-4} if the uniaxial load is acting along the Y-axis. These values are about 2 to 6 times lower than those under bidirectional ground motions that are mentioned earlier. The estimated probability of incipient collapse $P_{C,b}$ under unidirectional ground motions is shown in Figure 5.16. Comparison of the results shown in Figures 5.13 to 5.16 again indicates that the estimated $P_{C,b}$ under bidirectional ground motion is consistently greater than that under unidirectional ground motions. The ratio of the former to the latter ranges from about 3 to 8. In general, the ratio increases as $\mu_{x,cap}$ or $\mu_{y,cap}$ increases. This indicates the importance of considering the bidirectional ground motions in estimate the probability of incipient collapse.

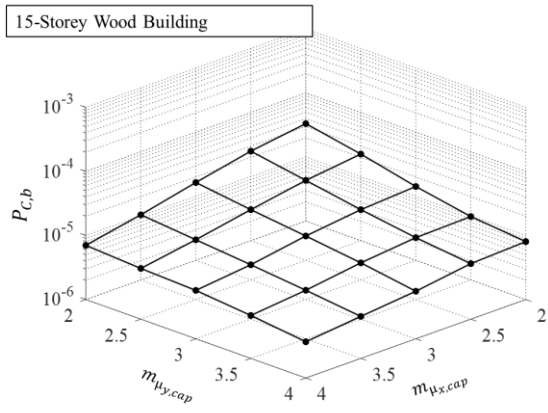


a)

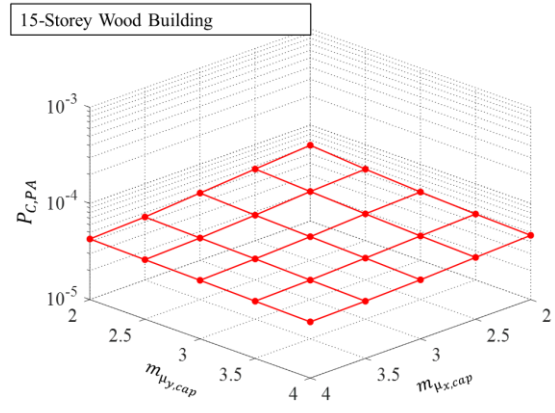


b)

Figure 5.13. Estimated $P_{C,b}$: and $P_{C,PA}$ for the model representing 10-storey: a) Estimated $P_{C,b}$; b) Estimated $P_{C,PA}$.



a)



b)

Figure 5.14. Estimated $P_{C,b}$: and $P_{C,PA}$ for the model representing 15-storey: a) Estimated $P_{C,b}$; b) Estimated $P_{C,PA}$.

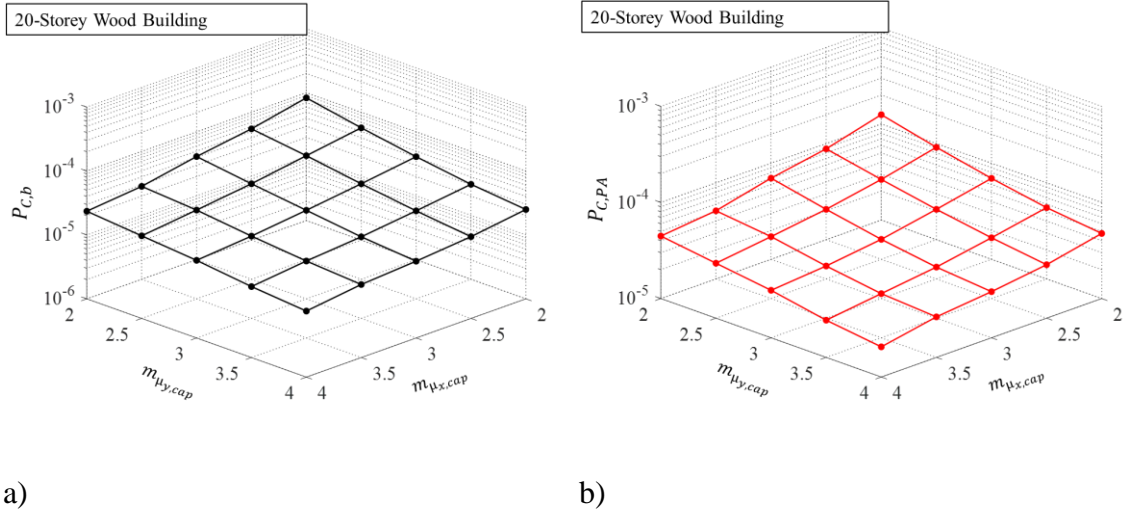


Figure 5.15. Estimated $P_{C,b}$ and $P_{C,PA}$ for the model representing 20-storey: a) Estimated $P_{C,b}$; b) Estimated $P_{C,PA}$.

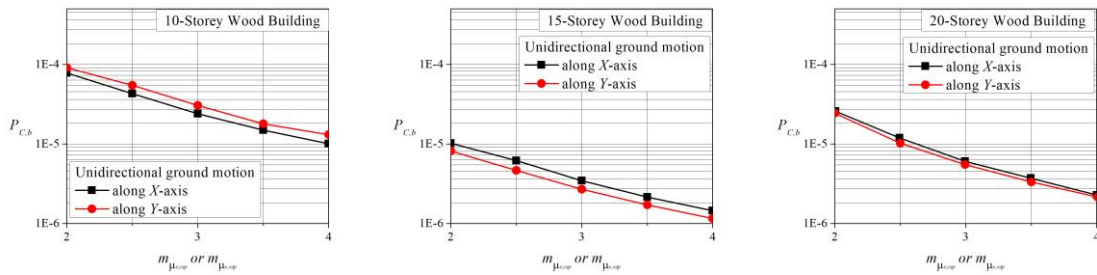


Figure 5.16. Estimated failure probability P_C by considering the unidirectional ground motion with the equivalent structural model shown in tables 5.1 and 5.2.

5.5 Conclusions

A simple procedure to estimate reliability of 3D bisymmetrical structures under bidirectional ground motions is proposed. The procedure is employed to estimate probabilities of incipient yield and of incipient collapse. The procedure considers that the seismic capacity of bisymmetric buildings can be represented by capacity surface which can be obtained through nonlinear static pushover analysis or incremental dynamic analysis. The capacity surface is then used as the bases to establish equivalent nonlinear inelastic two-degree-of-freedom system (2DOF). As the statistics of the ductility demand for the equivalent nonlinear inelastic 2DOF system can be established with relative ease, the probability of incipient yield and probability of incipient collapse of the equivalent 2DOF system can be evaluated once the probabilistic seismic hazard characteristics are available.

The established procedure is applied to estimate the failure probability of three designed mid-rise and high-rise wood buildings. The results indicate that the failure probabilities under bidirectional ground motions are greater than those obtained under unidirectional ground motion. Therefore, for assessing the reliability of building under seismic ground motions, the consideration of bidirectional ground motion can be important for seismic risk modeling and emergency preparedness.

5.6 References

- Boore, D. M., Joyner, W. B., and Fumal, T. E. (1997). Equations for estimating horizontal response spectra and peak acceleration from western North American earthquakes: a summary of recent work. *Seismological research letters*, 68(1), 128-153.
- Chung, S. T., and Loh, C. H. (2002). Identification and verification of seismic demand from different hysteretic models. *Journal of earthquake engineering*, 6(03), 331-355.
- Cornell, C. A., Jalayer, F., Hamburger, R. O., and Foutch, D. A. (2002). Probabilistic basis for 2000 SAC federal emergency management agency steel moment frame guidelines. *Journal of structural engineering*, 128(4), 526-533.

- Foliente, G. C. (1995). Hysteresis modeling of wood joints and structural systems. *Journal of Structural Engineering*, 121(6), 1013-1022.
- Goda, K., Hong, H. P., and Lee, C. S. (2009). Probabilistic characteristics of seismic ductility demand of SDOF systems with Bouc-Wen hysteretic behaviour. *Journal of Earthquake Engineering*, 13(5), 600-622.
- Han, S. W., and Wen, Y. K. (1997). Method of reliability-based seismic design. I: Equivalent nonlinear systems. *Journal of Structural Engineering*, 123(3), 256-263.
- Hong, H. P., and Goda, K. (2007). Orientation-dependent ground-motion measure for seismic-hazard assessment. *Bulletin of the Seismological Society of America*, 97(5), 1525-1538.
- Hong, H. P., and Hong, P. (2007). Assessment of ductility demand and reliability of bilinear single-degree-of-freedom systems under earthquake loading. *Canadian Journal of Civil Engineering*, 34(12), 1606-1615.
- Hong, H. P., Hong, P., and Wang, W. (2010). Reliability of steel frames designed in accordance with the National Building Code of Canada seismic provisions and its implication in codified design. *Engineering Structures*, 32(5), 1284-1291.
- Lee, C. S., and Hong, H. P. (2010). Statistics of inelastic responses of hysteretic systems under bidirectional seismic excitations. *Engineering Structures*, 32(8), 2074-2086.
- Lee, C.S. and Hong, H.P. (2012) Statistics of inelastic torsional responses of single-storey, *15th World Conference on Earthquake Engineering*, Lisbon, Portugal. September.
- Madsen, H. O., Krenk, S., and Lind, N. C. (1986). *Methods of structural safety*. Prentice Hall, Inc., Englewood Cliffs, N.J.
- Ma, F., Zhang, H., Bockstedte, A., Foliente, G. C., and Paevere, P. (2004). Parameter analysis of the differential model of hysteresis. *Journal of Applied Mechanics*, 71(3), 342-349.

- Melchers RE. (1999). Structural reliability analysis and prediction. 2nd edition. *John Wiley*.
- NRCC (2010). National Building Code of Canada, *NRC Canada*, Ottawa, Ontario, Canada.
- Park, Y. J., and Ang, A. H. S. (1985). Mechanistic seismic damage model for reinforced concrete. *Journal of structural engineering*, 111(4), 722-739.
- Park, Y. J., Ang, A. H. S., and Wen, Y. K. (1985). Seismic damage analysis of reinforced concrete buildings. *Journal of Structural Engineering*, 111(4), 740-757.
- Park, Y. J., Wen, Y. K., and Ang, A. (1986). Random vibration of hysteretic systems under bi-directional ground motions. *Earthquake engineering and structural dynamics*, 14(4), 543-557.
- Shome, N., and Cornell, C. A. (2000). Structural seismic demand analysis: Consideration of “Collapse”. In *8th ASCE Specialty Conference on Probabilistic Mechanics and Structural Reliability* (pp. 1-6). South Bend, Indiana: University of Notre Dame.
- Wang, C. H., and Wen, Y. K. (2000). Evaluation of pre-Northridge low-rise steel buildings. I: Modeling. *Journal of Structural Engineering*, 126(10), 1160-1168.
- Yeh, C. H., and Wen, Y. K. (1990). Modeling of nonstationary ground motion and analysis of inelastic structural response. *Structural Safety*, 8(1-4), 281-298.

Chapter 6

6 Conclusions and Recommendations for Future Work

6.1 Conclusions

This thesis is focused on the design, and seismic performance of mid- and high-rise wood buildings. Design of 10-, 15- and 20-storey wood buildings is carried out according to the requirements stipulated in Canadian design codes. The performance is assessed by considering the unidirectional and bidirectional horizontal ground motions. The assessment is concentrated on the structural capacity in sustaining the seismic load and the seismic reliability under uni- and bi-directional ground motions. The main conclusions and observations based on the analysis results of this study can be summarized as follows:

- 1) It was found the design of the three mid-rise or tall wood buildings are governed by inter-storey drift caused by earthquake load or wind load rather than the strength requirements if the NBCC is employed.
- 2) An assessment of the capacity curves of the design buildings is carried out using the IDA and NSPA. Comparison of the obtained capacity curves indicates that the NSPA curve approximates well the mean capacity curve estimated by using the IDA, although the use of the NSPA cannot characterize the uncertainty in the capacity curve caused by record-to-record variability.
- 3) It is observed that the post yield stiffness of the wood building system differs from steel frame structures, which influences the seismic ductility demand.
- 4) By considering the equivalent nonlinear inelastic SDOF system and the effect of record-to-record variability on the seismic ductility demand and, by incorporating the design considerations, the probabilities of the incipient of damage and of incipient collapse are estimated. The results indicate that the estimated probability of incipient collapse is similar to that obtained for steel frame structures designed according to codified Canadian design practice. This suggests that the use of the heavy timber as mid- and high-rise building construction material is adequate if the seismic hazard is of concern.

During this study, it was observed that, to gain further support in using heavy timber as building construction material, there is need and incentive to carry out experimental or detailed numerical investigation to gather sufficient statistical data on the ductility capacity of mid- and high-rise wood building systems so to further validate the estimated failure probability.

- 5) A procedure to develop seismic capacity surface under bidirectional horizontal ground motion is presented. It seems that the use of such a surface in defining the seismic capacity of a building has not been elaborated in the literature. The analysis procedure involves the use of incremental dynamic analysis (IDA), scaling the record components and rotating the incidence angle. Also, the use of nonlinear static pushover analysis (NSPA) with different incidence angle may also be considered. Most importantly, it is argued that use of capacity curve for building under bidirectional ground motion may not adequate since the structural responses may not remain in the same vertical plane and the inelastic behaviour of the structural for different vertical plane may differ. The obtained numerical analysis results for three designed mid-rise and tall wood buildings, by using the established procedure, indicate that the record-to-record variability is significant for the capacity surface, and that the yield capacity depends on the displacement path and the considered building.
- 6) Comparison of the capacity surface obtained from IDA and NSPA indicates that the results obtained from the latter could be considered as a good approximation for the former. However, it is worth mentioning that the use of NSPA does not provide information on the record-to-record variability on the estimated capacity surface.
- 7) A simple and practical procedure to estimate reliability of 3D bisymmetrical structures under bidirectional ground motions is proposed. The procedure considers that the seismic capacity of bisymmetric buildings can be represented by capacity surface which is then used as the bases to establish equivalent nonlinear inelastic two-degree-of-freedom system (2DOF). This largely facilitates the reliability of structural under bidirectional ground motions.

8) The procedure described in 7) is applied to estimate the failure probability of three designed mid-rise and high-rise wood buildings. The results indicate that the failure probabilities under bidirectional ground motions are about 3 to 8 times greater than those obtained under unidirectional ground motion if the incipient collapse is considered, and are about 2 to 6 times greater than those obtained under unidirectional ground motion if the incipient yield is considered. Therefore, the consideration of bidirectional ground motions in assessing the reliability of building under seismic ground motions can be important for seismic risk modeling and emergency preparedness.

6.2 Recommendations for future work

Several future works could be recommended. In particular, during this study, it was observed that, to gain further support in using heavy timber as building construction material, there is need and incentive to carry out experimental or detailed numerical investigation to gather sufficient statistical data on the ductility capacity of mid-rise and tall wood building systems. Such statistics can significantly impact the estimated failure probability of the buildings under seismic excitations.

Both equivalent nonlinear inelastic SDOF or 2DOF systems are used as the basis to evaluate the reliability of the buildings. However, these equivalent systems do not include the effect of torsion which can be important for nonsymmetric systems. An effort in extending the equivalent 2DOF system to 3DOF system could be valuable and simplify the reliability analysis for unsymmetrical systems

Curriculum Vitae

Name: Shucheng Yang

Post-secondary Education and Degrees: University of Western Ontario
London, Ontario, Canada
2013-2017 Ph.D.

Chang'an University
Xi'an, Shaanxi, China
2010-2012 M. Eng.

Chang'an University
Xi'an, Shaanxi, China
2006-2010 B.E.Sc.

Honours and Awards: 2013 – 2016 Chinese Government Scholarship (CGS)
2011 – 2012 1st place of National Graduate Scholarship

Related Work Experience Instructor
CEE 4458 – Risk Analysis and Decision Making in Engineering
University of Western Ontario
2016

Teaching Assistant
University of Western Ontario
2013-2017

Publications:
Peer-reviewed Journal Articles

Yang, S. C., Liu, T. J., and Hong, H. P. (2017). Reliability of Tower and Tower-Line Systems under Spatiotemporally Varying Wind or Earthquake Loads. *Journal of Structural Engineering*, 143(10), 04017137.

Yang, S. C., and Hong, H. P. (2016). Nonlinear inelastic responses of transmission tower-line system under downburst wind. *Engineering Structures*, 123, 490-500.

Conferences and Presentations

Yang, S.C., Hong, H.P. and Bartlett, M.F. (2016). Capacity Curves of Designed 10- and 15-storey Wood Buildings under Seismic Excitations, *Proceedings of the Annual Conference of the CSCE*

Yang, S.C., Hong, H.P. and Bartlett, M.F., Capacity Surface of Timber Buildings under Uni-directional Seismic Excitations, Presentation at NEWBuilds Annual Meeting, Vancouver, 2015.05

Yang, S.C., Hong, H.P. and Bartlett, M.F., Capacity Surface of Hybrid Timber Buildings under Uni- and Bi-directional Seismic Excitations, Presentation at NEWBuilds Annual Meeting, Vancouver, 2014.05